UNIVERSIDADE DE LISBOA

FACULDADE DE CIÊNCIAS

Photosynthetic metabolism in microphytobenthos: modulation by temperature and dissolved inorganic carbon

Doutoramento em Biologia

Especialidade em Ecofisiologia

Sónia Catarina Reis Vieira

Tese orientada por:

Professor Doutor Jorge Marques da Silva e pelo Doutor Paulo Cartaxana

Documento especialmente elaborado para a obtenção do grau de doutor

2016

UNIVERSIDADE DE LISBOA

FACULDADE DE CIÊNCIAS

Photosynthetic metabolism in microphytobenthos: modulation by temperature and dissolved inorganic carbon

Doutoramento em Biologia

Especialidade em Ecofisiologia

Sónia Catarina Reis Vieira

Tese orientada por:

Professor Doutor Jorge Marques da Silva e pelo Doutor Paulo Cartaxana

Júri:

Presidente:

- Doutora Vanda Costa Brotas Gonçalves

Vogais:

- Doutor Paulo Jorge Sousa Dias Cartaxana
- Doutor João António de Almeida Serôdio
- Doutor Rui Orlando Pimenta Santos
- Doutora Maria da Glória Calado Inglês Esquível
- Doutora Vanda Costa Brotas Gonçalves
- Doutora Ana de Jesus de Melo de Amorim Ferreira

Documento especialmente elaborado para a obtenção do grau de doutor

2016

PUBLICATIONS

CHAPTER 2
Vieira S, Utkin AB, Alexander L, Santos NM, Vilar R, Marques da Silva J, Cartaxana P (2011) Effects of intertidal microphytobenthos migration on biomass determination via laser-induced fluorescence. Marine Ecology Progress Series 432:45-52.

CHAPTER 3
Vieira S, Ribeiro L, Jesus B, Cartaxana P, Marques da Silva J (2013) Photosynthesis assessment in microphytobenthos using conventional and imaging pulse amplitude modulation fluorometry. Photochemistry and Photobiology 89:97-102.

CHAPTER 4
Vieira S, Ribeiro L, Marques da Silva J, Cartaxana P (2013) Effects of short-term changes in sediment temperature on the photosynthesis of two intertidal microphytobenthos communities. Estuarine, Coastal and Shelf Science 119:112-118.

CHAPTER 5
Vieira S, Cartaxana P, Máguas C, Marques da Silva J (2016) Photosynthesis in estuarine intertidal microphytobenthos is limited by inorganic carbon availability. Photosynthesis Research (in press) DOI 10.1007/s11120-015-0203-0.

CHAPTER 6
Cartaxana P, Vieira S, Ribeiro L, Rocha RJM, Cruz S, Calado R, Marques da Silva J (2015) Effects of elevated temperature and CO_2 on intertidal microphytobenthos. BMC Ecology 15:10.

ACKNOWLEDGEMENTS / AGRADECIMENTOS

Eu quero agradecer a todos os que me apoiaram e permitiram a realização da minha tese de doutoramento:

Fundação para a Ciência e Tecnologia (FCT) pela concessão da bolsa de doutoramento (SFRH/BD/63940/2009) e à Faculdade de Ciências da Universidade de Lisboa (FCUL).

Ao Professor Jorge Marques da Silva pela orientação e supervisão do trabalho, pela frontalidade e disponibilidade para discutir todos os aspetos do trabalho. Pela paciência e ajuda que tem tido para comigo ao longo deste trabalho.

Ao Paulo Cartaxana pela orientação e supervisão do trabalho, pela frontalidade e disponibilidade para discutir todos os aspetos do trabalho. Pela paciência e calma nesta fase final de escrita e pela ajuda incansável nas coreções finais. Pela amizade, pelas conversas, pelas risadas durante as horas de almoço.

Professores e investigadores do Departamento de Biologia Vegetal e MARE, que me ajudaram neste trabalho.

Dona Manuela pela crucial ajuda em muitos trabalhos laboratoriais, solucionando sempre os problemas. Pela amizade, pelas conversas, pelo carinho, pelas palavras de coragem e força.

A todas as pessoas que colaboraram na realização dos trabalhos laboratorias e de campo, pois sem elas teria sido impossível.

A todas as pessoas que participaram nos meus trabalhos: Lourenço Ribeiro, Bruno Jesus, Alexander Lavrov, Andrei Utkin, Sónia Cruz, Ricardo Calado, Rui Rocha, Cristina Máguas.

Ana Rita e Carla Gameiro e pelas conversas e amizade.

Professor Arrabaça e professora Belucha pelas conversas e motivação científica.

Aos meus amigos que me acompanharam ao longo deste percurso (Ricardo, Beto, Catarina, meninas, Zé, Vasco, Carlota, Pantufa, Campeão, Mia, Pipoca, Mana).

Maria Rita, minha filha por me lembrar todos os dias que temos um caminho e percurso a seguir.

Aos meus pais e família por acreditarem e tornarem isto possível.

A todos OBRIGADO!

Table of Contents

List of Abbreviations

α - initial slope of the *r*ETR

CCMs - carbon concentrating mechanisms

Chl *a* - chlorophyll a

DIC – dissolved inorganic carbon

DD - diadinoxanthin

DT - diatoxanthin

E_k - light saturation parameter

E - photosynthetic photon flux density

F_o - minimum fluorescence of dark-adapted samples

F_m' - maximal fluorescence of light-adapted samples

F - steady-state fluorescence of light-adapted samples

F_v/F_m - maximum efficiency of dark-adapted PSII

$\Delta F/F_m'$ - effective quantum yield of PSII

HPLC - high performance liquid chromatography

Imaging-PAM- imaging pulse amplitude modulated

LIF - laser induced fluorescence

MPB - microphytobenyhos

NDVI - normalised difference vegetation index

PAM fluorometer – pulse amplitude modulated fluorometer

PI - phytobenthos index

PSI - photosystem I

PSII - photosystem II

RLC- rapid light curves

*r*ETR - relative photosynthetic electron transport rate

ETR_{max} - maximum relative electron transport rate

V_{max} - inorganic carbon-saturated photosynthesis rate

K_m - half-saturation constant

$\delta^{13}C$ and $\delta^{15}N$ - carbon and nitrogen Isotope composition

Summary

Main primary producers of estuarine systems include benthic microalgae, predominantly diatoms, and cyanobacteria that colonize subtidal and intertidal zones, commonly referred to as microphytobenthos (MPB). MPB communities account for about 50% of the primary productivity of estuarine systems (e.g. MacIntyre et al., 1996; Barranguet et al., 1998; Underwood and Kromkamp, 1999; Serôdio and Catarino, 2000). This is highly relevant considering that estuarine systems are among the most productive ecosystems in the biosphere (Constanza et al., 1997). Despite the extreme variability of environmental parameters (irradiance, temperature and salinity) that characterizes the estuarine habitat, these communities are able to display high photosynthetic rates. It is common to distinguish two types of MPB communities: epipelic communities (typical of muddy sediments) composed of motile species and epipsammic communities (typical of sandy sediments) composed largely by non-motile species attached to sand grains. Contrary to epipsammic, epipelic diatoms exhibit circadian and circatidal migratory rhythms (Palmer and Round, 1967; Palmer, 1973; Admiraal et al., 1982; Serôdio and Catarino, 2000).

Being MPB critical for the function of estuarine and coastal ecosystems, understanding the impact of climate change on its structure and productivity is mandatory. In particular, the increase of temperature and inorganic carbon availability can markedly affect photosynthesis, diversity and productivity of estuarine MPB communities. However, studies of the impact of climate changes on MPB are still scarce, and in particular the effects of the interaction between increased temperature and inorganic carbon availability are, to a large extent, still unknown.

Thus, in this project we studied the effects of temperature and dissolved inorganic carbon (DIC) availability in two MPB communities of the Tagus estuary, in central Portugal, applying new methods of remote sensing, namely laser induced fluorescence (LIF) and modulated imaging fluorescence (Imaging-PAM). The LIF methodology (**chapter 2**) was used to trace migratory rhythms of benthic epipelic microalgae typical of mud sediments. Indeed, it was confirmed that, during the diurnal low tide these microalgae migrate to the surface of sediment to drive photosynthesis and then migrate in depth before the arrival of the tide.

Furthermore, epipelic diatoms show photophobic migration when exposed to high light levels, a process known as behavioral photoprotection. This technique proved to be adequate to the study of MPB communities, both for the determination of surface biomass and the study of migratory rhythms. The possibility of using LIF for middle-range remote sensing under natural light conditions opens good perspectives for its use in environmental monitoring of estuarine systems.

In the last decades, conventional pulse amplitude modulated fluorescence (PAM) has been increasingly applied to estuarine MPB communities (Serôdio et al., 1997; Kromkamp et al., 1998; Paterson et al., 1998; Serôdio et al., 2001; Honeywill et al., 2002; Perkins et al., 2002; Serôdio, 2003; Stephens et al., 2003; Forster and Kromkamp, 2004; Murphy et al., 2004; Serôdio, 2004; Forster and Jesus, 2005; Murphy et al., 2005). Lower resolution imaging systems allow the mapping of fluorescence parameters over large areas, making it a unique technique to study the spatial heterogeneity of the photosynthetic activity across an autotrophic surface (Scholes and Rolfe, 1996; Hill et al., 2004. This can be particularly relevant in the study of MPB biofilms, characterized by a "patchy," heterogeneous distribution and can provide useful information about the spatial distribution of biomass and productivity in sediments. Yet, important hardware differences exist between conventional and imaging systems and therefore a comparative study of the results obtained with these technologies in MPB was required **(chapter 3**). In fact, we observed significant differences between the results obtained with conventional and imaging systems, especially in what refers to the analysis of rapid fluorescence curves as a function of irradiance (RLCs, Rapid Light Curves). Lower values of α (initial slope of the *r*ETR vs. E curve), ETR_{max} (maximum relative ETR), E_k (light saturation parameter) and F_v/F_m (maximum quantum efficiency of photosystem II of dark-adapted samples) were obtained using the Imaging- PAM system. The discrepancy between instruments was dependent on sample type, being more pronounced in mud than in sandy MPB sediments. The differences may be largely explained by the interplay between the different depth-integration of the fluorescence signal, dependent on the thickness of the photosynthetic layer, and the different attenuation coefficients of the light sources used by the two types of instrument. It is therefore important to take into account the specificity of each fluorescence system when interpreting and comparing chlorophyll fluorescence data of

MPB communities, taking full advantage of the application of imaging fluorescence to the MPB communities, in particular in what refers to its unique ability to study the spatial heterogeneity of their photosynthetic activity.

The in-depth understanding of the primary production processes of MPB is a prerequisite to assess the impacts of climate change on estuarine systems. Among the global change variables, increased temperature and atmospheric CO_2 (and concomitantly dissolved inorganic carbon, DIC) are expected to have the most significant impact over the primary productivity in estuaries. Therefore, we studied their effect, as well as their interaction, on the photosynthesis of MPB biofilms. The short-term effect of increasing temperature in the photosynthetic activity of two communities of MPB (Alcochete and Trancão) was studied **(chapter 4)**. The Trancão MPB community had higher photosynthetic electron transport capacity (higher ETR_{max}) being photoacclimated at higher irradiance (higher E_K) and had lower energy conversion efficiency at limiting irradiance (lower α) .The differences in the species composition and size class may explain the results obtained for the two sites, since smaller cells are generally more metabolically active. However, for the both MPB communities photosynthetic capacity increased with temperature up to 35 °C and decreased with extreme temperature of 42 °C. Photosynthetic efficiencies at low irradiance (α) were not affected by the temperature in the 15-35 °C range, and decreased at 42 °C. These MPB estuarine communities were able to increase the photosynthetic capacity under exposure to short-term high temperatures sediments, similar to happens during the summer midday in the diurnal low tides.

We also studied the effect of dissolved inorganic carbon availability (DIC) in photosynthesis, on the two intertidal MPB communities, taking as reference the model diatom species *Phaeodactylum tricornutum*, using fluorescence imaging (on intact MPB communities) and polarographic oxygen measurement (in cell suspensions) **(chapter 5)**. The parameters of DIC acquisition kinetics (V_{max} and K_m (DIC)) estimated for MPB communities were higher ((K_m (DIC) = 0.31 mM; V_{max} = 7.78 nmol min^{-1} μg (Chl a)$^{-1}$), than those obtained for *Phaeodactylum tricornutum* (K_m (DIC) = 0.23 mM; V_{max} = 4.64 nmol min^{-1} μg (Chl a)$^{-1}$), showing that these communities have species with low affinity for DIC and high photosynthetic capacity. The net photosynthesis of MPB suspensions reached saturation at DIC concentrations of 1-1.5 mM,

lower than those found in the sediment top 5 mm interstitial water, suggesting that the photosynthesis of these communities is not limited by DIC availability. However, when $NaHCO_3$ was added to intact MPB samples, an increase in the maximum photosynthetic electron transport rate (ETR_{max}) was observed. These results suggest that the local depletion of DIC in the photic layer of the sediment, where the microalgae accumulate during diurnal low tide, limits the photosynthetic activity of MPB, providing the first experimental evidence of DIC limitation of the productivity of intertidal MPB communities.

The interactive effects of temperature and DIC in biomass, species composition and photosynthetic performance of MPB was studied using a microcosm ELSS ('experimental life support system') with tide regime **(chapter 6)**. The longer term effect of increased temperature (24 ° C) had a negative effect on MPB biomass and photosynthetic performance under both simulated DIC conditions (pH = 7.4 and pH = 8.0). Furthermore, at elevated temperatures there was a change in the relative abundance of the major species of diatoms and an increase of cyanobacteria. The long term effect of increasing DIC (pH = 7.4) under low temperature (18 °C) had a positive effect on biomass MPB, possibly due to decreased local depletion of dissolved inorganic carbon. No significant effects were found on the relative abundance of the major groups of microalgae. Our results suggest that the interactive effects of increased temperature and DIC availability of estuarine MPB communities can have a negative impact on the structure, diversity and productivity of these communities, eventually affecting the entire estuarine ecosystems. Therefore, a deepen understanding of the potential impacts of climate change in these complex ecosystems is required.

Keywords: Microphytobenthos, climate change, pulse amplitude modulated fluorometry, photosynthesis, temperature, carbon, diatoms.

Resumo

Entre os principais produtores primários dos sistemas estuarinos encontram-se as microalgas bênticas, predominantemente diatomácias, e cianobactérias que colonizam as zonas subtidais e intertidais, geralmente designadas por microfitobentos (MPB). Estas comunidades de MPB são responsáveis por cerca de 50% da produtividade primária dos sistemas estuarinos (e.g. MacIntyre et al., 1996; Barranguet et al., 1998; Underwood and Kromkamp, 1999; Serôdio and Catarino, 2000). Este facto é particularmente relevante considerando que os estuários se encontram entre os ecossistemas mais produtivos da biosfera (Constanza et al., 1997). Apesar da extrema variabilidade em parâmetros ambientais (tais como luz, temperatura e salinidade) que caracteriza o habitat estuarino, estas comunidades apresentam elevadas taxas fotossintéticas. Na literatura é comum encontrar as comunidades de MPB divididas em comunidades epipélicas (típicas de sedimentos vasoso), com células capazes de se deslocarem entres as particulas de sedimento, e comunidades epipsâmicas (típicas de sedimentos arenosos), maioritariamente constituídas por células fixas aos grãos de areia. Ao contrário destas últimas, as diatomáceas epipélicas apresentam ritmos migratórios circadianos e circatidais (Palmer and Round, 1967; Palmer, 1973; Admiraal et al., 1982; Serôdio and Catarino, 2000).

Os ecossistemas costeiros e estuarinos são habitats particularmente sensíveis às alterações climáticas, prevendo-se que sofram profundas alterações nas próximas décadas. O aumento da temperatura e do CO_2 atmosférico são duas variáveis importantes nos cenários de alterações globais, tendo, presumivelmente, efeitos significativos na fotossíntese, diversidade e produtividade das comunidades de MPB estuarino. Uma vez que os estudos de alterações climáticas ao nível do MPB são escassos, é particularmente importante estudar os efeitos interativos destes dois parâmetros ambientais nestas comunidades.

Numa primeira fase desta tese, fomos estudar os parâmetros fotossintéticos, ritmos migratórios e mecanismos de fotoproteção comportamental das comunidades de MPB, aplicando novas metodologias de deteção remota como a fluorescência induzida por laser (LIF) e imagiologia de fluorescência (Imaging-PAM). Por um lado, a metodologia LIF foi usada, para seguir os ritmos migratórios das microalgas bênticas epipélicas **(capítulo 2)**. Por outro

lado, permitiu determinar mecanismos de fotoproteção comportamental característicos destas comunidades epipélicas. Durante a baixa-mar diurna estas microalgas migram para a superfície do sedimento (acumulação de biomassa na superfície) e seguidamente migram em profundidade antes da chegada da maré. A migração em direcão à superficíe do sedimento permite às células chegar à zona fótica e captar luz indispensável à fotossíntese. Por outro lado, a migração vertical descendente sob níveis de luz elevados, pode ser interpretada como um mecanismo de fotoproteção comportamental evitando deste modo níveis de luz fotoinibitórios. Esta técnica mostrou-se adequada ao estudo das comunidades de MPB quer na determinação da biomassa superficial quer no estudo dos seus ritmos migratórios.

Nas últimas decadas, a fluorescência de pulso modulado (PAM), tem sido aplicada ao estudo das comunidades de MPB estuarino de forma exaustiva (Serôdio et al., 1997; Kromkamp et al., 1998; Paterson et al., 1998; Serôdio et al., 2001; Honeywill et al., 2002; Perkins et al., 2002; Serôdio, 2003; Stephens et al., 2003; Forster and Kromkamp, 2004; Murphy et al., 2004; Serôdio, 2004; Forster and Jesus, 2005; Murphy et al., 2005). A imagiologia de fluorescência permite o mapeamento de parâmetros de fluorescência numa área alargada, tornando-se uma técnica única em estudos de heterogeneidade espacial da atividade fotossintética (Scholes and Rolfe, 1996; Hill et al., 2004). Isto pode ser particularmente relevante no estudo de biofilmes de MPB, podendo fornecer informações úteis sobre a distribuição espacial de biomassa e produtividade em sedimentos. Deste modo, e tendo em conta que estas técnicas foram optimizadas para plantas superiores, era importante um estudo comparativo entre a fluorometria convencional e de imagem ao nível destas comunidades **(capítulo 3)**. Verificámos que o nível de discrepância entre os sistemas convencionais e de imagem foi dependente do tipo de amostra sendo mais pronunciado em sedimentos vasosos de MPB. Estas diferenças podem ser explicadas pelas diferenças da integração de profundidade do sinal de fluorescência relacionado com a espessura da camada fotossintética e pelos coeficientes de atenuação de luz. Deste modo, é necessário ter algum cuidado ao interpretar e comparar dados de fluorescência da clorofila das comunidades de MPB. Contudo a aplicação do Imaging-PAM ao MPB estuarino permite a obtenção de mapas de fluorescência tornando-se uma técnica única para o estudo da heterogeneidade espacial da atividade fotossintética destas comunidades.

O efeito a curto prazo do aumento da temperatura na atividade fotossintética de duas comunidades de MPB (Alcochete e Trancão) foi o primeiro parâmetro a ser estudado utilizando imagiologia de fluorescência (Imaging-PAM) **(capítulo 4**). As comunidades de MPB do Trancão apresentaram maior capacidade fotossintética (maior ETR_{max}), estando fotoaclimatadas a irradiâncias mais elevadas (maior E_K) e apresentaram menor eficiência para irradiâncias limitantes (menor α). As diferenças na composição taxonómica e na classe de tamanhos podem justificar os resultados obtidos para os dois locais, uma vez que, as células de menor tamanho são geralmente mais ativas, devido à maior superfície relativamente ao volume. Em ambas as comunidades de MPB estuarino a capacidade fotossintética aumentou com a temperatura até 35 °C e decresceu com a temperatura extrema de 42 °C. As eficiências fotossintéticas não foram afetadas pela temperatura no intervalo 15-35 °C e decreceram a 42 °C. Estas comunidades de MPB estuarina foram capazes de aumentar a capacidade fotossintética sob exposição a curto prazo de temperaturas elevadas do sedimento, semelhante ao observado durante o verão na baixa-mar diurna.

Foi também investigado o efeito da disponibilidade do carbono inorgânico dissolvido (DIC) na fotossíntese, nas duas comunidades intertidais de MPB (Alcochete e Trancão) e na diatomácia modelo *Phaeodactylum tricornutum*, utilizando a imagiologia de fluorescência (Imaging-PAM) **(capítulo 5).** Os parâmetros da cinética de aquisição de DIC para as comunidades de MPB foram mais elevados do que os obtidos para *Phaeodactylum tricornutum*, mostrando que estas comunidades têm espécies com baixa afinidade para o DIC e elevada capacidade fotossintética. Quando comparamos a taxa fotossintética líquida de suspensões de MPB, verificamos que esta atingiu a saturação a concentrações de DIC de 1-1,5 mM, e que estes valores são inferiores aos encontrados na água intersticial do sedimento (0-5 mm) sugerindo que não há limitação de DIC na fotossíntese para estas comunidades. Contudo, quando adicionamos $NaHCO_3$ a amostras intactas de MPB verificou-se um aumento da capacidade fotossintética (ETR_{max}). Estes resultados sugerem depleção local de DIC, na camada fótica dos sedimentos, onde as microalgas se acumulam durante a baixa-mar diurna. Assim, este estudo fornece a primeira evidência experimental da limitação de DIC nas comunidades intertidais de MPB.

Por último, o efeito interativo destes dois parâmetros ambientais (temperatura e CO_2) na biomassa de MPB, composição taxonómica e performance fotossintética foi estudo usando um sistema de suporte de vida com regime de maré **(capítulo 6).** As temperaturas mais elevadas (24°C) tiveram um efeito negativo na biomassa de MPB e no desempenho fotossintético sob ambas as condições de CO_2 simuladas (correspondentes a pH=7,4 e pH= 8,0). Por outro lado, sob temperaturas elevadas houve uma mudança na abundância relativa das principais espécies de diatomáceas bem como um aumento de cianobactérias. O efeito do aumento de CO_2 (pH=7,4) sob temperatura baixa (18°C) teve um efeito positivo sobre a biomassa de MPB, possivelmente devido à diminuição da depleção local do carbono inorgânico dissolvido. Contudo, nenhum efeito significativo deste parâmetro foi verificado relativamente aos principais grupos de microalgas e espécies de diatomáceas. Os efeitos interativos do aumento de temperatura e CO_2 ao nível das comunidades de MPB estuarino podem ter um impacto negativo na estrutura, diversidade e produtividade destas comunidades e eventualmente nos servicos naturais que estes ecossistemas nos prestam. São cruciais novos estudos sobre o efeito das alterações climáticas nestes complexos ecossistemas.

Palavras-chave: Microfitobentos, alterações climáticas, fluorometria de pulso modulado, ritmos migratórios, fotossíntese, diatomáceas.

Chapter 1

Introduction

Estuarine intertidal flats and microphytobenthos

Estuaries are at the interface of terrestrial and marine environments and are amongst the most productive ecosystems in the biosphere (Constanza et al., 1997). The functioning of an estuary is dependent on a wide range of factors that include geomorphology, tidal and freshwater flushing time, tidal range, nature and extent of intertidal areas and climatic conditions. The intertidal flats of estuarine systems (mud and sand flats) are highly dynamic, characterized by rapid changes in environmental variables. Daily fluctuations in light, salinity, temperature, water content, oxygen, and other environmental parameters are induced by day/night and tidal cycles (Huggets et al., 1986; Serôdio and Catarino, 1999).

The most important estuarine primary producers are the benthic microalgae and cyanobacteria that colonise intertidal and shallow subtidal areas, generally designated microphytobenthos (MPB). The taxonomic composition of MPB is the result of a complex interaction of factors, the most important being light, salinity, nutrients, grazing and sediment type (Oppenheim, 1988; Pinckney and Sandulli, 1990; Delgado et al., 1991; Underwood, 1994; Defew et al., 2004; Van der Grinten et al., 2004; Jesus et al., 2005; Van der Grinten et al., 2005). These communities form transient biofilms during the period of low tide on the surface of the sediments and are mostly dominated by diatoms (phylum Bacillariophyta) and cyanobacteria (the prokaryotic phylum Cyanophyta). Diatoms are important marine photoautotrophic organisms that account for up to 25% of the primary production on Earth, fixing more than 10 billion tons of inorganic carbon each year (Falkowski and Raven, 1997). MPB provide critical functions to the estuarine ecosystem, contributing up to 50% of estuarine primary production (Pomeroy, 1959; Sullivan and Moncreiff, 1988; Pinckney and Zingmark, 1993; MacIntyre et al., 1996; Barranguet et al., 1998; Meyercordt and Meyer-Reil, 1999; Underwood and Kromkamp, 1999; Serôdio and Catarino, 2000) while stabilizing sediments (Paterson, 1989; Yallop et al., 1994; Sutherland et al., 1998; Paterson and Black, 1999) and providing an important resource for grazers (Fréchette and Bourget, 1985; Middelburg et al., 2000). Benthic microalgae and cyanobacteria of estuarine habitats have developed different behavioural and physiological adaptations that optimize their primary production. One adaptation to these harsh conditions is vertical migration within the sediment (Consalvey et al., 2004). Frequently, benthic diatoms exhibit a periodic vertical migration whereby cells migrate up onto the sediment surface

during diurnal low tide and migrate down into the sediment in anticipation of flood (Serôdio et al., 2008). Upward migration during diurnal low tide periods allows cells to reach the photic zone and absorb light to drive photosynthesis. Downward migration has been associated with the avoidance of resuspension into the water column (e.g., Kingston, 1999), grazing (e.g., Buffan-Dubau and Carman, 2000) and high light exposure (Kromkamp et al., 1998; Perkins et al., 2001, 2002; Serôdio et al., 2005; Cartaxana et al., 2011).

Benthic diatoms are subjected to a highly variable and extreme light regime caused by rapid changes in water cover and by the direct exposure to sunlight for prolonged periods during diurnal low tides. Exposure to solar light after long periods of darkness may take place when diatoms buried in aphotic layers of the sediment are resuspended and brought to the surface. In order to cope with these harsh conditions, MPB developed efficient mechanisms of photoacclimation and photoprotection. An increasing amount of recent literature has shown that motile benthic microalgae may use their migratory ability to actively search for optimal light levels for photosynthesis, thus maximizing light absorption while avoiding exposure to photoinhibiting light levels – behavioural photoprotection (Kromkamp et al., 1998; Perkins et al., 2001; Serôdio et al., 2006; Cartaxana et al., 2011). Another adaptation to high light stress is the activation of physiological photoprotective mechanisms that include photorespiration, cyclic electron transport and photo-reduction of molecular oxygen by PSI (see review by Niyogi, 1999). However, the most important physiological photoprotective mechanism in diatoms is the xanthophyll cycle which allows the thermal dissipation of excess energy in the antennae of photosystem II (PSII), involving the de-epoxidation of diadinoxanthin (Dtx) to diatoxanthin (Ddx) (Young et al., 1997). Non-photochemical quenching (NPQ) induced by the xanthophyll cycle has been shown to be 3 to 5 times larger in diatoms than in higher plants (Ruban et al., 2004).

MPB photosynthesis: temperature and carbon availability

Photosynthesis is the biological conversion of light energy to chemical bond energy stored in the form of organic carbon compounds. Approximately 40% of the annual photosynthesis on Earth occurs in aquatic environments (Falkowski, 1994). All photosynthetic organisms, whether they are prokaryotes, eukaryotic algae, or higher plants, use membranes to organize

photosynthetic electron processes and separate these processes from carbon fixation (Bryant, 1994; Drews, 1985; Redlinger and Grant, 1983). Photosynthetic electron transport takes place in the thylakoid membrane located within specialized organelles called chloroplasts. In diatoms the plastid ultrastructure and the organization of the photosynthetic apparatus differ from that in higher plants. The thylakoid membranes are grouped by bands of three all along the plastid and they are not very tightly associated since they are spaced by 2 nm (Pyszniac and Gibbs, 1992). The process of photosynthesis can be separated into two parts, the photochemical reactions and the carbon reduction reactions. The photochemical reactions begin with the absorption of light by the antenna complex. The light-harvesting pigments-proteins complexes are a diverse group of proteins that bind pigments absorbed excitation energy to the photosynthetic reaction center. The light-harvesting pigments include chlorophylls *a* (Chl *a*) and *c*, xanthophylls, and β-carotene. These pigments transfer the absorption of light energy to the reaction centers, where the energy is used in the photosynthetic electron transport chain. The main components of the photosynthetic electron transport chain are: the PSII, the cytochrome b_6f complex, the photosystem I (PSI) and the ATP- synthase complex. The photosynthetic electron transport chain based on the apparent redox potentials of the two reaction centers (called Z-scheme) can be divided into three segments: (a) the donor side of PSII, which includes the reactions responsible for the injection of electrons into PSII from water, (b) the intersystem electron transport chain, which includes all the carriers between PSII and PSI, and (c) the acceptor side of PSI, in which the primary reducing agent, NADPH, is formed and exported for the carbon fixation. The transport of four electrons via the thylakoid membrane causes the transport of protons across the membrane, leading to formation of a pH gradient. The gradient provides the driving force for the ATPase to synthesize ATP (adenosine triphosphate) from ADP (adenosine diphosphate) and phosphate. In the case of the linear electron transport, ferredoxin gives its charge to the enzyme ferredoxin-NADP-oxidoreductase. This facilitates the synthesis of NADPH from NADP. The fundamental products of photosynthesis (ATP, NADPH) are then available for a number of secondary pathways, including carbon reduction, nitrate reduction, sulphate reduction, and ATP production (Falkowski and Raven, 1997; Behrenfeld et al., 2004). These photosynthetic products couple the light reactions to carbon fixation and to cell growth. Approximately 95%

of NADPH and more than 60% of ATP are used to assimilate and reduce inorganic carbon (Falkowski and Raven, 1997).

The uptake of inorganic carbon into a cell is the first step in the photosynthetic assimilation of carbon. All oxygenic photoautotrophs incorporate CO_2 into organic matter by adding four electrons and four protons to the carbon atom to forming carbohydrate. The primary metabolic pathway responsible from carbon reduction is the Calvin-Benson cycle, alternatively called the C_3 pathway. This pathway for inorganic carbon fixation invariably involves the enzyme Ribulose-1,5-Bisphosphate Carboxylase/Oxigenase (Rubisco). Rubisco can only use CO_2 as substrate. Hence, inorganic carbon uptake must ultimately lead to the formation of CO_2 in the chloroplast stroma (Falkowski and Raven, 1997).

CO_2 is found in the atmosphere as a gas but in aquatic systems (aqueous solution) the dissolved CO_2 reacts with water (equation 1). The equilibrium reactions are shifted toward the right at high pH and toward the left at low pH.

$$CO_2\ (aq) + H_2O \Leftrightarrow H_2CO_3 \Leftrightarrow H^+ + HCO_3^- \Leftrightarrow 2H^+ + CO_3^{2-} \quad \text{(equation 1)}$$

The inorganic carbon system is one of the most important chemical equilibrium in aquatic systems and is largely responsible for controlling the pH of seawater. Dissolved inorganic carbon (DIC) exists in seawater in three major forms: bicarbonate ion (HCO_3^-), carbonate ion (CO_3^{2-}), and aqueous carbon dioxide (CO_2 (aq)), which here also includes carbonic acid (H_2CO_3). At a pH of 8.2, 88% of the carbon is in the form of HCO_3^-, 11% in the form of CO_3^{2-}, and only 0.5% of the carbon is in the form of dissolved CO_2. When CO_2 dissolves in seawater, H_2CO_3 is formed. Most of the H_2CO_3 quickly dissociates into a hydrogen ion (H^+) and HCO_3^-. A hydrogen ion can then react with a CO_3^{2-}, to form bicarbonate. Therefore, the net effect of adding CO_2 to seawater is to increase the concentrations of H_2CO_3, HCO_3^-, and H^+, and decrease the concentration of CO_3^{2-} and lower pH. These reactions are fully reversible and their basic thermodynamics in seawater are well known (Millero et al., 2002). CO_2 usually accounting for less than 1% of the total inorganic carbon and thereby, the expected CO_2 concentration of seawater is approximately 10 µmol L^{-1} (at atmospheric equilibrium at 25°C) (Badger et al. 1998). The photosynthesis of marine diatoms could be limited by inorganic carbon availability (Badger et al., 1998), but is generally not limited due to the operation of carbon concentrating

mechanisms (CCMs) (e.g. Giordano et al., 2005; Roberts et al., 2007) that maintain efficient photosynthetic rates. Recent results indicate a central role of the C_4 pathway in the photosynthesis of diatoms acclimated to low CO_2 concentrations (Reinfelder and Morel, 2004), operating as CCMs. The key enzyme in C_4 metabolism is phosphoenolpyruvate carboxylase (PEPC) and has higher temperature optima and C affinity then Rubisco (Kelly and Latzko, 2006). The former enzyme is one of the most catalytically active enzymes and is especially important in the ocean, where free CO_2 concentrations are so low but the concentration of HCO_3^- is large. The PEPC function supplying the CO_2 to a CO_2-specific enzyme such as a carboxylase, facilitate the diffusive transport of inorganic carbon into the cells. The activity of PEPC is often found in the plasmalemma, and can facilitate the CO_2 diffusion by accelerating the formation of CO_2 near the cell surface.

A few studies on diatoms as part of highly productive MPB biofilms suggest limitation of photosynthesis by inorganic carbon availability (Admiraal, 1982; Cook and Roy, 2006). Admiraal et al. (1982) found that the diffusion of inorganic carbon limited the productivity of dense unialgal mats of the diatom *Navicula salinarum*. Cook and Roy (2006) found an increase on photosynthetic rates of MPB natural communities in subtidal sandy sediments after the addition of HCO_3^-.

Temperature can have a major influence on rates of MPB photosynthesis (Blanchard et al., 1996; Guarini et al., 1997). Temperature influences algae photosynthesis by changing the photosynthetic rate or by inducing phenotypic or genotypic changes among algae species (Davison, 1991). Intertidal sediment temperature fluctuations occur on long (seasonal) and short (daily and hourly) time scales, depending on factors such as meteorological conditions, time of day and tidal inundation. In summer, intertidal sediment temperature can easily change 10-15°C during an emersion period, reaching values higher than 35°C at midday (Blanchard et al., 1997; Serôdio and Catarino, 1999). Increased temperature generally results in higher metabolic activity and thus increased growth rates. Short-term (hours) temperature changes, similar to those experienced by intertidal MPB communities during a tidal cycle, have been shown to have a significant effect on the photosynthesis of cultured benthic diatoms (Admiraal, 1984; Morris and Kromkamp, 2003; Salleh and McMinn, 2011) and suspensions of intertidal MPB (Blanchard et al., 1996, 1997). Extreme temperatures limit electron transport

and carbon fixation. Much less is known on the effect of temperature changes on MPB at longer time-scales or on undisturbed natural MPB communities.

MPB and climate change

Rising global temperatures and increasing atmospheric CO_2 concentrations, expected to occur due to global warming, are causing changes to a wide range of ecosystems, including estuarine systems (De Jonge and De Jong, 2002). Little is known about the combined impacts of temperature and future CO_2 increases on the productivity and physiology of MPB communities. To our knowledge, Hicks et al. (2011) is the only study addressing the combined effect of these two parameters. Using a nontidal experimental mesocosm in a 7-day experiment, these authors report a negative effect of combined elevated atmospheric CO_2 concentrations and temperature on MPB biomass.

Chlorophyll *a* fluorescence

Photosynthetic activity of intertidal benthic microalgae is increasingly assessed using Chl *a* fluorescence techniques, particularly pulse amplitude modulated (PAM) fluorescence techniques. PAM fluorescence was originally introduced by Schreiber et al. (1986) for the study of terrestrial phototrophs, but since its introduction it has been applied to numerous aquatic organisms (Beer & Björk, 2000; Schlensog and Schroeter, 2001; Villareal and Morton, 2002; Carr and Bjork, 2003; Gevaert et al., 2003; Kromkamp and Forster, 2003). PAM fluorometry is a powerful and non-intrusive technique for probing photosynthesis based on Chl *a* fluorescence quenching analysis. The measurements assume that the Chl fluorescence is proportional to the inherent photosynthetic properties of the phototroph. This non-invasive technique is generally used to estimate the effective quantum yield of PS II ($\Delta F/F_m'$) (Genty et al., 1989). This parameter reflects the short-term variability of photosynthetic activity and can be used to assess the linear electron transport rate (ETR) through PS II. This technique has been used successfully to assess photosynthetic activity of the MPB communities on intact sediment cores or isolated microalgae (Kromkamp et al., 1998; Barranguet and Kromkamp, 2000; Perkins et al., 2001, 2002; Serôdio et al., 2005). Additionally, the fluorescence signal

has be used to estimate biomass (Honeywill et al. 2002; Serôdio et al. 2001) and follow cell vertical migration (Kromkamp et al., 1998; Serôdio et al., 1997).

Objectives

The main objectives of this thesis were:

- To improve the application of chlorophyll fluorescence tools to study photosynthesis of intertidal MPB communities.
- To evaluate the effects of short-term changes in temperature and available inorganic carbon on the photosynthetic metabolism of intertidal MPB communities of the Tagus estuary.
- To assess the interactive effects of elevated temperature and CO_2, expected to occur due to climate change, on the structure and productivity of intertidal MPB.

Chapter 2

Effects of intertidal microphytobenthos migration on biomass determination via laser-induced fluorescence

Abstract

Laser-induced fluorescence (LIF) spectra of intertidal microphytobenthos (MPB) communities were obtained in the laboratory with a 532 nm pulsed Nd: YAG laser. The laser-induced chlorophyll (chl) fluorescence emission spectra of MPB in mud and sand sediments were characterized by a band in the red region with a maximum at ca. 685 nm. Biomass accumulation on the surface of the mud due to cell migration caused a shift to longer wavelengths (up to 5 nm) of the red emission maximum and the development and increase of an emission shoulder at the far-red region (maximum at ca. 732 nm), probably owing to increased re-absorption of chl fluorescence within the denser microalgae biofilm. Direct relations were observed between MPB biomass proxies (normalized difference vegetation index [NDVI] and phytobenthos index [PI]) and fluorescence intensity. LIF was used to track migratory rhythms of epipelic benthic microalgae in muddy sediments, which are absent in epipsammic communities in sand: progressive accumulation of biomass occurred at the sediment surface during diurnal low tide periods and was followed by a rapid downward migration before tides began to cover the sampling site. When exposed to high light, surface biomass decreased in migratory biofilms, indicating that diatom cells avoid photoinhibitory light levels. This phenomenon is known as behavioral photoprotection. For the first time, LIF was applied to study intertidal MPB communities to adequately describe surface biomass, which included changes due to migration.

Introduction

Microphytobenthos (MPB) are a generic grouping of microalgae that colonize intertidal and shallow subtidal flats in estuarine and coastal ecosystems. MPB can form dense, micro-algal, diatom-dominated biofilms on the upper layers of intertidal sediments that range from fine silt and mud to sand and have a productivity that can exceed 300 g C m^{-2} yr^{-1} (MacIntyre et al., 1996; Underwood and Kromkamp, 1999). MPB represent an important food source for benthic invertebrates (e.g. Montagna et al., 1995) and have been implicated in protecting sediments from erosion through the production of extracellular polymeric substances (e.g. Underwood and Paterson, 2003). The large spatio-temporal variability of MPB and the difficulty of accessing tidal flats that cover many square kilometers of estuarine and coastal ecosystems make the use of remote sensing techniques particularly useful in assessing MPB distribution.

A unique feature of some of these benthic epipelic (motile, fine sediment-inhabiting) diatom communities is the exhibition of vertical migratory movements within the uppermost layers of the sediment (see review by Consalvey et al., 2004). Typically, motile diatoms move towards the surface of the sediment during diurnal low tide and then back to deeper layers before high tide or night, causing reversible several fold changes in surface biomass (Round and Palmer, 1966; Serôdio et al., 1997). Upward migration benefits microalgae by placing them on the surface during low tide when light is readily available for photosynthesis. However, rapid downward diatom movement has been observed upon exposure to high light levels (Kromkamp et al., 1998; Perkins et al., 2001; Cartaxana and Serôdio, 2008), indicating that benthic diatoms may also use migration to avoid photoinhibitory light levels, a phenomenon known as behavioural photoprotection (Admiraal, 1984; Serôdio et al., 2006). Recently, Perkins et al. (2010) have shown that vertical cell movement is a primary response of epipelic benthic biofilms to increasing light exposure. Epipsammic diatoms, i.e. those attached to particles of sandy sediments, depend exclusively on physiological mechanisms to photoregulate (Jesus et al., 2009).

Laser-induced fluorescence (LIF) has been successfully used in remote sensing of terrestrial plants (e.g. Subhash and Mohanan, 1997; Richards et al., 2003; Anderson et al., 2004), phytoplankton (Barbini et al., 1998) and macroalgae (Kieleck et al., 2001). The chlorophyll (chl) fluorescence spectrum of plant leaves typically includes 2 maxima, one in the red (684 to 695 nm) and one in the far-red (730 to 740 nm) region, which are primarily dependent on the concentration of chl *a* (see review by Buschmann, 2007). Changes in red to far-red fluorescence ratios (F685/F735), as well as shifts in the peak center of chl fluorescence bands, are correlated to changes in chl concentration in plants under stress (Lichtenthaler and Rinderle 1988; McMurtrey et al., 1994; Subhash and Mohanan, 1997; Schuerger et al., 2003).

In the present study, LIF was used as a remote sensing technique to study MPB biomass of muddy and sandy sediments of the Tagus Estuary, Portugal. LIF was used successfully to estimate MPB biomass and, in the case of epipelic diatom communities, to track micro algal migration caused by diurnal and tidal cycles and changes in irradiance levels. To our knowledge this is the first application of LIF in the study of MPB communities.

Materials and methods

Sampling

Sediment samples were collect at Alcochete, Tagus Estuary, Portugal (38° 44' N, 09° 08' W), on several occasions between February and July 2010. This estuary has a large inner bay with extensive intertidal flats covering an area of approximately 100 km^2 (Brotas and Catarino, 1995). The Tagus Estuary is mesotidal with a mean tidal range of 2.4 m, which ranges from about 1 m at neap tides to about 4 m at spring tides. Sampling was carried out during low tide periods at 2 stations with different sediment types: a mud site with 97% of particles <63 µm, and a sand site composed of a mixture of very fine to coarse sand ranging in diameter between 125 and 1000 µm, hereafter called mud and sand, respectively. Sediment samples were collected by means of plexiglass cores (8 cm internal diameter) and taken to the laboratory. All experimental measurements were carried out on the day after sampling. The sediment was left overnight in the laboratory in shallow water (±2 cm) collected from the site and carefully added to avoid re-suspending the sediment.

Effects of diurnal and tidal cycles on MPB surface biomass

Just before the start of the diurnal low tide emersion that was predicted to occur at the original sampled sites, the water was removed from the mud and sand cores in the laboratory. To promote cell migration to the sediment surface, the cores were exposed to low light (70 µmol photons m^{-2} s^{-1}) provided by a halogen lamp (Philips focusline, 250 W) through fiberoptics (model 460-F, Heinz Walz). Light intensity was measured with a quantum sensor (model QMSW-SS, Apogee). The in vivo LIF spectra of these 2 types of sediment were obtained every 30 min with an Nd: YAG laser (model NL303, EKSPLA) along a diurnal tidal cycle. Reflectance spectra were recorded in the same sediment area immediately before LIF measurements were taken. The experiment was repeated during a second diurnal tidal cycle for each sediment type. Additional measurements of reflectance spectra and LIF were recorded in areas covering a wide range of surface microalgal biomass.

Effects of irradiance levels on MPB surface biomass

Just before the start of the diurnal low tide emersion predicted for the original sampled site, the water was removed from the mud cores and the cores were exposed to low light as described in the above sub-section. Sediment in the cores was sampled with plexiglass minicores (2 cm diameter) for the following treatments: addition of filtered water from the sampling site only (control) and addition of latrunculin A dissolved in filtered site water to inhibit diatom motility (Lat A). Three replicates were used for each treatment. Treatments were applied once the biofilm had become established at the sediment surface as assessed by the stabilization of the normalized difference vegetation index (NDVI) (see 'Spectral reflectance').

A concentrated Lat A solution (1 mM) was prepared as a fresh stock on the morning of the experiment by dissolving purified Lat A (Sigma-Aldrich) in DMSO. A solution of 20 µM Lat A was prepared by diluting the stock solution in filtered water collected at the sampling site. Small volumes of this solution (total of 200 µL) were carefully pipetted directly onto the sediment surface of the minicores until a continuous thin layer completely covered the sample. The amount of Lat A needed to sufficiently inhibit diatom migration in benthic biofilms was previously determined (Cartaxana and Serôdio, 2008; Perkins et al., 2010). Filtered site water (200 µl) without the addition of Lat A was added to all control cores to mimic chemical treatments. After 30 to 45 min, LIF spectra were obtained in control and Lat A-treated sediments for sequential light treatments in the following order: low light (LL1): 70 µmol photons m^{-2} s^{-1}; high light (HL): 1200 µmol photons m^{-2} s^{-1}; low light (LL2): 70 µmol photons m^{-2} s^{-1}; and dark (D). LIF spectra were recorded after a period of 30 min in each light level.

Laser-induced fluorescence

In vivo LIF spectra of sediment MPB communities were recorded with an Nd: YAG laser. The laser provided 30 mJ pulses of 4 ns at the wavelength of 532 nm (second harmonic), with a pulse repetition rate of 10 Hz. The distance of the laser to the sediment was ca. 1 m and the diameter of the laser spot hitting the sediment surface was ca. 1.5 cm. To obtain a good fluorescence signal, relatively high laser excitation energy was necessary, which was sufficient to cause reaction center closure (Rosema et al., 1998).

Photosystem II (PSII) operating efficiencies, also known as the Genty factor (Genty et al., 1989), were measured with a pulse-amplitude modulated (PAM) fluorometer (model Diving-PAM, Walz) before and immediately after laser pulses. Mean (±SD) PSII operating efficiencies were 0.746 ± 0.056 and 0.705 ± 0.057 (n = 8), before and after the laser pulse, respectively (5.5 ± 3.9% lower after laser measurements). This showed that the laser pulse had an actinic effect on the samples. This effect was fully reverted before the next laser pulse, 30 min later, indicating that the decrease on the yield was not due to damages to the photosynthetic apparatus.

The fluorescence emission signal was collected by a telescope (model F810SMA, Thorlabs) situated ca. 40 cm from the sample. To protect the light-detecting electronics from very strong elastically scattered radiation of the second laser harmonic, the telescope was equipped with a long-wave pass filter of $\lambda \geq 550$ nm. The collected radiation was transmitted into a spectrometer (model USB4000, Ocean Optics) via an optical fiber. The spectrometer was synchronized with the laser pulse, which enabled the signal to be measured for about 10 µs (minimum exposure permissible by the spectrometer control software) after each laser pulse. To achieve a reliable signal-to-noise ratio, the fluorescence spectra were obtained by collecting and averaging signals from 100 to 1000 laser pulses.

Spectral reflectance

Reflectance spectra were measured over a 350 to 1000 nm bandwidth by means of a USB4000 spectrometer with a VIS-NIR optical configuration connected to a 400 µm diameter fiber optic (model QP400-2-VIS/NIR, Ocean Optics). The light spectrum reflected from the sample was normalized to the spectrum reflected from a clean polystyrene plate. The polystyrene plates differed by <3% from a calibrated 99% reflectance standard plate (SpectralonTM, Forster and Jesus, 2006). A reflectance spectrum measured in the dark was subtracted from both spectra to account for the dark current noise of the spectrometer. The fiber optic was positioned perpendicular to the sediment surface by means of a micromanipulator (model MM33, Diamond General) maintained at a fixed distance from the sample surface and set to match the area measured by LIF. Sample and reference spectra were measured under a constant irradiance of 70 µmol photons m^{-2} s^{-1}. Microalgae biomass present in the surface layers of the sediment was estimated by calculating NDVI (Rouse et al., 1973) and a modified version of the phytobenthos index (PI) (Méléder et al., 2003;

Jesus et al., 2006; Murphy et al., 2008) from reflectance spectra. Biomass indices NDVI and PI were calculated as follows:

$$NDVI = (R750 – R675)/ (R750 + R675)$$

and

$$PI = (R750 – R636)/ (R750 + R636),$$

where R750, R675 and R636 represent the diffusive reflectance (R) at 750, 675 and 636 nm, respectively.

Statistical analysis

Significant differences were determined with 2-way ANOVA for effects of irradiance levels (light treatment) and chemical treatment on MPB surface biomass (fluorescence peak area). Data complied with the assumptions of ANOVA. Multiple comparisons among pairs of means were performed with Tukey's Honestly Significant Difference (HSD) test.

Results

LIF spectra of the 2 different intertidal sediments of the Tagus Estuary showed a chl fluorescence band in the red region, with a peak maximum between 684.7 and 689.9 nm. Typical fluorescence emission spectra for both sediments, with fluorescence maxima at 685.3 and 686.5 nm for mud and sand, respectively, are shown in Figure 1. Emission spectra corresponding to mud sediments had consistently higher fluorescence intensities than those of sand sediments (Figure 1). There was a positive correlation between peak area and the wavelength shift of peak maxima ($p < 0.001$, $r = 0.763$). In other words, for areas of sediment with higher surface microalgal biomass the red emission maxima occurred at longer wavelengths. This is de - picted in Figure 2, in which the sediment sample with less biomass (NDVI = 0.695) exhibits a maximum fluorescenc at 686.3 nm, while samples with higher surface chl concentrations show maxima at 689.6 nm (NDVI = 0.827) and 689.9 nm (NDVI = 0.849). Furthermore, in the latter samples, there was a clear development and increase of an emission shoulder at the far-red region (maximum at ca. 732 nm, Figure 2).

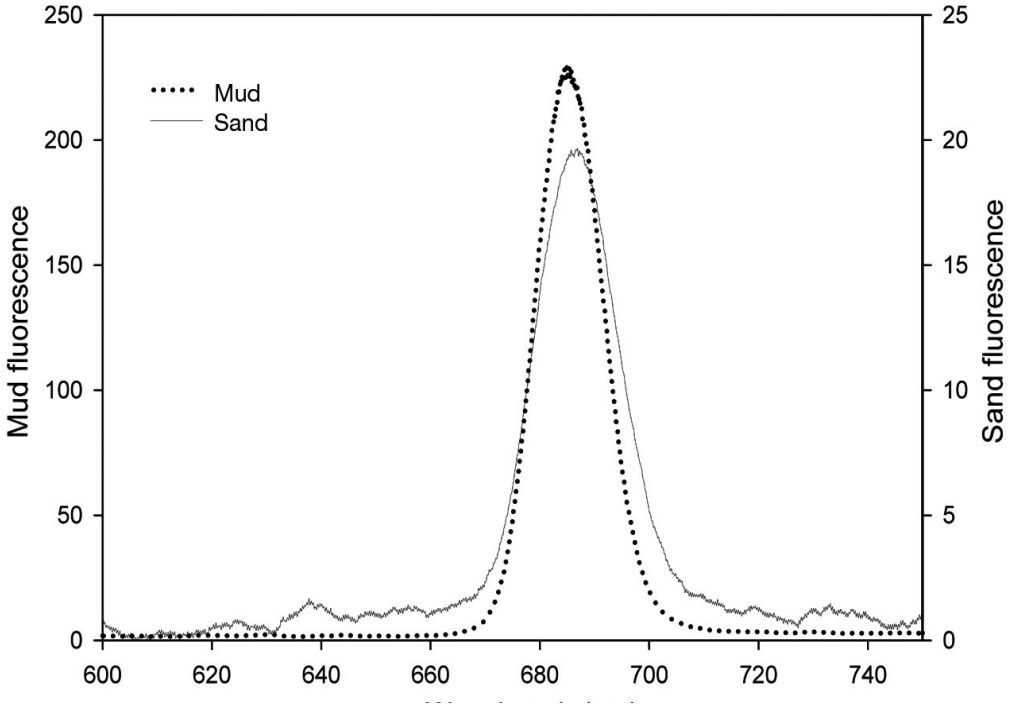

Figure 1. Typical laser-induced fluorescence spectra of microphytobenthos in mud and sand intertidal sediments. Units on the y-axis are arbitrary.

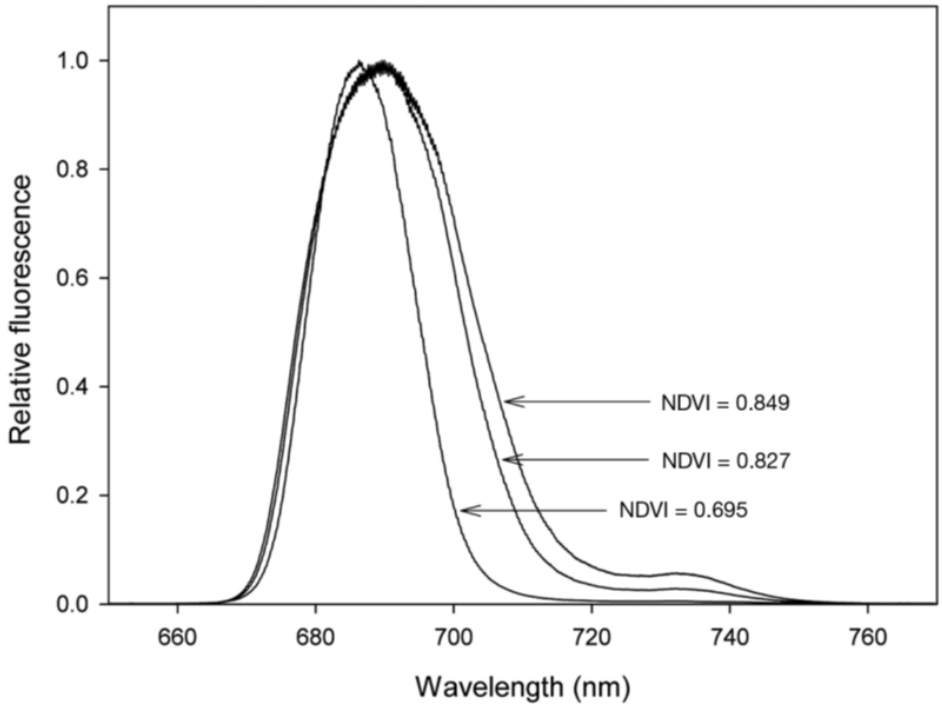

F**igure 2.** Laser-induced relative fluorescence spectra of 3 samples of microphytobenthos with increasing biomass in mud intertidal sediments (two samples with high biomass and one with low biomass). Normalized difference vegetation index (NDVI) is shown for the 3 samples.

Fluorescence intensities, measured by calculating the ln-transformed data of peak area, were found to vary linearly with both biomass indices NDVI and PI (Figure 3). Highly significant correlations were obtained between ln (peak area) and NDVI ($r = 0.968$, $p < 0.001$, Figure 3A) and PI ($r = 0.943$, $p < 0.001$, Figure 3B). Similar results were obtained using intensity calculated by ln-transforming data of peak height instead of peak area in these correlations.

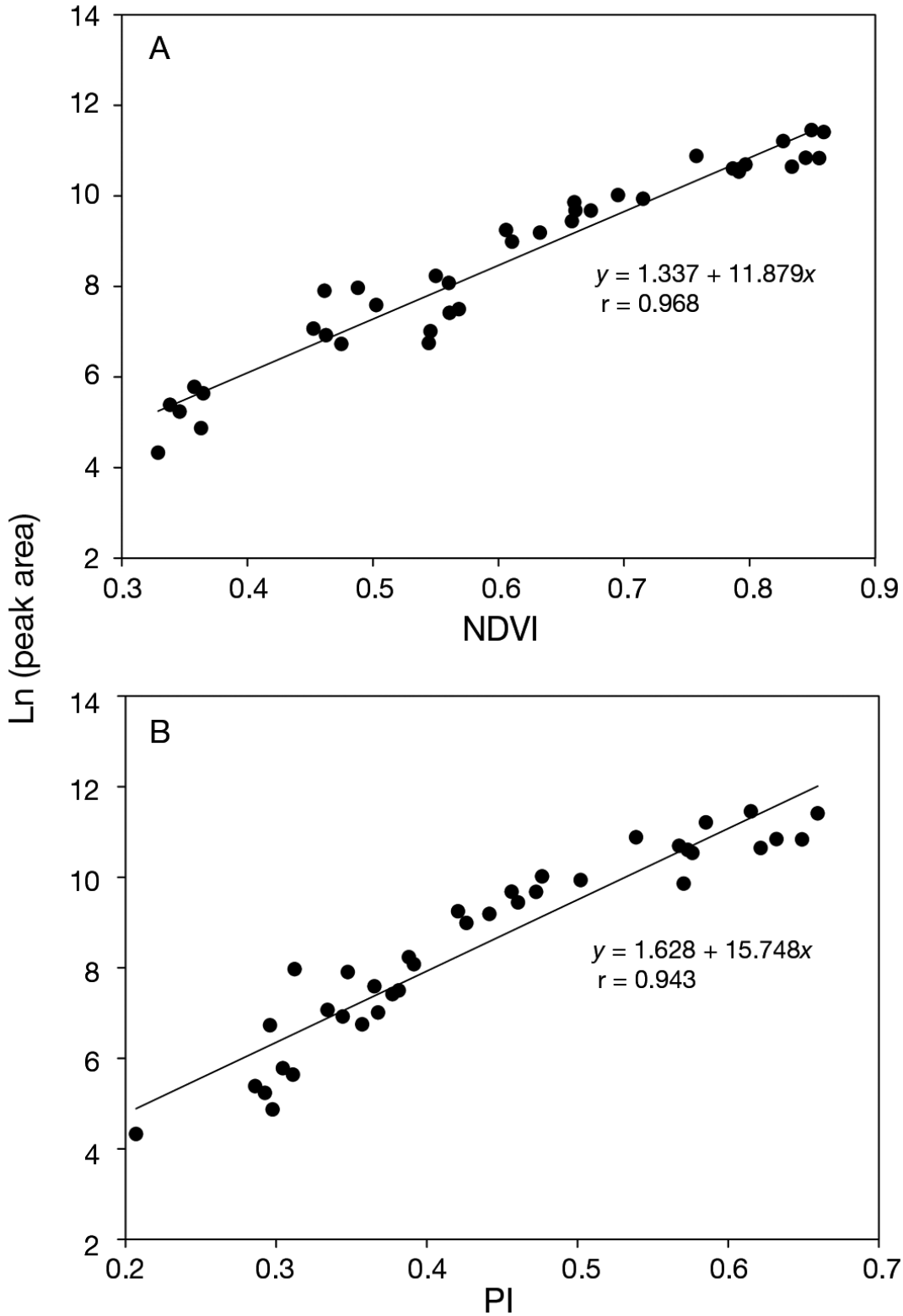

Figure 3. Linear regressions between biomass indices, (A) normalized difference vegetation index (NDVI) and (B) phytobenthos index (PI) and laser-induced fluorescence measured as ln (peak area) of microphytobenthos of intertidal sediments

Fluorescence intensities measured in mud sediments were clearly related to migratory rhythms of epipelic benthic diatoms. A typical increase in relative fluorescence following exposure to low light that coincided with the emersion period is shown in Figure 4. A rapid decrease of fluorescence was observed closer to though clearly before the start of the immersion (high tide) period in the natural environment (Figure 4).

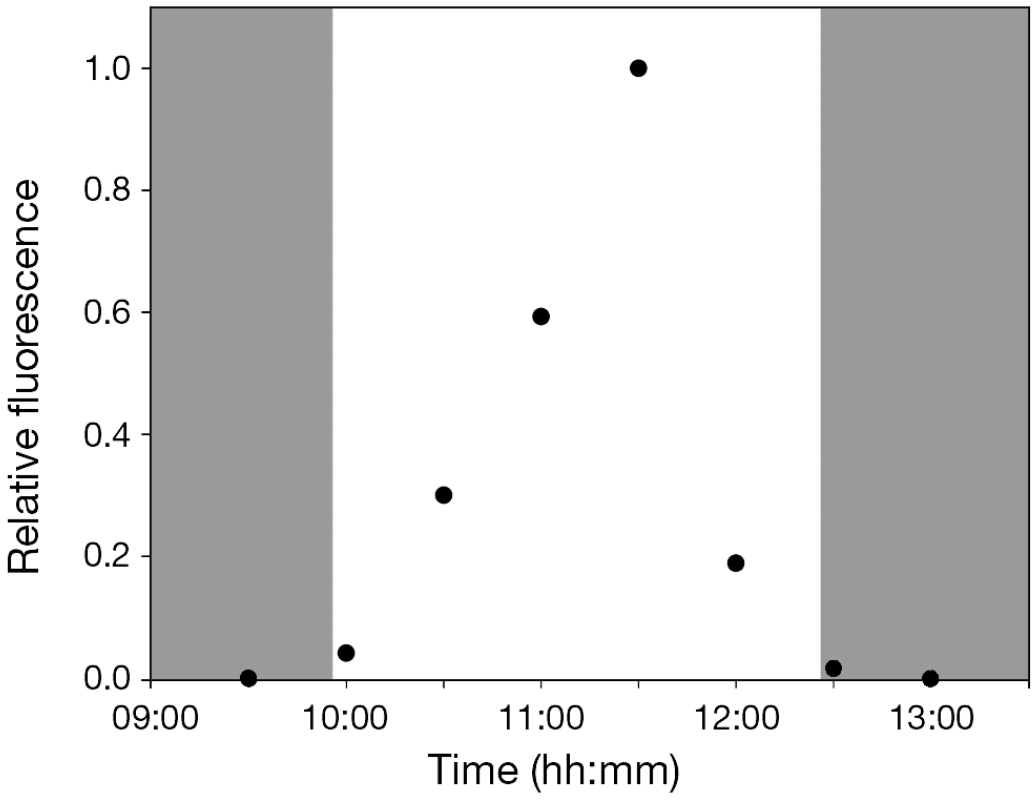

Figure 4. Variation of laser-induced relative fluorescence of microphytobenthos in a mud intertidal sediment along a diurnal tidal cycle. The sample was kept emersed and under constant low light. Gray and white bars represent immersion and emersion periods, respectively, at the field site where the sample was collected.

These fluctuations of fluorescence intensity were not observed in epipsammic communities of sandy sediments. Effects of different irradiance levels on MPB surface biomass of mud sediments were investigated by applying the diatom motility inhibitor Lat A applied to the sediment surface after the biofilm was established during low tide. Fluorescence peak areas (intensity) were compared for a sequence of light treatments for control and Lat A-treated sediment samples (Figure

5). There was a significant effect of light ($F_{3,16}$ = 4.604, $p < 0.05$) and chemical ($F_{1,16}$ = 10.446, $p < 0.01$) treatment on fluorescence intensity. Exposure to high light levels (1200 µmol photons m^{-2} s^{-1}) caused a significant (Tukey's test, $p < 0.05$) decrease of fluorescence peak area in control sediment (Figure 5). Re-exposure of the control sediment to low light led to an increase in fluorescence peak area, which was followed by a decrease when samples were transferred to the dark near the time of arrival of high tide in the natural environment (Figure 5). No significant differences were observed in fluorescence peak area for Lat A-treated sediment samples, as diatom migration was inhibited.

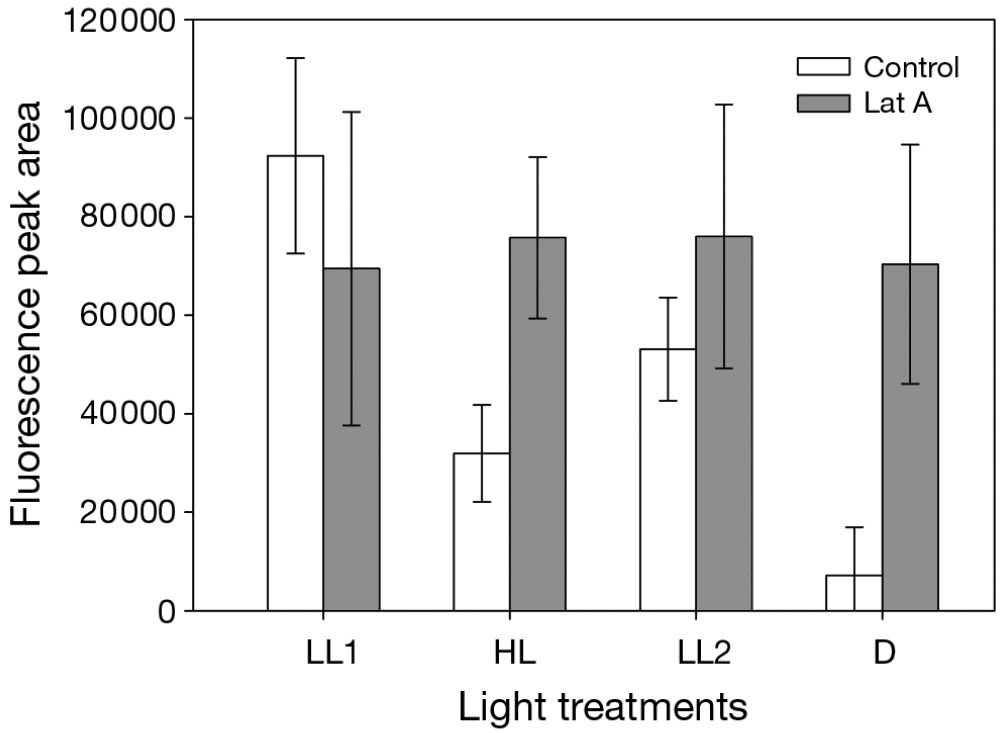

Figure 5. Variation of laser-induced fluorescence measured as peak area (arbitrary units, mean ± SD) for control and Lat Atreated intertidal mud sediments during a sequence of 30 min light treatments: low light (LL1), 70 µmol photons m^{-2} s^{-1}; high light (HL), 1200 µmol photons m^{-2} s^{-1}; low light (LL2), 70 µmol photons m^{-2} s^{-1}; and dark (D)

Discussion

Chl fluorescence emission spectra of MPB measured by means of LIF were characterized by a band in the red region (maximum at ca. 685 nm) and a shoulder at the far-red region (maximum at ca. 732 nm). Similar results were observed for leaves of higher plants, with 2 fluorescence emission bands, one in the red (684 to 695 nm) and one in the far-red (730 to 740 nm) region (see review by Buschmann, 2007). It is generally assumed that most of this fluorescence arises from photosystem II (PSII) (Govindjee, 1995), in which the 684 to 695 nm band arises from the main electronic transitions and the 730 to 740 nm band arises from vibrational sublevels whose relative intensities are increased in vivo through self-absorption (Franck et al., 2002).

Surface microalgal biomass accumulation on mud sediments caused a shift to longer wavelengths of the red emission maximum and the increase of the emission shoulder at the far-red region. Chl fluorescence can be partially reabsorbed within a cell or by other micro phytobenthic cells. Naturally, at higher chl *a* concentrations in sediment, reabsorption of emitted chl fluorescence increases. The increase of reabsorption with increasing chl concentration leads to a shift in the position of the red chl fluorescence maximum of plant leaves towards longer wavelengths as shown by Gitelson et al. (1998). Furthermore, since the red chl fluorescence maximum at around 685 nm is more strongly affected by the reabsorption than the long-wavelength maximum in the far-red region around 735 nm, the chl fluorescence ratio of F685/F735 decreases with increasing leaf chl content (Buschmann, 2007).

The MPB communities studied were composed exclusively of benthic diatoms as confirmed by microscopic examination of resuspended sediment samples and high performance liquid chromatography pigment analysis. Differences in both the excitation and emission spectra related to differences in pigment composition have been used to characterize the taxonomic structure of microalgae in vivo (see review by MacIntyre et al., 2010). If cyanobacteria were present in the MPB, phycobilins would be able to absorb the excitation energy of the laser at 532 nm. In this case, emission peaks around 570 nm and/or 655 nm would be expected depending on the abundance of phycoerythrins and phycocyanins, respectively (MacIntyre et al., 2010).

In the present study, MPB biomass was estimated non-destructively with LIF by establishing a direct relationship between ln-transformed data on fluorescence intensity of MPB communities and the biomass proxies NDVI and PI. NDVI is based on the in vivo chl *a* absorption maximum around 675

nm. It constitutes a long-established index developed in the context of remote sensing of terrestrial vegetation and is currently the most commonly used index to quantify MPB biomass (Jesus et al., 2006; Kromkamp et al., 2006; Serôdio et al., 2006; Cartaxana and Serôdio, 2008). Indices based on the absorption at 675 nm have the advantage of being specific for chl *a*, thus allowing detection and quantification of photosynthetic biomass without the interference of secondary pigments. However, saturation of NDVI for high MPB biomass has been pointed out and attributed to the saturation of light absorption (Méléder et al., 2003). The fact that a linear relationship of NDVI with fluorescence intensity was established with ln-transformed data suggests that the relationship between NDVI and chl *a* would approximate an exponential relationship. The PI is also commonly used to estimate MPB biomass (Méléder et al., 2003; Cartaxana and Serôdio, 2008) and is based on the absorption of the diatom pigment chl *c* and the close relationship of the concentration of this pigment with reflectance at 636 nm (Murphy et al., 2008). Ln-transformed fluorescence intensity data was not fully linear with PI, which is less sensitive than NDVI to saturation at high chl *a* concentrations (Méléder et al., 2003; Barillé et al., 2007).

Complex diatom migratory patterns in epipelic motile biofilms can also be followed in a non-destructive way through chl fluorescence measurements with LIF. Motile diatoms moved towards the surface of the sediment during diurnal low tide and back to deeper layers before high tide causing several-fold changes in surface biomass as previously shown by other authors (e.g. Round and Palmer, 1966; Serôdio et al., 1997). Upward migration during diurnal low tide periods allows cells to reach the photic zone and to absorb light to drive photosynthesis. The reasons for downward migration before high tide or darkness are less clear, but might include the prevention of cells being washed away during immersion or grazing by predators, and facilitating nutrient and carbon uptake or cell division (Admiraal, 1984; Decho, 1990; Saburova and Polikarpov, 2003). Serôdio et al. (1997) have shown that these rhythms are partially endogenous as they were maintained in the absence of external stimuli.

Benthic epipelic diatoms were also found to migrate as a response to irradiance levels. Rapid downward diatom movement was observed upon exposure to 30 min of 1200 µmol photons m^{-2} s^{-1}, followed by upward migration when light levels were reduced to 70 µmol photons m^{-2} s^{-1}. Thus, diatoms exhibit behavioural photoprotection by avoiding photoinhibitory light levels (Admiraal, 1984; Kromkamp et al., 1998; Perkins et al., 2001, 2010; Serôdio et al., 2006). This is in agreement

with the 'microcycling' proposed by Kromkamp et al. (1998) in which a turnover of taxa at the sediment surface results in a reduction in photodose over time and emphasizes the role of vertical movement demonstrated in other experiments that used Lat A as a motility inhibitor (Cartaxana and Serôdio, 2008). Cell migration may well be more energetically avorable than physiological photoprotection processes such as non-photochemical quenching induction (Perkins et al., 2010).

In the last 2 decades, research has increasingly focused on spectral reflectance and PAM fluorescence techniques that employ the optical properties of chl to remotely sense MPB biomass in intertidal flats of estuarine and coastal ecosystems (Serôdio et al., 2001, 2009; Méléder et al., 2003; Jesus et al. 2006; Kromkamp et al., 2006). LIF presents some advantages over these remote sensing techniques for the study of intertidal MPB. Spectral reflectance is a passive method of remote sensing that depends on stable and uniform illumination, making it difficult to take measurements under overcast and partly cloudy conditions. In contrast, LIF instruments use their own illumination source to actively excite fluorescence. Results obtained with hand-held LIF instruments studying beans and wheat have shown that this technique can be used for remote sensing under a diversity of light conditions, including full darkness, at dawn and dusk and under rapidly changing light environments similar to those encountered on partly cloudy days (Richards et al., 2003). The lighting conditions described are generally unsuitable for spectral reflectance remote sensing systems.

PAM fluorometry (Schreiber et al., 1986) was first applied to MPB by Serôdio et al. (1997) and Kromkamp et al. (1998) and led to major advances in the comprehension of the ecophysiology and productivity of MPB communities. However, PAM techniques rely on short saturating pulses delivered at close range, making them impractical for most remote sensing applications. LIF techniques overcome this limitation and have been successfully used in the remote sensing of terrestrial plants (e.g. Subhash and Mohanan, 1997; Richards et al., 2003; Anderson et al., 2004), phytoplankton (Barbini et al. 1998) and macroalgae (Kieleck et al. 2001). More recently, a laser-induced fluorescence transient (LIFT) fluorometer, which uses a fast repetition rate technique (Kolber and Falkowski, 1993), has been developed to operate with relatively low excitation power with subsaturating flashes for measurement of fluorescence parameters from a distance of up to 50 m (Kolber et al., 2005; Pieruschka et al., 2010). The results shown in our study, together with the

discussed advantages over spectral reflectance and PAM fluorometry, make LIF a promising technique for the remote sensing of intertidal MPB communities.

Chapter 3

Photosynthesis assessment in microphytobenthos using conventional and imaging pulse amplitude modulation fluorometry

Abstract

Imaging pulse amplitude modulated (Imaging-PAM) fluorometry is a breakthrough in the study of spatial heterogeneity of photosynthetic assemblages. However, Imaging and conventional PAM uses a different technology, making comparisons between these techniques doubtful. Thereby, photosynthetic processes were comparatively assessed using conventional (Junior PAM and PAM 101) and Imaging-PAM on intertidal microphytobenthos (MPB; mud and sand) and on cork oak leaves. Lower values of α (initial slope of the *r*ETR, relative photosynthetic electron transport rate) *vs.* E (incident photosynthetic active radiation) curve), ETR_{max} (maximum relative ETR), E_k (light saturation parameter) and F_v/F_m (maximum quantum efficiency of photosystem II of dark-adapted samples) were obtained using the Imaging-PAM. The level of discrepancy between conventional and Imaging-PAM systems was dependent on the type of sample, being more pronounced for MPB muddy sediments. This may be explained by differences in the depth integration of the fluorescence signal related to the thickness of the photosynthetic layer and in the light attenuation coefficients of downwelling irradiance. An additional relevant parameter is the taxonomic composition of the MPB, as cyanobacteria present in sandy sediments rendered different results with red and blue excitation light fluorometers. These findings emphasize the caution needed when interpreting chlorophyll fluorescence data of MPB communities.

Introduction

Pulse amplitude modulated (PAM) fluorometry was introduced by Schreiber (Schreiber, 1986) as a methodology for the study of in vivo photosynthesis in plants. In the last few decades, the measuremen of chlorophyll (Chl) fluorescence has become an universal technique in the study of virtually all types of photosynthetic organisms,including corals (Ralph et al., 2005), seagrasses (Ralph et al., 1998), macroalgae (Beer et al., 2000) and microphytobenthos (MPB; e.g. Serôdio et al., 1997; Kromkamp et al., 1998; Jesus et al., 2005). In contrast with other techniques where inadequate replication, long incubation times and substantial alteration of the environmental conditions are common drawbacks, PAM fluorometry allows minimal intrusive, rapid and reproducible measurements of photosynthetic parameters with intact MPB biofilms (Underwood and Kromkamp, 1999).

On the basis of the calculation of the fluorescence index $\Delta F/ F_m'$ (where ΔF is the difference between the maximal fluorescence (F_m') and the steady-state fluorescence (F) of light-adapted samples), which measures the effective quantum yield of photosystem II (PSII; Genty et al., 1989), PAM fluorometry allows the construction of rapid light curves (RLC) relating the rate of photosynthetic electron transport rate (ETR) and incident photon irradiance (E; e.g. Serôdio et al., 2005; Perkins et al., 2006). However, in intact MPB biofilms the determination of $\Delta F/F_m'$ can be strongly affected by the vertical attenuation of downwelling measuring, actinic and saturating light, and of upwelling fluorescence (Forster and Kromkamp, 2004; Serôdio, 2004). In fact, the signal detected by the fluorometer is generated by cells at different depths in the photic zone and therefore subjected to different actinic irradiances, which in turn result in different quantum yields. Hence, the quantum yield calculated from depth-integrated measurements may vary with factors not related to microalgal physiology, such as the optical characteristics of the sediment or the vertical distribution of the microalgal biomass (reviewed in Perkins et al., 2010).

The development of Chl fluorescence imaging systems by a number of research groups (e.g. Omasa et al., 1987; Oxborough and Baker, 1997; Nedbal et al., 2000), together with the emergence of commercially available models by PSI (Brno, Czech Repuplic), Walz Systems (Effeltrich, Germany), and Technologica Ltd. (Colchester, UK), has greatly increased the versatility of Chl*a* fluorometry as a noninvasive technique (reviewed in Oxborough, 2004). Systems that image at the microscopic level allow to measure PSII photochemical efficiencies from chloroplasts within intact leaves and from individual algal cells within mixed populations (Oxborough and Baker, 1997; Meng et al, 2001; Nebdal et al., 2000). On the other hand, lower resolution imaging systems allow the mapping of fluorescence parameters over large areas, making it a unique technique to study the spatial heterogeneity of the photosynthetic activity across an autotrophic surface (Scholes and Rolfe, 1996; Hill et al., 2004). This can be particularly relevant in the study of MPB biofilms, characterized by a "patchy," heterogeneous distribution.

Currently, only three studies have dealt with the application of imaging fluorescence to MPB, all using the microscope fluorescence technique developed by Oxborough and Baker (1997) for measurements at cellular and subcellular levels. Oxborough et al. (Oxborough et al., 2000) used this technique to determine PSII photochemical efficiency of different taxa within MPB biofilms. Perkins et al. (2002) studied the effects of PSI Chl fluorescence and cell vertical migration on the estimation

of ETR and Underwood et al. (2005) reported diel patterns of $\Delta F/F_m'$ in several benthic species over an emersion period. To our knowledge, lower resolution Chl fluorescence imaging systems were never applied to MPB, albeit they might provide useful insights into the spatial distribution of biomass and productivity in sediments.

Recently, Nielsen and Nielsen (2008) found that ETR measured using conventional and Imaging-PAM fluorometry in thin- and thick-blade marine macroalgae and its relation to gross O_2 evolution was dependent of the type of PAM used. Reportedly, conventional PAM fluorometers detect fluorescence emission from the entire tissue, although Imaging-PAM may only acquire fluorescence data from the outermost cell layers of thick algae. These two techniques use different technologies, namely in the detection processes of the fluorescence signal: a photodiode or phototube in conventional PAM fluorometry and a CCD (charged coupled device) camera in Imaging-PAM fluorometry. Our study addresses for the first time the quantitative analysis of the effects associated with the use of conventional (Junior PAM and a PAM 101) and Imaging-PAM fluorometry (Imaging-PAM) on the determination of fluorescence parameters in intact MPB samples. Two sediment types with substantially different light attenuation characteristics and species composition were compared, together with cork oak leaves, to evaluate the effects of depth-integrated measurements in both techniques. Finally, spatial and temporal variability in MPB biomass was followed during a diurnal low tide period for the two intertidal sediments (mud and sand) using the Imaging-PAM system.

Material and methods

Sampling

Sediment samples were collected at Alcochete intertidal flats, Tagus estuary, Portugal (38°44'N, 09°08'W). Sampling was carried out during low tide at two stations with different sediment types: a muddy site with 97% particles <63 µm, and a sandy site composed of a mixture of very fine to coarse sand, between 125 and 1000 µm (here after called mud and sand, respectively). Sediment samples were collected using Plexiglas corers (8 cm internal diameter) and taken to the laboratory. All experimental measurements with MPB were carried out on the day following sampling. The sediment was left overnight in the laboratory at room temperature (ca. 25°C) with a shallow depth of site water (ca. 2 cm), carefully added so as not to resuspend the sediment. Experiments were also

carried out with detached cork oak (*Quercus suber* L.) leaves. The leaves were collected at the gardens of the Faculty of Science of the University of Lisbon, immediately before the fluorescence measurements.

Fluorescence analysis

Just before the start of the diurnal low tide emersion that was predicted to occur at the original sampled sites, the water was removed from the sediment samples and 15 minicores (2 cm diameter) were sub-sampled for each sediment type. Epipelic MPB show circadian and tidal migratory rhythms that are partially endogenous and maintained ex-situ (Serôdio et al., 1997; Vieira et al., 2011). Therefore, experiments were done in the laboratory in synchronization with diurnal low tides in the field to maximize migration of these communities to the sediment surface. Five minicores were used with each PAM fluorometer (Junior PAM, PAM 101 and Imaging-PAM). Sediment samples were exposed to low light (60 µmol photons m^{-2} s^{-1}) provided by a halogen lamp (Philips focusline, 250 W, Philips, Eindhoven, the Netherlands) through fiberoptics 460-F (Heinz Walz GmbH, Effeltrich, Germany), to promote cell migration to the sediment surface. After 1 h, rapid light curves (RLC) were carried out using the three different fluorometers in the five subsamples of each sediment type and immediately after curve completion samples were dark-adapted for 2 min to determine the maximum efficiency of dark-adapted PSII (F_v/F_m). RLC were constructed by calculating, for each level of actinic light, the relative ETR from the delivered actinic irradiance and the effective quantum yield of PSII by *r*ETR = E x $\Delta F/F_m'$. The light response was characterized by fitting the model of Platt et al. (1980) to *r*ETR *vs.* E curves and by estimating the parameters α (initial slope of the light curve), ETR_{max} (maximum *r*ETR) and E_k (light saturation parameter). The model was fitted iteratively using MS Excel Solver. Curve fit was very good ($r > 0.95$) in all cases. The efficiency of dark-adapted PSII was calculated by $F_v/F_m = (F_m-F_o)/F_m$, where F_m and F_o are, respectively, the maximum and the minimum fluorescence of dark-adapted samples. The dark adaptation period was restricted to 2 min to reduce the possibility of inducing downward vertical migration in the epipelic MPB biofilm (Serôdio et al., 2007, 2008). Simultaneously, the same procedure was repeated with five cork oak leaves using both the conventional (Junior PAM and PAM 101) and imaging (Imaging-PAM) systems.

Conventional PAM fluorometry

Fluorescence measurements were carried out using a Junior PAM (Portable Junior PAM; Gademann Instruments GmbH, Germany) and PAM 101 fluorometer (Walz). The PAM 101 uses a light-emitting diode of 650 nm (LED type: USBR; Stanley) providing the measuring pulse at a frequency of 1.6 kHz automatically increased to 100 kHz for F_m and F_m' determination. The fluorometer was connected to a PAM Data Acquisition System PDA 100 (Walz) controlled by the software WINCONTROL v2.08 (Heinz Walz GmbH, Effeltrich, Germany). The actinic light was provided by an external halogen source (Philips focusline, 250 W) through fiberoptics Lighting Unit FL-460 (Walz). The Junior PAM applied a modulated blue light (LED-lamp peaking at 470 nm, half-bandwidth of 31 nm) as source for measuring, actinic and saturating light, emitted at a frequency of 25 Hz when measuring the minimum fluorescence level (F_o) or 1.2 kHz when measuring other fluorescence parameters. The saturation pulse intensity was 6000 µmol photons m^{-2} s^{-1} for 0.8 s for both conventional PAM. For the construction of RLC the samples were exposed to nine incremental intensities of actinic light with an irradiance step duration of 30 s. The PAR (photosynthetically active radiation) steps used in Junior PAM RLC were: 0, 70, 115, 170, 270, 425, 650, 1000 and 1500 µmol photons m^{-2} s^{-1}. For the PAM 101 the light step intensities were: 0, 80, 110, 190,292, 383, 550, 1055 and 1600 µmol photons m^{-2} s^{-1}. For both conventional PAM the distance between the fluorometer fiber optic and the surface of sample was kept constant at 2 mm during all measurements.

Imaging-PAM fluorometry

Fluorescence measurements were carried out using the Mini Version of Imaging-PAM M-Series (Walz). The Mini version uses an IMAGE-K5 1/2" CCD camera (640 x 480 pixel resolution) with a 16 mm objective (Allied Vision Technologies GmbH, Stadtroda, Germany). The instrument is designed for measurements at a fixed working distance. The 24 x 32 mm area imaged by the Mini version is illuminated by a powerful Luxeon LED array (460 nm) of 12 high-power LED organized in four groups equipped with short-pass filters. This LED array provided the measuring beam, the actinic light and the saturation light pulses. The saturation pulse intensity was 6000 µmol photons m^{-2} s^{-1} for 0.8 s and the measuring pulse frequency was 8 Hz. For the construction of RLC the samples were exposed to 10 incremental intensities of actinic light: 0, 81, 111, 145, 223, 320, 491, 624, 996 and 1580 µmol photons m^{-2} s^{-1}, and each irradiance step was 30 s. Numerical values and images of the Chl

fluorescence parameters were extracted from the digital images using analytical software (Imaging Win; Walz). For each individual, replicate values were obtained with one "area of interest" (AOI) selected with the Imaging-PAM software (Heinz Walz GmbH). This was performed for each of the five replicates of the three samples (sand, mud and cork oak leaf). The AOI in the Imaging-PAM were selected taking into account the areas measured by the fiberoptics of the conventional PAM. To determine the spatial heterogeneity of MPB biomass, fluorescence measurements were made using the Imaging-PAM in both sediment types (2 cm diameter minicores) during a diurnal low tide period (5 h). Sediment samples were exposed to low light (60 µmol photons m^{-2} s^{-1}) for the entire low tide period and dark adapted for 2 min every 60 min along 5 h to determine F_o.

MPB taxonomic composition

After the fluorescence measurements, samples from each sediment type were collected by scraping the sediment surface with a scalpel (upper ca. 2 mm). Approximately 3 mL of sediment were collected and placed in disposable 5 mL polypropylene tubes, to which was added 1 mL of a 2.5% glutaraldehyde solution and stored at 4 °C for later processing.

Cells were extracted from the sediment following an isopycnic separation technique using silica sol Ludox® HS-40 (Ribeiro et al., 2010) that separates the organic material from mineral particles and is, thus, able to remove both migratory and non-migratory fractions of the diatom assemblages, as well as cyanobacteria, euglenids and other microphytobenthic algal groups. Total MPB cell counts were made directly from these extracts in anOlympus BX50 optical microscope (Olympus Corporation, Tokyo, Japan) at a 400× magnification. A total of 50 random fields (700–2000 individual cells) were counted in muddy and sandy extracts and separated into major microalgal taxonomical groups.

Diatom analysis was conducted after cleaning the cells of organic material, by incinerating the extracts in a muffle oven during 2 h at 450 °C, leaving the diatom frustules intact. Permanent slides, mounted in Naphrax™ (Northern Biological Supplies Ltd., Ipswich, UK), were made for each sample. Phase and differential interference contrast optical microscopy were used to identify and count diatoms at a magnification of 1000×. For each sample, a minimum of 370 frustules were counted and identified to the species level, following Ribeiro (2010) and references therein.

Statistical analysis

The existence of significant differences was tested using two-way analysis of variance (ANOVA) for the effects of PAM flurometer (Junior PAM, PAM 101 and Imaging-PAM) and sample type (mud, sand and plant leaves) on RLC parameters (α, ETR_{max} and E_k), and on maximum efficiency of PS II of dark-adapted samples (F_v/F_m). Assumptions for normality and equal variance were satisfied. Multiple comparisons among pairs of means were performed using Tukey HSD. All statistical analyses were carried out using STATISTICA 10 (StatSoft Inc., Tulsa, OK).

Results

Figure 1 shows fluorescence RLC measured in the three study sample types (cork oak leaves, mud and sand) using the different PAM fluorometers (Junior PAM, PAM 101 and Imaging-PAM). It was clear that the Imaging-PAM always yielded lower *r*ETR values, especially at higher irradiances. The RLCs obtained with the two conventional PAM and with the Imaging-PAM using the cork oak leaves were more similar when compared with the RLC measured in MPB biofilms. In the latter samples, Imaging-PAM yielded lower *r*ETR values for both sub-saturating and saturating irradiances. The differences were more pronounced in the mud. Fluorescence measurements in the sandy samples with the Junior PAM and the Imaging-PAM yielded lower *r*ETR for higher irradiances compared with the PAM 101 (Figure 1).

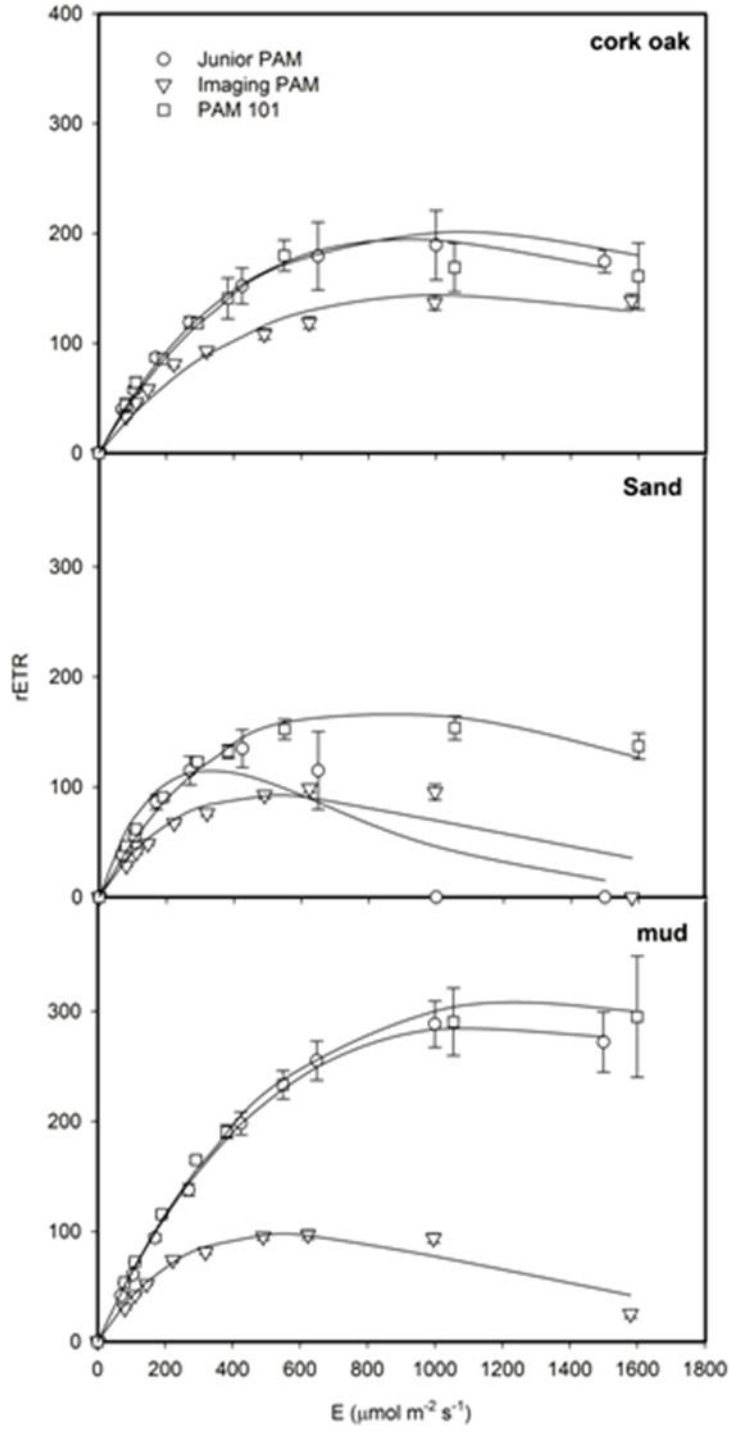

Figure 1. Relative photosynthetic electron transport rate (*r*ETR) *vs.* incident photon irradiance (E; mean ± SD, n = 5) rapid light curves (RLC) for cork oak leaves and MPB from sandy and muddy sediments, obtained with conventional (Junior PAM and PAM 101) and imaging (Imaging-PAM) fluorometers

There were significant (two-way ANOVA) effects of both sample type and PAM fluorometer on all three RLC parameters: α, ETR_{max} and E_k. The RLC parameters measured using the Imaging-PAM were consistently lower when compared with the values obtained using the two conventional PAM (Table 1). For cork oak leaves, ETR_{max} and α values were significantly ($P < 0.05$) lower using Imaging-PAM and no significant differences were found for E_k. In mud, significantly ($P < 0.05$) lower α, ETR_{max} and E_k were obtained using the Imaging-PAM (Table 1), but no significant differences were found between the two conventional PAM. In the sand, significant ($P < 0.05$) differences were found using the three PAM fluorometers in all RLC parameters. For F_v/F_m, consistently higher values were obtained using the two conventional PAM, for leaves, sand and mud. F_v/F_m values were higher for cork oak leaves than those in MPB communities. In the latter communities, F_v/F_m values were higher in the mud than those in the sand. Obtained using the two conventional PAM, for leaves, sand and mud. F_v/F_m values were higher for cork oak leaves than those in MPB communities. In the latter communities, F_v/F_m values were higher in the mud than those in the sand.

Table 1. RLC parameters α, ETR_{max}, E_k and F_v/F_m (mean ± SD, n = 5) measured with the conventional (Junior PAM and PAM 101) and imaging (Imaging-PAM) PAM for cork oak leaves and MPB of sand and mud. Different letters (a–c) indicate significant differences between fluorometers for $P < 0.05$.

	α			ETR_{max}			E_k			F_v/F_m		
	Junior PAM	Imaging-PAM	PAM 101	Junior PAM	Imaging -PAM	PAM 101	Junior PAM	Imaging -PAM	PAM 101	Junior PAM	Imaging-PAM	PAM 101
Cork oak	a 0.581 ± 0.035	b 0.382 ± 0.015	a 0.540 ± 0.019	a 185 ± 19	b 144 ± 7	a 177 ± 20	ns 322 ± 14	ns 377 ± 5	ns 329 ± 37	a 0.797 ± 0.039	b 0.692 ± 0.026	a 0.794 ± 0.016
Sand	a 0.953 ± 0.079	b 0.484 ± 0.039	c 0.620 ± 0.017	a 115 ± 15	b 86 ± 10	c 169 ± 8	a 121 ± 9	b 178 ± 8	c 272 ± 13	a 0.597 ± 0.039	b 0.487 ± 0.032	a 0.627 ± 0.015
Mud	a 0.673 ± 0.036	b 0.555 ± 0.014	a 0.683 ± 0.040	a 289 ± 38	b 103 ± 3	a 320 ± 81	a 429 ± 53	b 187 ± 3	a 476 ± 149	a 0.669 ± 0.033	b 0.579 ± 0.028	c 0.708 ± 0.010

ns, not significant.

Figure 2A depicts images of F_o values along a period corresponding to the diurnal low tide at the field site for the muddy sediment that can be related to biomass changes at the surface due to migratory rhythms of epipelic (motile, fine sediment-inhabiting) MPB. A typical increase in F_o is observed upon exposure to low light coinciding with the expected emersion period at the field site. Heterogeneity of the surface MPB biomass is higher at 10:45, close to the peak of low tide in the field (11:00). A general decrease in F_o and biomass heterogeneity is then observed before the arrival of the water to the sampling site (13:00) (Figure 2A)

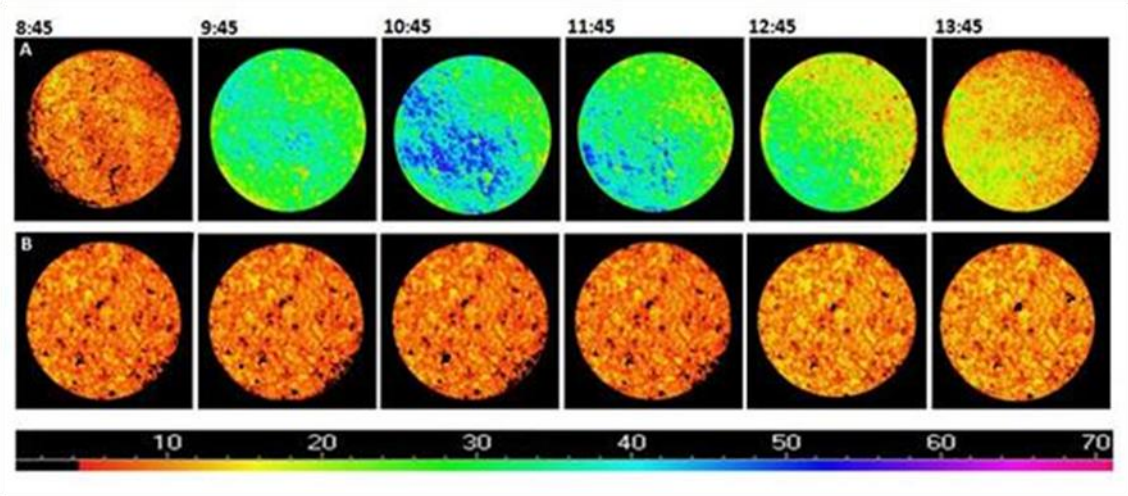

Figure 2. Images of minimum fluorescence of a dark-adapted sample (F_o) during a diurnal low tide for mud (A) and sand (B). False color scale in 20 mm diameter sediment circles.

The described fluctuations of F_o were not observed in epipsammic communities of sandy sediments (Figure 2B). MPB taxonomic composition in the muddy sediment, the MPB was composed exclusively of diatoms, whereas the MPB community in the sandy sediment was comprised by a mixed assemblage of diatoms (54.4%), cyanobacteria (45%), dinoflagellates (0.5%) and euglenids (0.1%). Most of the cyanobacteria cells were part of colonies of *Merismopedia, Oscillatoria and Gloeocapsopsis* species. Diatom assemblages found in the muddy sediment were dominated by motile epipelic species (80.1%), such as *Navicula gregaria* Donkin, *N.* cf. *phyllepta* Kützing or *Gyrosigma fasciola* (Ehrenberg) Griffith & Henfrey. Non-motile tychoplankton (16.2%), e.g. *Thalassiosira* cf. *pseudona*na Hasle and Heimdal & *T. minima* Gaarder, was the second most abundant life-form. In the sandy sediment, the diatom assemblages were mainly composed by epipsammic species (96.6%), in particular adnate forms (64.2%), like *Planothidium delicatulum*s s.1.

l. (Kützing) Round & Bukhtiyarova, *Catenula adhaerens* (Mereschkowsky) Mereschkowsky *a*nd *Cocconeis hauniensis* Witkowski emend. Witkowski. Small motile epipsammic species (e.g. *Cocconeiopsis breviata* (Hustedt) Witkowski, Lange-Bertalot & Metzeltin), and the stalked diatom *Opephora guenter-grassii* (Witkowski & Lange-Bertalot) Sabbe & Vyverman were also found. Large motile epipelic diatoms were absent.

Discussion

As demonstrated here, Imaging-PAM fluorometry is a particularly useful tool in determining spatial heterogeneity of MPB biomass and photophysiology across a sediment surface. However, differences observed between conventional and Imaging-PAM fluorescence and different sediment types makes quantitative comparison between studies difficult. A priori, the main hardware components that may explain the differences obtained with conventional and Imaging-PAM are those related with the detection of the fluorescence signal and the type of measuring light:

(1) Higher intensity of measuring light pulses is required in imaging systems because the CCD cameras used require integration times that may reach several seconds, much longer than the time required by photodiodes or phototubes used in conventional PAM (Oxborough, 2004). Therefore, in the Imaging-PAM a significant actinic effect may have been induced by individual measuring light pulses, as these are relatively intense, causing a significant overestimation of F_o (Oxborough, 2004), leading to a decrease of F_v (= F_m -F_o) and affecting other measured parameters such as F_v/F_m. However, although intense, measuring pulses were applied at very low frequencies, to avoid an actinic effect (Walz, 2006). Furthermore, we tested the measuring light pulses in *Q. suber* leaves and for the selected intensity no actinic effect was found. Thereby, a significant contribution of the measuring light pulses to the lower F_v/F_m measured with the Imaging-PAM might be excluded.

(2) The correct measurement of the effective quantum yield is critically dependent on the accurate measurement of the fluorescence increase caused by the saturation pulse over actinic light (Fm'). Close to light saturation an underestimation of Fm' by a few percent will induce a large underestimation of $\Delta F/F_m'$ and, hence, also of *r*ETR (= $\Delta F/F_m' \times E$). Under high actinic irradiation, ΔF (=F_m' - F) is minimal (because the plastoquinone pool is already strongly reduced) posing technical difficulties to its correct determination with any type of PAM, but mostly when the imaging technology is used. In fact, as the Imaging-PAM uses the same LED for providing the measuring light,

the actinic illumination and the saturating pulses, when a pulse is triggered there is a heating effect on the LED that decreases the measuring light intensity (Walz, 2006). This leads to an underestimation of the fluorescence peak and therefore to a strong underestimation of $\Delta F/F_m'$ and hence of *r*ETR.

(3) Different measuring light wavelengths are used in the devices tested: red in the case of the PAM 101 and blue for the Junior PAM and the Imaging-PAM. The depth range of the red and the blue measuring light may have been considerably different. Kühl and Jorgensen (1994) showed that in abiotic sand sediments light attenuation increased gradually from the infrared to the blue part of the spectrum. In coastal sediments with diatoms, blue light (450–550 nm) was also strongly attenuated in the surface layer, whereas red light (675 nm) showed an absorption peak deeper in the sediment (Kühl and Jorgensen, 1994). Vogelmann and Han (2000) showed that a leaf irradiated with actinic blue light showed a peak of fluorescence 50 µm below the surface, whereas when the actinic light was red, fluorescence peaked 100 µm below the surface. Thus, it is extremely probable that the blue measuring light used in the Junior PAM and Imaging-PAM had a lower penetration in the substrates, measuring fluorescence of a thinner surface layer subjected to higher light intensities.

The differences observed between the conventional and Imaging-PAM systems were clearly dependent on the type of sample studied and were particularly relevant for the mud MPB biofilms. Although the differences between PAM 101 and Imaging-PAM still hold in sandy MPB, in this substrate Junior PAM, albeit showing higher ETR_{max} than the Imaging-PAM, presented no electron transport for E higher than 600 µmol photons m^{-2} s^{-1}. Differences between the three instruments were less evident for cork oak leaves most probably due to the thinner photosynthetic layer (ca. 230 µm), whereas Chl *a* is present in the sediments at a depth of several centimeters. Previous results in thick-leaved macroalgae have shown discrepancies between ETR measured with imaging and conventional PAM (Nielsen and Nielsen, 2008).

Sediments are optically dense, so all types of light involved in the fluorescence measurement are subject to very strong attenuation, leading to complete light extinction within the photosynthetic viable community (Serôdio, 2004). Therefore, values of F and F_m' measured at the sediment surface represent the integration of F and F_m' at different sediment depths. Hence, light curves derived from depth-integrated measurements appear to saturate at higher irradiances, or to be less

photoinhibited when compared to the physiological response of the microalgae (Forster and Kromkamp, 2004; Serôdio, 2004; Perkins et al., 2010; Jesus et al., 2006), due to the recruitment of fluorescence from the deeper cell layers, which are reached by lower PAR and thereby present higher $\Delta F/F_m'$. Serôdio (2004) has shown that the effects of depth integration on RLC parameters are small for α, but extremely relevant for ETR_{max} and E_k. The effects of depth integration in these parameters are more pronounced in sediments where the attenuation coefficients (K_p) are higher (Serôdio, 2004). Accordingly, the K_p values of the studied sediments, and consequently the degree of the effect of depth integration on RLC parameters, were significantly higher for mud (8.6 ± 0.9 mm^{-1}) than that for sand (1.6 ± 0.5 mm^{-1}; Campbell et al., 1998).

In addition to this influence on the depth integration of the fluorescence signal, the wavelength of the measuring light is also relevant in what concerns the type of photosynthetic organisms sampled. In fact, whereas in plants, green algae and diatoms fluorescence emission can be induced by either red or blue light excitation, in cyanobacteria blue light is mostly ineffective in variable fluorescence induction, although some basal (F_o) fluorescence is still observed (Schubert et al., 1989), leading to a significant decrease of the measured quantum yield. Furthermore, cyanobacterial fluorescence signals differ in fundamental ways from the ones of green algae and diatoms, as the principal light-harvesting complexes are phycobilisomes peripheral to the thylakoid membranes, instead of the integral membrane Chl*a*/*b*-binding proteins, which capture light in green algae and diatoms (for a review of Chl fluorescence analysis in cyanobacteria see Campbell et al., 1998). Therefore, the significant presence of cyanobacteria in the sandy sediments (accounting for 45% of the MPB assemblage), in contrast with their total absence in muddy sediments, may explain the differences observed between these two substrates, namely the very low ETR measured with the blue light excitation fluorometers (JuniorPAM and Imaging-PAM) in the epipsammic communities.

Conclusions

Previous studies have shown that estimates of $\Delta F/F_m'$ and *r*ETR in MBP biofilms are influenced by the optical properties of the sediments (e.g. Forster and kromkamp, 2004; Serôdio, 2004), hence not directly comparable. In our study, we have shown that *r*ETR computed from fluorescence measurements of conventional and Imaging-PAM are not directly comparable, even for sediments

with similar optical characteristics. This is related to differences in conventional and Imaging-PAM, such as the type and intensity of measuring light pulses.

In addition, the heating effect caused by saturating pulses on the LED may have lead to a strong underestimation of $\Delta F/F_m'$ in the imaging system used. The manufacturer not only provides a method to correct the underestimated measurements (F_m factor) but also recommends that actinic light higher than 700 µmol photons m^{-2} s^{-1} should not be used in *r*ETR *vs.* E curves, as the accuracy of the results cannot be granted. In fact, the instrument manual does not show any light curves with actinic light intensities higher than 500 µmol photons m^{-2} s^{-1} (Walz, 2006). This, of course, is a strong drawback of this Imaging-PAM that users must keep in mind.

Furthermore, the species composition of MPB biofilms may interact differently with different fluorometers. In particular, the presence of cyanobacteria requires different approaches to the interpretation of the fluorescence signal (Campbell et al., 1998) and may render different results with red and blue excitation light fluorometers.

Accurate determination of fluorescence parameters requires the application of super-saturating pulses of light that are typically several hundred milliseconds in length at a photon irradiance of several thousand µmol photons m^{-2} s^{-1}. When imaging large areas, this requirement for high photon irradiances presents a significant technical challenge (Oxborough, 2004). Users of this type of Imaging-PAM should keep this in mind and previously determine and reject areas where light is heterogeneous.

The level of discrepancy between conventional and Imaging-PAM systems was particularly relevant for MPB communities. These findings highlight the caution needed when interpreting Chl fluorescence data of MPB.

Chapter 4

Effects of short-term changes in sediment temperature on the photosynthesis of two intertidal microphytobenthos communities

Abstract

Intertidal microphytobenthos (MPB) has been found to maintain high productivity rates despite the variability in various key environmental parameters, namely rapid temperature changes during emersion. The effects of short-term (30 min and 2 h) changes in temperature (15, 25, 35 and 42°C) on the photosynthetic activity of two intertidal MPB communities (Trancão and Alcochete) of the Tagus estuary were studied using imaging pulse amplitude modulated (Imaging-PAM) fluorometry. MPB communities differed in species composition and size-class distribution: Trancão was dominated by diatoms of the size-class 100-250 μm^3, particularly *Navicula* cf. *phyllepta*, whereas Alcochete had higher relative abundances for size-class 250-1000 μm^3, dominated by a mixture of diatom species of the genera *Navicula, Thalassiosira* and *Gyrosigma*. The Trancão MPB community had higher photosynthetic capacity (higher ETR_{max}), was photoacclimated to higher irradiances (higher E_k) and had lower efficiency at limiting irradiances (lower α). The different taxonomic composition and size-class distribution could explain the observed results, as small cells are usually more active due to larger surface to volume ratios. Photosynthetic capacities of the two studied MPB communities increased with temperature until 35°C. Photosynthetic efficiencies were not affected by temperature in the 15-35°C range and both ETR_{max} and α decreased at the extreme temperature of 42°C. MPB communities were able to increase photosynthetic capacity and productivity under transient exposure to high sediment temperatures, similar to that observed during summer midday low tides.

Introduction

The intertidal flats of estuaries are characterized by the presence of microphytobenthos (MPB) communities dominated by diatoms, forming highly dense biofilms on the sediment surface. Intertidal MPB communities are responsible for a significant fraction of the total primary productivity of estuaries (Underwood and Kromkamp, 1999), despite the extreme variability in various key environmental parameters (e.g. irradiance, salinity or temperature).

Intertidal sediment temperature fluctuations occur on long (seasonal) and short (daily and hourly) time scales, depending on factors such as meteorological conditions, time of day and tidal inundation. In summer, intertidal sediment temperature can easily change 10-15 °C during an

emersion period, reaching values as high as 35 °C at midday (Blanchard et al., 1997; Serôdio and Catarino, 1999). Short-term (hours) temperature changes, similar to those experienced by intertidal MPB communities during a tidal cycle, have been shown to have a significant effect on the photosynthesis of cultured benthic diatoms (Admiraal, 1984; Morris and Kromkamp, 2003; Salleh and McMinn, 2011) and suspensions of intertidal MPB (Blanchard et al., 1996, 1997). In these studies, the described relationship between maximum photosynthetic capacity (P_{max}) and temperature is a progressive increase of P_{max} with increasing temperature up to an optimum value, beyond which P_{max} declines rapidly (Blanchard et al., 1996). Although both approaches (cultures and suspensions) may provide valuable information regarding the potential photosynthetic responses of benthic diatoms to short-term changes in temperature, the results thus obtained may not accurately represent the photosynthesis of these organisms while part of an MPB biofilm.

The aim of this study was to characterize the effects of short-term temperature changes on the photosynthetic activity of two intertidal MPB communities of the Tagus estuary. Most studies on MPB ignore species composition and treat the assemblages as a black box (Underwood, 2005). In this study, we present a detailed description of the diatom taxonomic composition of the two studied MPB communities. A chlorophyll (Chl) *a* fluorescence imaging system was used to determine photosynthetic parameters, allowing the simultaneous analysis of several sediment samples. We hypothesize that community-level photosynthetic rates and productivity of intertidal MPB biofilms increase with transient high temperatures, similar to those observed during summer midday exposure.

Material and methods

Sampling and sample preparation

Sediment samples were collected in two different intertidal flats of the Tagus estuary (Portugal) at Alcochete (38° 44´45´´N, 08° 59´04´´W) and Trancão (38° 47´46´´N, 09° 05´33´´W). Both sediments are fine mud with more than 97% particles <63 µm. Alcochete site is exposed for up to 3 h during low spring tides, being subtidal during neap tides. Trancão is a steep intertidal flat, exposed for periods of up to 6 h during low tide in both spring and neap tides. Sampling was carried out in June 2011 at spring tides when the intertidal flats were exposed. The surface layer of sediment (approximately the 0-1 cm) was collected using a spatula.

In the laboratory, the sediment was mixed and then evenly spread in trays to a depth of about 2 cm. The sediment was left overnight in the dark with a shallow depth of site water to mimic the tidal rhythm and avoid dessication. The following morning, at the start of the low tide emersion period predicted for the original sample site, the shallow layer of site water was removed. Portions of the surface layer of the sediment were transferred to 6-well plates using a small spatula, making sure the sediment reached the surface of the wells as the Imaging PAM is designed for measurements at a fixed working distance. The well plates were exposed to a homogeneous light field provided by a halogen lamp (Philips focusline, 250W) through fiberoptics 460-F (Walz GmbH, Effeltrich, Germany), delivering a constant irradiance of 60 µmol photons m^{-2} s^{-1} at the sample surface. Low light levels induced cell migration to the sediment surface and the formation of a biofilm. After 60 min of biofilm establishment, a total of eight 6-well plates were used: two sampling sites (Trancão and Alcochete) four temperatures (15, 25, 35 and 42 °C). Temperature treatments were set using temperature-controlled water baths and sediment temperatures followed using a ScanTemp 410 infrared thermometer (Tematec GmbH, Hennef, Germany). Photosynthetic activity was assessed using non-invasive fluorescence analysis after 30 min and 2 h at each temperature.

Fluorescence analysis

Chlorophyll fluorescence was measured using an imaging-PAM fluorometer (Mini PAM M-Series, Walz GmbH) with an IMAGE-K5 1/2'' CCD camera (640 × 480 pixel resolution) equipped with a 16 mm objective. The 24 x 32 mm area imaged by the Mini version is illuminated by a powerful Luxeon LED array (460 nm) covering a 6-well plate, so that 6 sediment samples could be monitored simultaneously. The LED array provided the measuring beam, the actinic light and the saturation light pulses. The saturation pulse intensity was 8000 µmol photons m^{-2} s^{-1} for 0.8 s and the measuring pulse frequency was 10^3 kHz. Photosynthetic activity was assessed using rapid light curves (RLC). For the construction of RLC, the samples were exposed to 12 intensities of actinic light: 0, 3, 23, 43, 61, 111, 223, 320, 491, 624, 782 and 996 µmol photons m^{-2} s^{-1}. The duration of each irradiance step was 30 s. Numerical values and images of the chlorophyll fluorescence parameters were extracted from the digital images using analytical software (Imaging Win, Walz), selecting a priori areas of interest (AOI) that corresponded to the total sediment surface of each well. RLC were constructed by calculating, for each level of actinic light, the relative electron transport rate (*r*ETR)

from the delivered actinic irradiance (E) and the effective quantum yield of PSII ($\Delta F / F_{m'}$) by *r*ETR= E x $\Delta F / F_{m'}$. The light response was characterized by fitting the model of Platt et al. (1980) to *r*ETR vs E curves and by estimating the initial slope of the light curve α (light utilization coefficient), ETR_{max} (maximum *r*ETR) and E_k (light saturation parameter), where $E_k = ETR_{max}/\alpha$.

MPB taxonomic composition

Sediment trays of both sampling sites were also subjected to low light levels (60 µmol photons m^{-2} s^{-1}) to induce cell migration to the sediment surface and the formation of a biofilm. Sediment samples were collected directly from the trays after 60 min of biofilm establishment by scraping the sediment surface with a scalpel (upper 2 mm). Approximately 3 mL of sediment per sample were collected and placed in disposable 5 mL polypropylene tubes, to which was added 1mL of a 2.5% glutaraldehyde solution and stored at 4 °C for later processing. Cells were extracted from the sediment following an isopycnic separation technique using silica sol Ludox® HS-40 (Ribeiro, 2010) that separates the organic material from mineral particles and is, thus, able to remove both migratory and non-migratory fractions of the diatom assemblages, as well as cyanobacteria, euglenids and other microphytobenthic algal groups. However, optical microscope analysis of these extracts with an Olympus BX50 at a 400× magnification revealed that exclusively diatoms composed the MPB communities. Diatom analysis was conducted after cleaning the cells of organic material, by incinerating the extracts in a muffle oven during 2 h at 450 °C, leaving the diatom frustules intact. Permanent slides, mounted in Naphrax, were made for each sample. Phase and differential interference contrast optical microscopy were used to identify and count diatoms at a magnification of 1,000×. For each sample, a minimum of 400 frustules were counted and identified to the species level, following Ribeiro (2010) and references therein. Diatom taxa relative abundances were also allocated to four size-classes which comprised the average cell biovolumes of <100 μm^3, 100-250 μm^3, 250-1000 μm^3 and >1000 μm^3. Cell biovolume calculation was based on equations proposed by Hillebrand et al. (1999) and derived from biometric measurements.

Statistical analysis

The data set was separated in two groups corresponding to the 30 min and 2 h measurements. The existence of significant differences was tested using two-way analysis of variance (ANOVA) for the

effects of the independent variables temperature (15, 25, 35 and 42 °C) and sampling site (Alcochete and Trancão) on fluorescence RLC parameters (α, ETR_{max} and E_k). Data normality and homogeneity of variances were tested with Shapiro-Wilk and Bartlett tests, respectively. Data were transformed whenever necessary to comply with ANOVA assumptions. Multiple comparisons among pairs of means were performed using Tukey HSD. Statistical analyses were carried out using Statistica 10 (StatSoft Inc., USA).

Results

MPB taxonomic composition

A total of 42 diatom species were identified in the intertidal MPB communities of the two study sites of the Tagus estuary, in Alcochete and in Trancão, occurring in both sites (Table 1). Differences were found in the major species present in each community. Diatom assemblages found in the muddy sediment from Alcochete were dominated by *Navicula gregaria* Donkin (24.3%), *Navicula* cf. *phyllepta* Kützing (17. 3%), *Thalassiosira* cf. *pseudonana* Hasle & Heimdal (12.1%) and *Gyrosigma fasciola* (Ehrenberg) Griffith & Henfrey (10.2%). The muddy sediment samples from Trancão were dominated mainly by *Navicula* cf. *phyllepta* Kützing (60.5%). Nevertheless, other species were also relatively abundant, namely *Thalassiosira* cf. *pseudonana* Hasle & Heimdal (13.9%), *Navicula spartinetensis* Sullivan & Reimer (5.4%) and *Staurophora salina* (W. Smith) Mereschkowsky (3.0%) (Table 1).

Both assemblages were composed of ca. 80% of motile epipelic diatoms and 16-18% of tychoplanktonic species (e.g. *T.* cf. *pseudonana*) in Alcochete and Trancão, respectively. Truly epipsammic and planktonic species had only residual contributions. The differences in relative abundances of the motile epipelic species were responsible for distinct size-class distributions (Figure 1). Trancão was clearly dominated by diatoms of the size-class 100-250 μm^3, while Alcochete showed a more even distribution of small, medium and large-size diatoms, but with higher relative abundances of the size class 250-1000 μm^3.

Table 1. Species composition, size class (µm^3) and relative abundance (%) of two microphytobenthos communities of the Tagus estuary (Alcochete and Trancão).

Taxa	Relative abundance (%)		Size-class (µm^3)
	Alcochete	Trancão	
Actinocyclus normanii (Gregory) Hustedt	0.3		>1000
Amphora cf. *pediculus* (Kützing) Grunow	0.3		<100
Aulacoseira subartica (O. Müller) Haworth	1.3		100–250
Biremis ambigua (Cleve) Mann	0.5		>1000
Climaconeis fasciculata (Grunow ex Cleve) Cox	1.3		>1000
Cyclotella cf. *ambigua* Grunow in Cleve & Grunow	0.5	1.7	<100
Cyclotella atomus Hustedt	0.3		<100
Cylindrotheca closterium (Ehrenberg) Reimann & Lewin		1.3	100–250
Cylindrotheca cf. *gracilis* (Brébisson in Kützing) Grunow	4.3	2.1	250–1000
Entomoneis paludosa var. *paludosa* (W. Smith) Reimer		0.2	>1000
Fallacia cf. *teneroides* (*Hustedt*) *Mann*		0.4	100–250
Fragilaria cf. *sopotensis* Witkowski & Lange-Bertalot	0.3		<100
Frustulia interposita (Lewis) De Toni	0.8		>1000
Gyrosigma acuminatum (Kützing) Rabenhorst	1.1		>1000
Gyrosigma fasciola (Ehrenberg) Griffith & Henfrey	10.2	0.6	>1000
Gyrosigma cf. *limosum* Sterrenburg & Underwood	1.9	0.6	>1000
Gyrosigma wansbeckii (Donkin) Cleve	0.3	0.2	>1000
Navicula gregaria Donkin	24.3	1.5	250–1000
Navicula cf. *mollis* (W. Smith) Cleve	1.1		>1000
Navicula pargemina Underwood & Yallop		0.2	<100
Navicula cf. *phyllepta* Kützing	17.3	60.5	100–250
Navicula spartinetensis Sullivan & Reimer	8.1	5.4	250–1000
Nitzschia cf. *aequorea* Hustedt	7.3	2.4	100–250
Nitzschia cf. *aurariae* Cholnoky	0.8		<100
Nitzschia cf. *distans* Gregory	0.3		>1000
Nitzschia frustulum (Kützing) Grunow		0.2	<100
Nitzschia cf. *parvula* W. Smith non Lewis		0.4	100–250
Nitzschia sigma (Kützing) W. Smith	0.5		>1000
Nitzschia sp.1	0.3		100–250
Nitzschia sp.2		0.4	100–250
Nitzschia sp.3		1.7	100–250
Nitzschia sp.4		0.4	<100
Plagiogrammopsis minima (Salah) Sabbe & Witkowski	0.8		<100
Planothidium sp.1	0.3		<100
Staurophora salina (W. Smith) Mereschkowsky		3.0	>1000
Surirella atomus Hustedt	0.5		250–1000
Thalassiocyclus lucens (Hustedt) Håkansson & Mahood		1.3	100–250
Thalassiosira minima Gaarder	3.0	0.2	100–250
Thalassiosira proschkinae Makarova		0.6	<100
Thalassiosira cf. *pseudonana* Hasle & Heimdal	12.1	13.9	<100

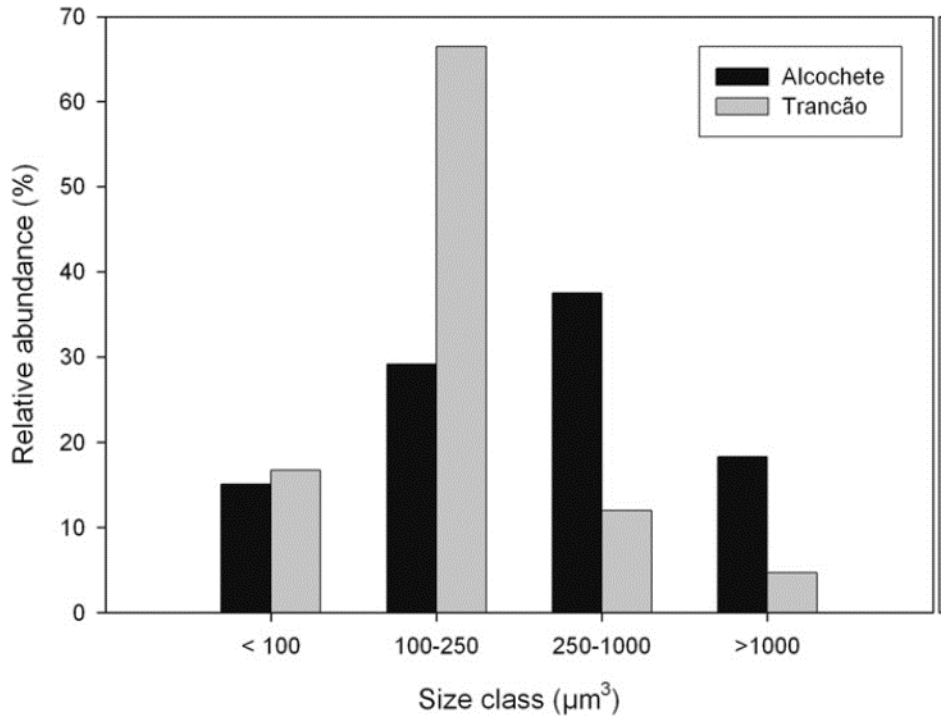

Figure 1. Size-class distribution of relative abundance of microphytobenthos from two sites of Tagus estuary (Alcochete and Trancão).

Influence of temperature on photosynthetic parameters

Relative photosynthetic electron transport rate (*r*ETR) versus incident photon irradiance (E) rapid light curves (RLC) of MPB from Alcochete and Trancão are shown in Figure 2 and 3, respectively. There is a clear effect of short-term temperature treatments (15, 25, 35 and 42°C) on RLC curves in both Alcochete and Trancão with higher *r*ETR found at 35°C. *r*ETR found in Trancão at 15, 25 and 35°C were higher than those obtained in Alcochete for the 30 min treatment (Figure 2A and 3A).

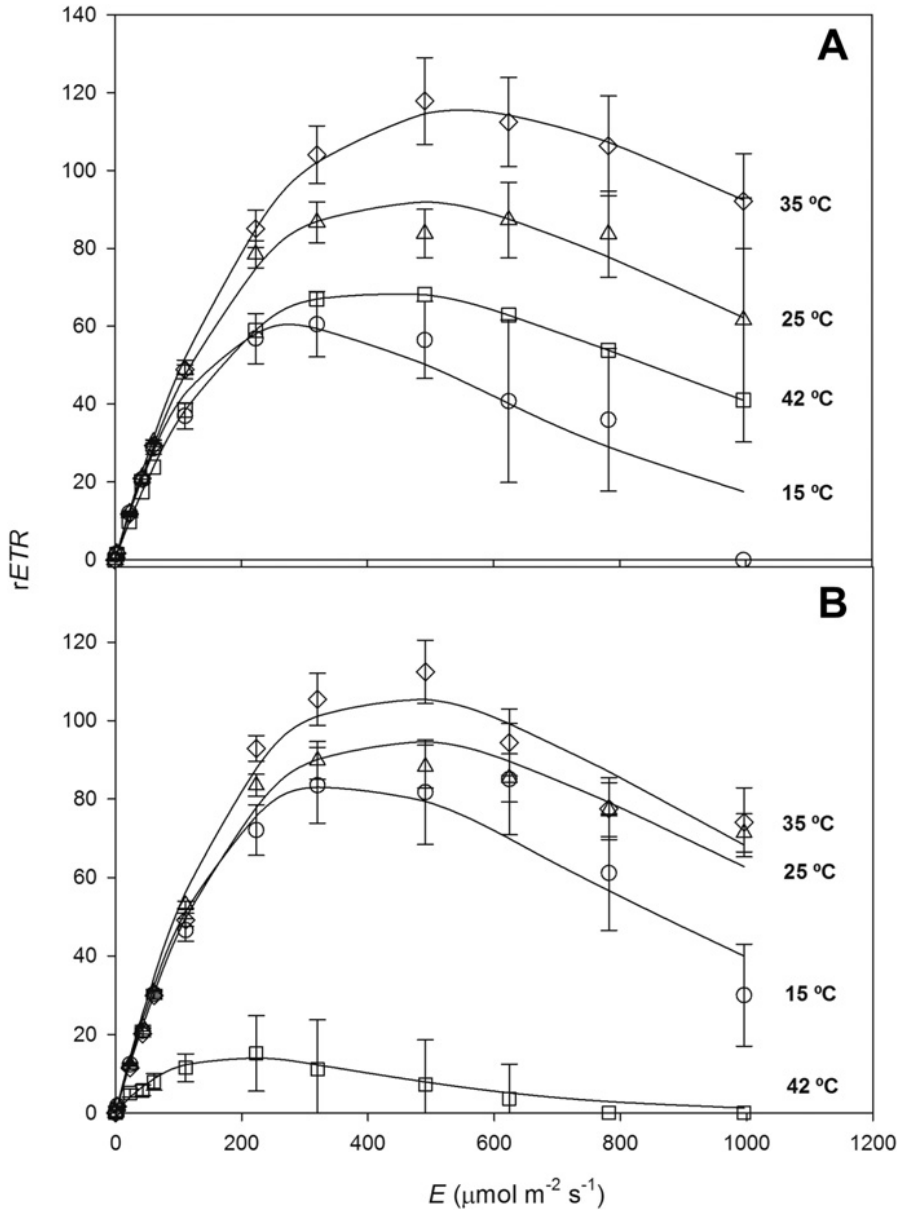

Figure 2. Relative photosynthetic electron transport rate (*r*ETR) versus incident photon irradiance (E) (mean ± standard deviation, n=6) rapid light curves (RLC) of microphytobenthos from Alcochete (Tagus estuary) after 30 min (A) and 2 h (B) at the four temperature treatments (15, 25, 35 and 42 °C).

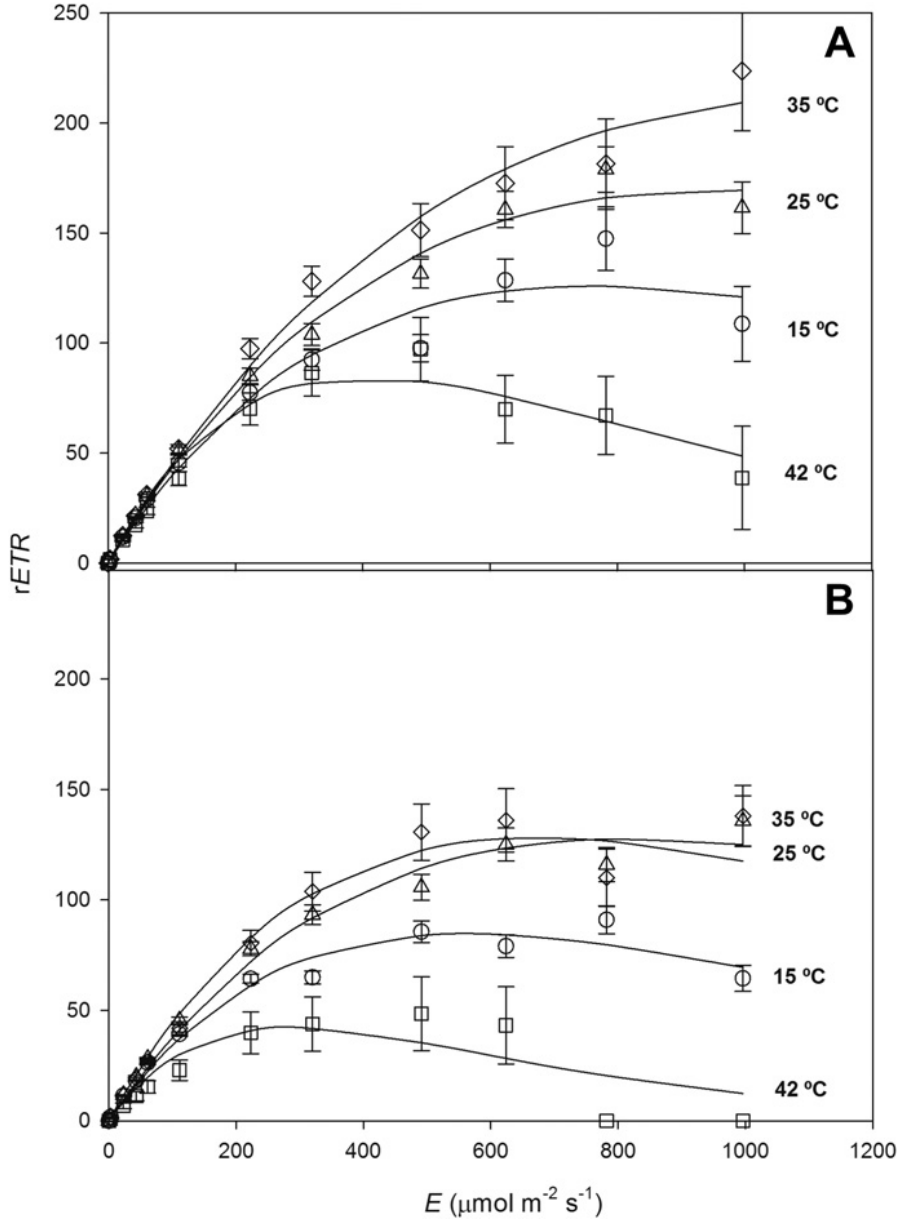

Figure 3. Relative photosynthetic electron transport rate (*r*ETR) versus incident photon irradiance (E) (mean ± standard deviation, n =6) rapid light curves (RLC) of microphytobenthos from Trancão (Tagus estuary) after 30 min (A) and 2 h (B) at the four temperature treatments (15, 25, 35 and 42 °C).

Differences between sites were less visible for the 2 h treatments as *r*ETR values decreased significantly in Trancão (Figure 3). RLC measured at 42 °C were similar in the two study sites and usually the temperature at which lowest *r*ETR were obtained (Figure 2 and 3). RLC in sediment samples from Alcochete showed photoinhibition (β decline in *r*ETR for higher E levels) at all

temperatures tested, whereas in Trancão photoinhibition was only observed in RLC measured at 42°C.

There were significant (ANOVA, $P < 0.001$) effects of both independent variables (temperature and sampling site) in ETR_{max} (maximum *r*ETR) (Figure 4A). For the 30 min treatment, this parameter increased significantly (Tukey, $P < 0.001$) with temperature from 15 to 35°C, declining abruptly at 42 °C. For the 2 h treatment, values of ETR_{max} increased significantly ($P < 0.001$) from 15 to 25°C, but were not significantly different between 25 and 35°C (Figure 4A). ETR_{max} values were significantly (Tukey, $P < 0.001$) higher at Trancão than at Alcochete for both treatment durations (30 min and 2 h).

There were significant (ANOVA, $P < 0.01$) effects of both independent variables (temperature and sampling site) in α (light utilization coefficient) (Fig. 4B). The light utilization coefficient remained independent of temperature from 15 to 35°C, declining significantly (Tukey, $P < 0.001$) at 42°C. α values were significantly (Tukey, $P < 0.01$) higher at Alcochete for both treatment durations (30 min and 2 h).

As α was relatively insensitive to temperature (except for the decline at 42°C), E_k (light saturation parameter) trends reflected those of ETR_{max} (Figure 4C). There were significant (ANOVA, $P < 0.001$) effects of both independent variables (temperature and sampling site) in E_k. For the 30 min treatment, this parameter increased significantly (Tukey, $P < 0.001$) from 15 to 25°C and from 25 to 35°C, while for the 2 h treatment differences were not significantly between 25 and 35°C (Figure 4C). Values decreased significantly (Tukey, $P < 0.001$) at 42°C. E_k values were significantly (Tukey, $P < 0.001$) higher at Trancão for both treatment durations (30 min and 2 h).

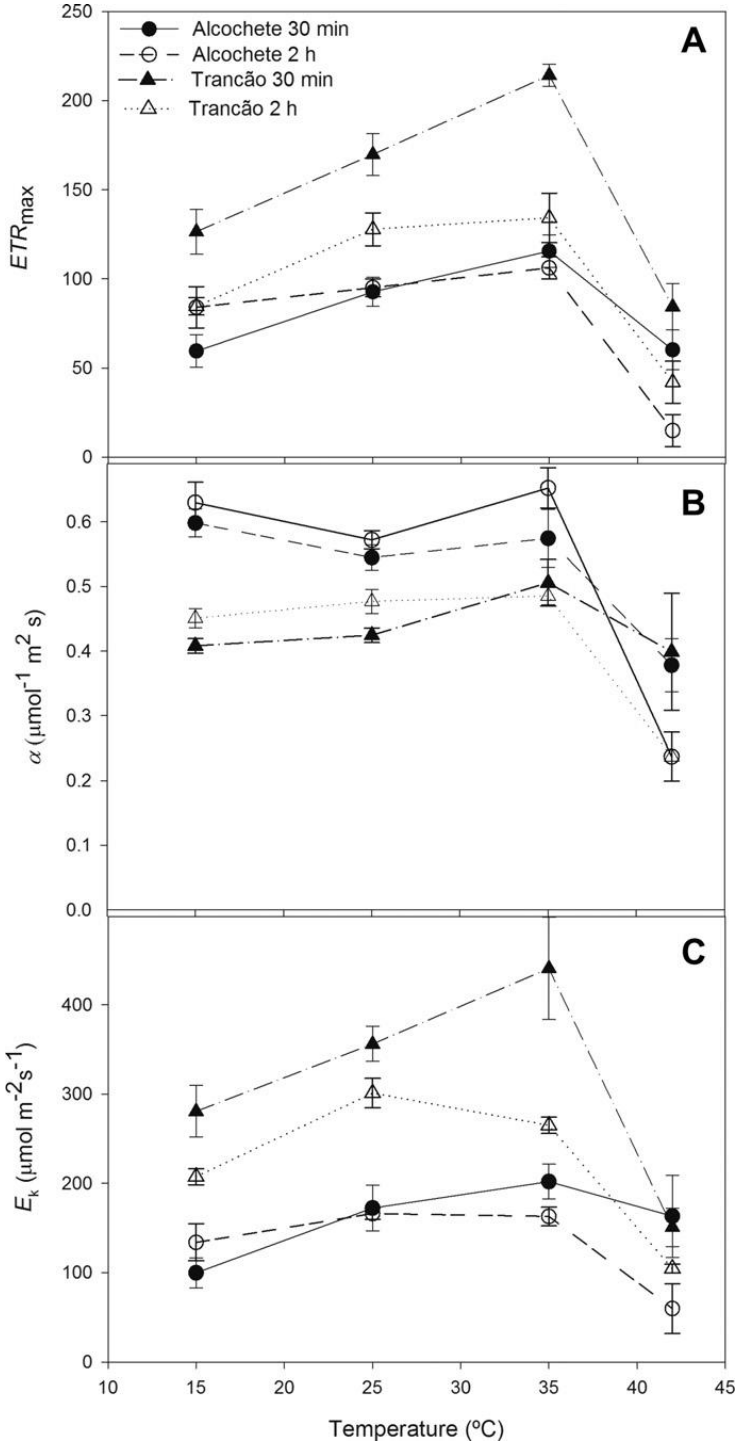

Figure 4. Variation (mean ± standard deviation, n =6) of maximum electron transport rate (ETR_{max}, A), light utilization coefficient (a, B) and light saturation parameter (E_k, C) with temperature in microphytobenthos from two sites of the Tagus estuary (Alcochete and Trancão). Fluorescence measurements were obtained after 30 min and 2 h at each temperature

Discussion

Mean daily air temperatures in the Tagus estuary can reach values over 30°C in the summer months (Gameiro et al., 2007). During midday, the exposed dark-coloured mudflat can reach significantly higher temperatures. Serôdio and Catarino (1999), studying the variability of light and temperature in intertidal sediments of the Tagus estuary, recorded sediment temperatures of ca. 35°C during summer low tides occurring at the middle of the day. In the latter study, temperature was measured at the top first cm of the sediment. It is possible that temperature of the photic zone, the very thin uppermost layer of the sediment (ca. 0-400 µm in very fine, muddy sediments; Cartaxana et al., 2011), where most of the MPB is concentrated, was actually higher. Under strong solar heating, during the summer months, temperature vertical gradients in excess of 100 C ml were recorded in the tidal mudflats of the Forth estuary (Harrison and Phizacklea, 1987).

Photosynthetic capacities (ETR_{max}) of the two studied MPB communities increased with temperature in the 15-35°C range and decreased at 42°C. Fitting of the Blanchard et al. (1996) model to our ETR data showed good agreement between the experimental data points and the fitted model with estimated optimum temperature (TOPT) between 34 and 35°C. Rates of light-saturated photosynthesis are generally limited by carbon metabolism, namely fixation by ribulose-1, 5-diphosphate carboxylase/oxygenase (Davison, 1991). Changes in the photosynthetic capacity with short-term (hours) changes in temperature have been reported for benthic diatom cultures (Morris and Kromkamp, 2003; Salleh and McMinn, 2011) and MPB suspensions (Blanchard et al., 1997). However, the estimated TOPT of 34-35°C observed in our study was higher than those previously reported. TOPT of 30°C and 25°C were found for cultures of the benthic diatom *Cylindrotheca closterium* (Morris and Kromkamp, 2003) and suspensions of intertidal epipelic MPB (Blanchard et al., 1997), respectively. Salleh and McMinn (2011), testing both thermal and irradiance stress in cultures of benthic diatoms, found TOPT of ca. 20°C and strong photoinhibition under elevated temperature and irradiance levels. Differences in the thermal environment to which the diatoms were previously acclimated to and in the species composition can explain the differences in TOPT found in these studies. Furthermore, in experiments using benthic cultures or diatom MPB suspensions, the cells are completely removed from the sediment environment. This may have significant effects on the photosynthetic activity of the benthic cells, namely in the vulnerability to high irradiance levels. Hancke and Glud (2004) found lower TOPT of 12-15°C in intact MPB

communities subjected to short-term changes in temperature. However, in the latter study, the MPB was subtidal (water depth <4 m) and collected during winter months in temperate and high artic locations.

Photosynthetic efficiencies at limiting irradiances (α) of the two studied MPB communities were not affected by temperature in the 15-35 °C range, while decreasing markedly at 42°C. This suggests impairment of energy capture and photosynthetic electron transport at extreme temperatures. Acute upper thermal tolerance of photosynthesis appears to be set by the thermal stability of photosystem II (PSII), especially of its donor side (Li et al., 2009). However, the upper thermal limit for long-term survival is dependent on different physiological processes and net photosynthesis can transiently occur at temperatures well above it (Davison, 1991). In the diatom *Phaeodactylum tricornutum*, significant increase in minimum fluorescence (F_o) resulting from inactivation of functional reaction centers associated with changes in the stability and organization of photosynthetic membranes was only observed above 43°C (Serôdio et al., 1997). Maximum temperatures (T_{max}) from 30 to 40°C have been reported for benthic diatoms and intertidal MPB suspensions (Blanchard et al., 1997; Morris and Kromkamp, 2003; Salleh and McMinn, 2011).

The two studied MPB communities differed in the diatom species composition and in the measured photosynthetic parameters. The Trancão MPB community was clearly dominated by smaller diatoms, particularly *Navicula* cf. *phyllepta*, whereas the Alcochete community showed a more even distribution of small, medium and large-size diatoms and was mainly composed by a combination of species of the genera Navicula, Thalassiosira and Gyrosigma. *Navicula* cf. *phyllepta* was previously observed in the intertidal flats of the Tagus estuary (Jesus et al., 2009) and corresponds morphologically to a strain of *N. phyllepta* found mainly in the lower salinity reaches of the Westerschelde estuary (Vanelslander et al., 2009). The dominance of this species was probably a consequence of the lower salinity found at this site due to the influence of fresh water discharges from the Trancão river.

The Trancão MPB community had higher photosynthetic capacity (higher ETR_{max}), was photoacclimated to higher irradiances (higher E_k) and had lower photosynthetic efficiency at limiting irradiances (lower α) than Alcochete community. Photosynthetic characteristics of each diatom taxon can cumulatively be responsible for the observed differences in the overall photosynthetic parameters observed in both MPB assemblages. The different size class distribution could also

explain the observed results as small cells are usually more active due to larger surface to volume ratios, allowing higher maximum photosynthetic rates (Taguchi, 1976). It is also possible that differences in ETR_{max} were related to different carbon availabilities at the sampling sites. There is strong evidence to suggest that DIC limitation may occur in natural MPB communities at times of high productivity (Cook and Roy, 2006).

After 2 h, particularly at the higher temperatures (35 and 42°C), the photosynthetic capacities of Trancão MPB community decreased compared to the 30 min treatment. It is possible that this is related to a joint effect of temperature and water stress, as this sediment had lower water content (63.0 ± 1.6 %) than that of Alcochete (68.5 ± 1.1%) and signs of drying were visible at Trancão sediment surface after 2 h at higher temperatures. Souffreau et al. (2010) observed the high sensitivity of benthic diatom cells when exposed simultaneously to temperature and desiccation stress.

It is possible that benthic diatoms may use migration for protection from long exposures to high temperatures found at the uppermost layer of the sediment, very much as the behavioral photoprotection mechanism described upon exposure to high irradiances (Serôdio et al., 2006; Cartaxana and Serôdio, 2008; Perkins et al., 2010; Vieira et al., 2011). Admiraal (1977) reported that lower temperatures are required for benthic diatoms to maintain high rates of cell division and Saburova and Polikarpov (2003) proposed a spatial disconnection between photosynthesis and cell division in MPB. The latter authors observed that epipelic diatom cells in different phases of mitosis were found almost exclusively in the aphotic anoxic zone of the sediment, arguing that deeper sediment layers provide more favorable nutrient conditions for cell growth and division. In a seasonal study, Hubas et al. (2006) observed that temperature influenced the benthic metabolism more than irradiance and suggested that migration prevented MPB from photoinhibition and high temperatures. Migratory behavior has often been referred as a major reason for the success of epipelic MPB in a highly unstable intertidal environment (Serôdio et al., 2001; Underwood et al., 2005).

Conclusions

Global climate change is expected to increase not only average temperature but also the frequency and the intensity of climate extremes such as heatwaves. Therefore, understanding the effect of changes in temperature on the primary productivity of estuarine MPB gains particular relevance. The present study shows that two intertidal MPB natural communities of the Tagus estuary increased maximum photosynthetic capacity when exposed to temperatures of up to 35°C for as long as 2 h. Although different diatom taxa within the same biofilm may respond differently to temperature, we conclude that community-level photosynthetic capacity of these intertidal MPB biofilms increases with transient high temperatures. Hence, MPB communities can exploit the rise in temperature associated with summer low tide emersion periods, increasing productivity.

Chapter 5

Photosynthesis in estuarine intertidal microphytobenthos is limited by inorganic carbon availability

Abstract

The effects of dissolved inorganic carbon (DIC) availability on photosynthesis were studied in two estuarine intertidal microphytobenthos (MPB) communities and in the model diatom species *Phaeodactylum tricornutum*. Kinetics of DIC acquisition, measured with a liquid-phase oxygen electrode, showed higher K_m (DIC) (0.31 mM) and V_{max} (7.78 nmol min^{-1} µg (Chl *a*)$^{-1}$) for MPB suspensions than for *P. tricornutum* (K_m (DIC) = 0.23 mM; V_{max} = 4.64 nmol min^{-1} µg (Chl *a*)$^{-1}$), suggesting the predominance of species with lower affinity for DIC and higher photosynthetic capacity in the MPB. The net photosynthetic rate of the MPB suspensions reached saturation at a DIC concentration of 1 to 1.5 mM. This range was lower than the concentrations found in the interstitial water of the top 5 mm sediment layer, suggesting no limitation of photosynthesis by DIC in the MPB communities. Accordingly, carbon isotope discrimination revealed a moderate activity of CO_2-concentrating mechanisms (CCMs) in the MPB. However, addition of $NaHCO_3$ to intact MPB biofilms caused a significant increase in the relative maximum photosynthetic electron transport rate ($rETR_{max}$) measured by imaging pulse-amplitude modulated (PAM) chlorophyll *a* fluorescence. These results suggest local depletion of DIC at the photic layer of the sediment (the first few hundred µm), where MPB cells accumulate during diurnal low tides. This work provides the first direct experimental evidence of DIC limitation of photosynthesis in highly productive intertidal MPB communities.

Introduction

The fixation of inorganic carbon is a central process of photosynthesis. The dissolved inorganic carbon (DIC) concentration in seawater is high and relatively constant (~2 mmol L^{-1}). However, the predominant form of DIC is HCO_3^-, CO_2 usually accounting for less than 1% of the total inorganic carbon. Thereby, the expected CO_2 concentration of seawater is approximately 10 µmol L^{-1} (at atmospheric equilibrium at 25°C) (Badger et al., 1998). As the K_m (CO_2) of ribulose-1,5-bisphosphate carboxylase-oxygenase (RUBISCO) is 30-60 µmol L^{-1}, photosynthesis of marine diatoms could be, in principle, limited by CO_2 supply (Badger et al., 1998). To maintain the photosynthetic activity under low carbon availability many diatom species have developed CO_2 concentrating mechanisms (CCMs) (Raven and Falkowski 1999; Giordano et al., 2005).

It is generally accepted that the biophysics and biochemistry of CCMs vary within and among the three dominant groups of eukaryotic marine phytoplankton (diatoms, coccolithophores, dinoflagellates), with diatoms possessing high-efficiency CCMs in what concerns energy and nutrient costs per unit of transported carbon (Reinfelder, 2011). CCMs increase the CO_2 concentration, and the CO_2/O_2 ratio, at the site of RUBISCO activity, increasing the rate of net C assimilation per unit RUBISCO. Therefore, as these mechanisms grant full saturation of RUBISCO catalytic centers it is believed that the photosynthesis of pelagic diatoms is not limited by dissolved CO_2 concentration (Tortell et al., 1997). CCMs are also expected to occur in microphytobenthos (MPB) biofilms, composed mainly by diatoms and cyanophytes. Accordingly to several authors (e.g. Raven et al., 2012) CCMs are ubiquitous in long-lasting low CO_2 microhabitats, including MPB where the high concentration of photosynthetic cells as well as the low carbon diffusion from the bulk medium into cells due to thick diffusion boundary layers (Raven et al., 2008) may decrease local DIC. However, albeit MPB communities are of critical importance to estuarine and coastal food webs, the methodological and technical difficulties inherent to the study these communities (e.g., sediment interferences and patchy distribution) have hindered the unravelling of DIC use and CCMs activity.

The application of stable isotope techniques, in particular $\delta^{13}C$, has provided the scientific community with new insights into understanding physiological and ecological processes related with carbon fixation and diffusion. Specifically, during photosynthetic uptake of aqueous carbon dioxide marine phytoplankton preferentially assimilate the lighter isotope (^{12}C), thus increasing the stable carbon isotopic signature (^{13}C) of the residual pool of dissolved inorganic carbon. Hence, marine algae always display more depleted ^{13}C particulate organic carbon than the DIC source they assimilate (Hayes, 1993). Field and laboratory studies have found numerous factors that affect the relationship between the concentration of dissolved CO_2 [CO_2 aq] and fractionation associated with photosynthesis including growth rate, nutrient and light limitation, cell size and geometry, diffusive limitations and the existence of carbon concentrating mechanisms (Raven et al., 2005, 2012). All of these factors can affect the relationship between (CO_2 aq) and $\delta^{13}C$ of organic matter; however, the existence of a CCM, particularly one which utilizes isotopically heavy HCO_3^- similarly to C_4 photosynthetic pathways (Mook et al., 1974) is especially significant.

Admiraal et al. (1982) provided indirect experimental evidence of inorganic carbon limitation in

benthic diatom mats cultured in the laboratory. In ^{14}C tracer column experiments, Cook and Roy (2006) found that increased rates of pore-water advection or addition of HCO_3^- increased photosynthesis in MPB of subtidal sandy sediments. Recently, Cartaxana et al. (2015) observed a beneficial effect of elevated CO_2 on intertidal MPB biomass in a microcosm experiment. However, to our knowledge, direct experimental evidence of inorganic carbon limitation in highly productive estuarine intertidal MPB has not been provided. To address this issue, we studied the effects of DIC availability on photosynthesis in two estuarine intertidal MPB communities of the Tagus estuary.

Materials and Methods

Sampling and culture growth conditions

The surface layer of sediment (approximately the top first 5 mm) was collect using a spatula at Trancão (38° 47' 46''N, 09° 05' 33''W) and Alcochete (38° 44' 45''N, 08 °59' 04''W) in the Tagus estuary (Portugal). Sampling was carried out in summer of 2012 at spring tides when the intertidal flats were exposed. Both sediments were fine mud with more than 97% particles <63 µm. In the laboratory, the sediment was mixed and then evenly spread in trays to a depth of about 2 cm. The sediment was left overnight with a shallow depth of site water, added so as not to re-suspend the sediment. The following morning, at the start of the low tide emersion period predicted for the original sampled site in the field, the shallow layer of water was removed.

Suspensions of MPB were obtained from trays with sediments collected at Trancão using the lens tissue method (Eaton and Moss 1966). Microalgae were collected by placing two pieces of lens tissue on the surface of the sediment shortly after the beginning of diurnal low tide at the Trancão sampling site. After *ca.* 1 h, the upper lens tissue was removed and microalgae were resuspended in approximately 20 ml of previously boiled seawater purged with N_2 for at least 1h.

The diatom model species *Phaeodactylum tricornutum* Bohlin (IO 108-01, ALISU Algal Collection, Centre of Oceanography, University of Lisbon) isolated from samples from Ria de Aveiro (Aveiro, Portugal) was grown in f/2 medium in a growth chamber (Fitoclima 250E, Aralab) at 15°C and 40 µmol photons m^{-2} s^{-1} irradiance (12 h photoperiod). Cultures were used in the exponential growth phase. Twenty ml of the culture were centrifuged and the pellets were resuspended in previously boiled seawater purged with N_2 for at least 1h.

Photosynthesis *vs* DIC response curves

The response of net photosynthesis to DIC concentration was measured in MPB suspensions and in cultures of *P. tricornutum.* Inorganic carbon-dependent photosynthetic oxygen evolution was measured polarographically at 25°C using a Clark-type oxygen electrode (S1, Hansatech Instruments Ltd) mounted in a liquid-phase oxygen electrode chamber (DW1, Hansatech Instruments Ltd) and controlled by a PC operated electrode control unit (Oxygraph, Hansatech Instruments Ltd). Two ml of MPB suspension (~ 11 µg Chl *a* mL^{-1}) for or *P. tricornutum* culture (~ 4 µg Chl *a* mL^{-1}) were placed in the O_2 electrode chamber, illuminated at a photon flux density of 140 µmol photons m^{-2} s^{-1} and cells allowed to reach the DIC compensation point (as shown by the cessation of apparent oxygen evolution). Then, 8 aliquots of a 200 mM $NaHCO_3$ solution (1, 2.5, 5, 10, 15, 20, 25 and 30 µl) were added sequentially to the cell suspension to create increasing DIC concentrations and to make a final concentration range of 0 to 3 mM $NaHCO_3$. After the addition of each aliquot the oxygen evolution rate was allowed to stabilize and steady-state net photosynthetic rates were computed. Net photosynthesis was selected in order to account for bacterial contamination. Even though the lens tissue method is selective for motile diatoms, bacterial contamination of the MPB samples is not to be excluded and in fact the respiratory rate of MPB (-7.1 ± 1.2 nmol O_2 min^{-1} μg^{-1} Chl) was higher than the respiratory rates of *P. tricornutum* culture (-2.2 ± 1.2 nmol O_2 min^{-1} μg^{-1} Chl). Before the addition of the next $NaHCO_3$ aliquot cells were again allowed to reach the DIC compensation point.

Kinetic parameters were obtained by fitting the net photosynthetic rate vs. DIC concentration plot with the Michaelis-Menten model: $V=Vmax*[DIC]/(K_m(DIC)+[DIC])$, where $K_m(DIC)$ is the DIC concentration required to give a half maximal photosynthetic rate and *Vm* is the DIC-saturated photosynthetic rate calculated from Michaelis-Menten fit.

The chlorophyll concentration of each cell suspension was measured using a spectrophotometer (Heλios β, Thermo Electron Corporation). The cells were harvested by centrifugation (Beckman-Coulter Avanti J-25I centrifuge) and chlorophyll was extracted overnight with 1.8 ml acetone at 4°C in the dark. After the addition of 0.2 ml of distilled water, samples were mixed and absorbance was measured at 630 nm (A630) and 664 nm (A664). The following equation was used to determine the chlorophyll *a* content (Jeffrey and Humphrey, 1975): [Chl *a*] = (A664*11.47-A630*0.40) µg ml^{-1}.

Effects of $NaHCO_3$ enrichment in MPB biofilm

Portions of the surface layer of the collected sediment (Trancão and Alcochete) were transferred to 6-well plates using a small spatula for Imaging PAM measurements as described by Vieira et al. (2013a). The well plates were exposed to a homogeneous light field provided by a halogen lamp (Philips focusline, 250W) through fiberoptics Lighting Unit FL-460 (Walz), delivering a constant irradiance of 60 µmol photons m^{-2} s^{-1} at the sample surface. Low light levels induced cell migration to the sediment surface and the formation of a biofilm. After biofilm establishment, 20 µl of seawater (control) or 20 µl of solution of 50 mM $NaHCO_3$ were added at the sediment surface. Six replicates were used for each treatment.

To assess the photosynthetic activity, a rapid light curve (RLC) was performed after 30 min of $NaHCO_3$ addition using an imaging-PAM fluorometer (Mini PAM M-Series, Walz GmbH) with an IMAGE-K5 1/2" CCD camera (640 x 480 pixel resolution) equipped with a 16 mm objective. The 24 x 32 mm area imaged by the Mini version is illuminated by a powerful Luxeon LED array (460 nm) covering the 6-well plate, so that 6 sediment samples could be monitored simultaneously. The LED array provided the measuring beam, the actinic light and the saturation light pulses. For the construction of RLC the samples were exposed to 12 intensities of actinic light: 0, 3, 23, 43, 61, 111, 223, 320, 491, 624, 782 and 996 µmol photons m^{-2} s^{-1}. The duration of each irradiance step was 30 s. Numerical values and images of the chlorophyll fluorescence parameters were extracted from the digital images using analytical software (Imaging Win, Walz). RLC were constructed by calculating, for each level of actinic light, the relative electron transport rate (r*ETR*) from the delivered actinic irradiance (*E*) and the effective quantum yield of PSII ($\Delta F/F_m'$) by *r*ETR = E x $\Delta F/F_m'$. The light response was characterized by fitting the model of Platt et al. (1980) to *r*ETR versus *E* curves and by estimating the initial slope of the light curve α (light utilization coefficient), $rETR_{max}$ (maximum *r*ETR) and E_k (light saturation parameter), where $E_k = rETR_{max} / \alpha$.

DIC concentration in sediment interstitial water

Five independent sediment samples (approximately the top 5 mm) were also collected at each study site (Trancão and Alcochete) for the determination of DIC concentrations. In the laboratory, the sediment samples were centrifuged at 10,000 g (Beckman-Coulter Avanti J-25I) and interstitial water was collected. Concentration of DIC in the interstitial water was determined using a carbon dioxide

(CO_2) analyzer (Corning 965). A sodium bicarbonate calibration curve was constructed with the following concentrations: 12.50, 6.25, 3.12, 1.56 and 0.78 mM.

Carbon and Nitrogen Isotope Composition ($\delta^{13}C$ and $\delta^{15}N$)

Five independent sediment samples (approximately the top 5 mm) were also collected at each study site (Trancão and Alcochete) for carbon isotope composition analysis. Suspensions of MPB were prepared using the lens tissue method (Eaton and Moss 1966) as described above. MPB was resuspended in filtered seawater of each site and lyophilized for 72 h (Alpha I-5 Christ, pressure 10^{-1} mbar at - 42ºC). The pellet was treated with 1 ml 1N HCl for 10 min, washed twice in milliQ water and lyophilized again. Subsequently, 8 mg of the pellet were used for each sample encapsulation.

Both carbon ($^{13}C/^{12}C$) and nitrogen ($^{15}N/^{14}N$) isotope ratios were determined by continuous flow isotope mass spectrometry (CF-IRMS). The standards used were IAEA-CH6 and IAEA-CH7 and the results were referred to Pee Dee Belemnite (PDB). Precision of the isotope ratio analysis, calculated using values from 6 to 9 replicates of laboratory standard material interspersed among samples in every batch analysis, was ≤ 0.2‰.

The samples were combusted under O_2 excess in an elemental analyzer (EuroVector EA, Italy), and converted to CO_2, N_2 and H_2O (Dumas-combustion). After removing H_2O with a water trap, the combustion products were flushed in a helium stream through the dilutor box into an Isotope Ratio Mass Spectrometer Sercon Hydra 20-22 (Sercon, UK), following standardized methods in CF-IRMS. Carbon and nitrogen isotope ratios were calibrated against international standards, namely, IAEA CH6 (sucrose) and IAEA CH7 (polyethylene) for carbon isotope ratio, and IAEA N1 (ammonium sulfate) for nitrogen isotope ratio. Analytical performance, stability and drift, was checked by inserting laboratory standards between samples. Precision (standard deviation of the set of standards analyzed in each batch, n = 6) was 0.06 % for carbon, 0.08 % for nitrogen. All results are given in δ-notation:

$$\delta^{13}C_{sample} = (R_{sample} - R_{standard}) / R_{standard}$$

where $R_{standard}$ is the $^{13}C/^{12}C$ ratios of PDB (Pee Dee Belemnite) and

$$\delta^{15}N_{sample} = (R_{sample} - R_{standard}) / R_{standard}$$

where $R_{standard}$ is the $^{15}N/^{14}N$ ratios of atmospheric N_2 and R_{sample} is the $^{15}N/^{14}N$ ratio of the sample.

Statistical analysis

Significant differences were tested with one-way analysis of variance (ANOVA) for the effects of carbon enrichment on fluorescence RLC parameters (α, $rETR_{max}$ and E_k) of MPB biofilms for each of the two study sites (Trancão and Alcochete). Data normality and homogeneity of variances were tested with Shapiro-Wilk and Bartlett tests, respectively. Data were transformed whenever necessary to comply with ANOVA assumptions. Mean values of DIC, K_m(DIC), V_{max}, $\delta^{13}C$ and $\delta^{15}N$ were compared by T-tests for independent samples. All statistical analyses were carried out using Statistica 10 (StatSoft Inc., USA).

Results

The photosynthesis vs. DIC response curves of Trancão MPB suspensions and of the diatom *P. tricornutum* are shown in Figure 1.

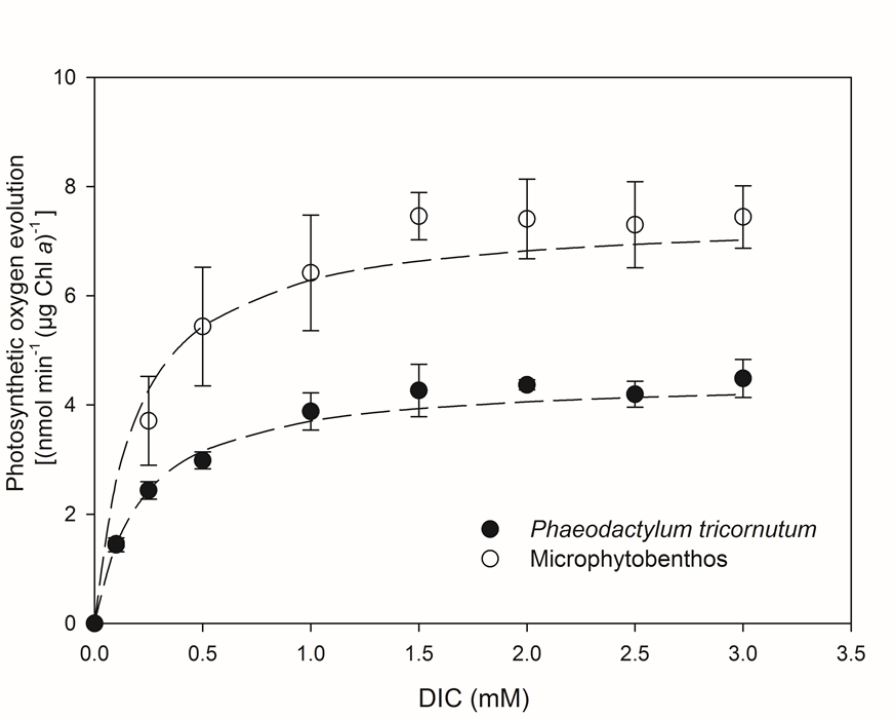

Figure 1. Photosynthetic oxygen evolution versus DIC curves (mean ± standard error, n=3) for microphytobenthos suspensions and for the model diatom species *Phaeodactylum tricornutum.* Lines were obtained by applying the Michaelis-Menten model to the experimental data.

Similar patterns were found for both MPB and *P. tricornutum,* with higher values of net photosynthetic oxygen evolution for MPB natural communities (Figure 1). For both MPB and *P. tricornutum*, photosynthetic rates saturated at about 1 to1.5 mM of DIC, clearly below the 3.53 mM concentration measured for interstitial sediment (0-5 mm layer) water in Trancão. For the MPB suspensions, K_m(DIC) was 0.31 ± 0.16 mM and the DIC-saturated photosynthetic rate (V_{max}) was 7.78 ± 1.08 nmol min^{-1} µg Chl a^{-1}. For *P. tricornutum* both K_m(DIC) and V_{max} were lower than for the MPB suspensions (0.23 ± 0.05 mM and 4.64 ± 0.50 nmol min^{-1} µg Chl a^{-1} respectively, Table1).

Table 1. Half-saturation constant (K_m) and inorganic carbon-saturated photosynthesis rate (V_{max}) (mean ± standard error, n=3) for microphytobenthos suspensions and for the model diatom species *Phaeodactylum tricornutum*. Values were obtained by applying the Michaelis-Menten model to the experimental data.

Sample	K_m (DIC) (mM)	V_{max} (nmol min^{-1} µg Chl a^{-1})
Phaeodactylum tricornutum	0.23 ± 0.05	4.64 ± 0.50
Microphytobenthos	0.31 ± 0.16	7.78 ± 1.08

Relative photosynthetic electron transport rate (*r*ETR) versus incident photon irradiance (E) rapid light curves (RLC) of control and inorganic carbon enriched MPB biofilms are shown in Figure 2 for the MPB communities of Trancão and Alcochete. For both communities, *r*ETR values at high irradiances were higher in DIC supplemented samples. This effect was more pronounced in MPB from Alcochete, were a large decrease of *r*ETR was observed in control samples at the higher irradiances tested (photoinhibition), but not in DIC enriched samples. There was a significant ($P<0.01$) effect of carbon enrichment on photosynthetic capacity ($rETR_{max}$) of MPB biofilms for the two sites (Figure 3). No significant effect of carbon enrichment on photosynthetic efficiency at limiting irradiances (α) was observed. The effect of carbon enrichment was more marked in MPB biofilms from Alcochete ($P<0.001$) than Trancão ($P<0.01$). For the light saturation parameter, E_k, a significant effect was found in MPB biofilms from Alcochete ($P<0.01$) but no significant differences were found in Trancão. Significant differences were also found between Alcochete and Trancão DIC concentrations in the sediment's interstitial water. Concentrations were significantly ($P<0.01$) higher in Trancão (3.53 ± 0.18 mM) than in Alcochete (1.87 ± 0.01 mM).

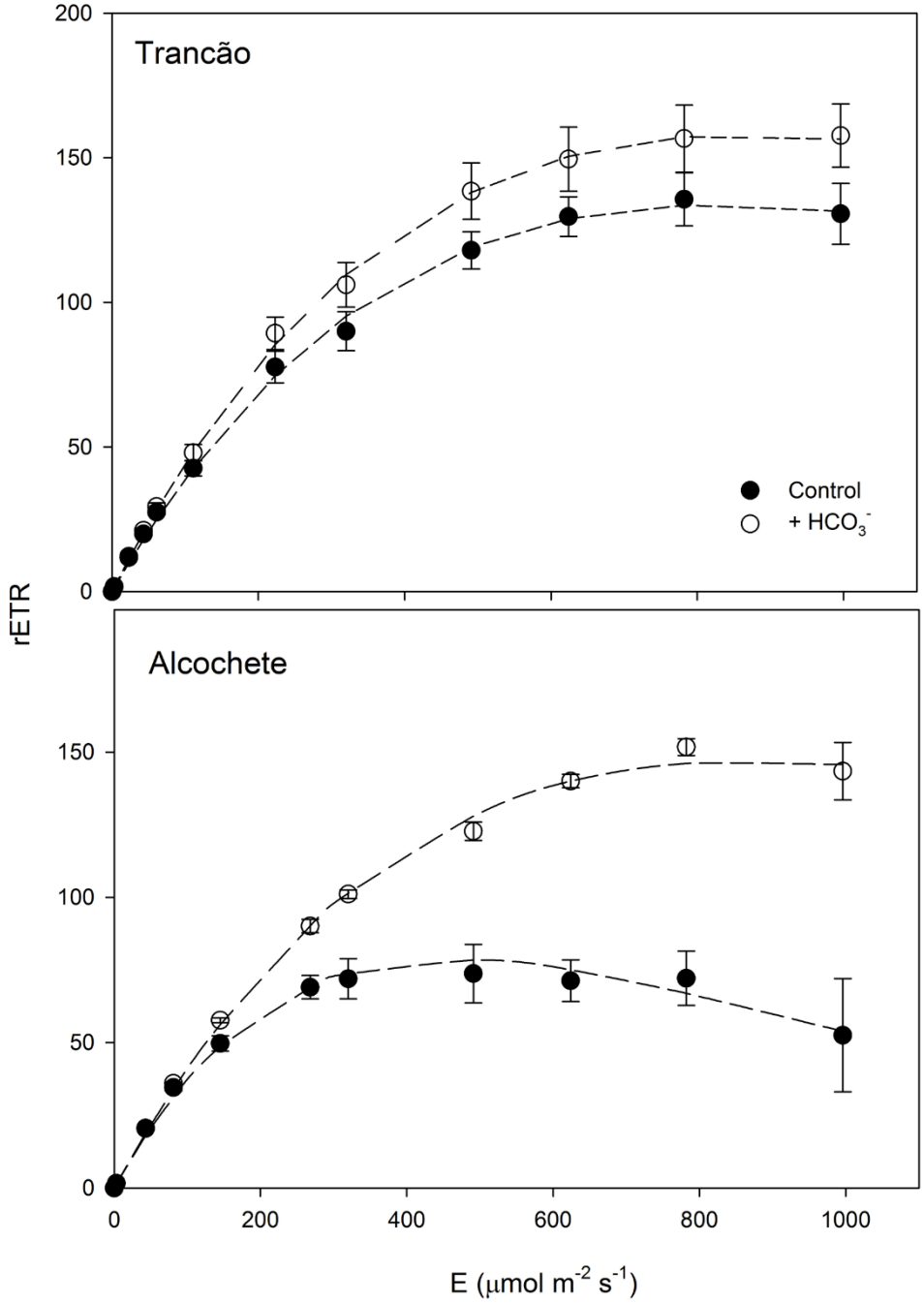

Figure 2. Relative photosynthetic electron transport rate (*r*ETR) versus incident photon irradiance (*E*) (mean ± standard deviation, n=6) rapid light curves (RLC) obtained using Imaging PAM fluorescence in control and carbon enriched intertidal microphytobenthos of the two studied communities (Trancão and Alcochete).

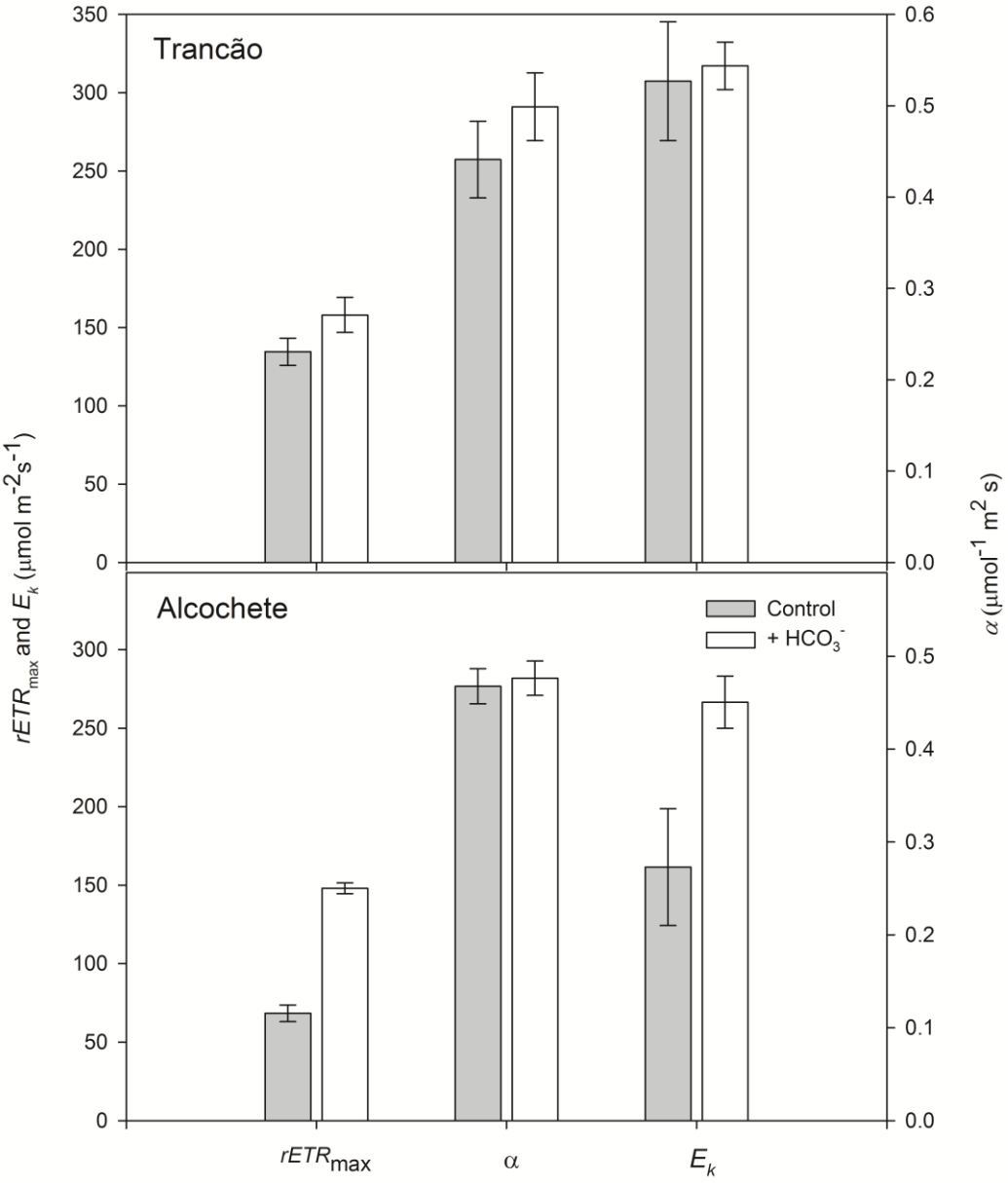

Figure 3. Maximum electron transport rate (*r*ETR$_{max}$), *α* (initial slope of the light curve) and E_k (light saturation parameter) (mean ± standard deviation, n=6) for control and carbon enriched microphytobenthos of the two studied communities (Trancão and Alcochete)

Carbon and nitrogen isotope composition, as well as the ratio C/N are shown in Table 2. Carbon and nitrogen isotope composition differed significantly (P<0.0001) between Alcochete (-19.98 ± 0.86‰ for δ^{13}C and 12.77± 0.26‰ for (δ^{15}N) and Trancão (-26.79 ± 0.37‰ for δ^{13}C and 4.72 ± 0.35‰ for

($\delta^{15}N$). The ratio C/N also vary between the two locations (6.24 ± 0.80 in Alcochete and 10.07 ± 3.28 in Trancão, $P<0.05$). The lower C/N ratio in Alcochete was mainly due to an increase in N.

Table 2. Carbon ($\delta^{13}C$) and nitrogen ($\delta^{15}N$) isotopic composition and Carbon / Nitrogen (C/N) ratio for microphytobenthos organic material collected from sediments located in Alcochete and Trancão.

Sample	$\delta^{13}C$	$\delta^{15}N$	*C/N*
Alcochete	-19.98 ± 0.86	12.77 ± 0.26	6.24 ± 0.80
Trancão	-26.79 ± 0.37	4.72 ± 0.35	10.07 ± 3.28

Discussion

Albeit a number of studies have previously determined the kinetic parameters of DIC acquisition in marine photoautotrophs such as phytoplankton, cyanobacteria and macrophytes (Caperon and Smith 1978; Turpin et al., 1985; Gimmler and Slovik 1995) data was not available for MPB communities. MPB showed higher K_m for DIC and higher V_{max} than the diatom model species *P. tricornutum,* suggesting that the MPB community includes species with lower affinity for DIC (explaining the higher K_m(DIC)) and higher photosynthetic capacity (explaining the higher V_{max}). The model marine diatom *P. tricornutum* has been intensively studied in regard to the inorganic carbon utilization mechanisms (e.g. Rotatore et al., 1995; Nimer et al., 1997; Burkhardt et al., 2001; Matsuda et al., 2001, 2002), being able to actively accumulate CO_2 and HCO_3^-. This microalgae has plastic photosynthetic and growth responses to changes in the external inorganic carbon concentration and may modify the mechanism of carbon acquisition (Johnston and Raven, 1996). This might explain its low K_m (DIC), when compared with the MPB community, where K_m (DIC) is the average of all photosynthetic species present.

The net photosynthetic rate of MPB suspensions reached saturation at a DIC concentration (1-1.5 mM) lower than the concentrations found in the interstitial water of the top 5 mm sediment layer (3.53 mM in Trancão and 1.87 mM in Alcochete), within the range (1.46 - 8.07 mM) found by Dvorak (2007) in four estuaries of southern Florida. It was therefore expected that the photosynthetic rates of natural communities of MPB were not limited by the availability of DIC. However, under experimental conditions, the addition of DIC to intact MPB biofilms caused an increase in the photosynthetic capacity when compared to control, non-enriched MPB. The MBP community

showed lower photosynthetic capacity ($rETR_{max}$) and higher photoinhibition in Alcochete than in Trancão in control sediment samples. However, when a surplus of DIC was experimentally supplied, the Alcochete MPB community showed a more pronounced increase of the photosynthetic capacity. Taken together, these results suggest a larger limitation by DIC of the Alcochete MPB community, which is in accordance with the lower interstitial DIC concentration in this location.

Several are the evidences that support the existence of CCMs in microalgae, which facilitate the photosynthetic activity under low CO_2 concentrations (Reinfelder et al., 2000; Raven and Johnston, 1991; Roberts et al., 2007; Meyer and Griffiths, 2013). Albeit indirectly, the measurement of the carbon isotope composition of MPB indicate the existence and activity of CCMs. The inorganic carbon available for photoautotrophic organisms consists ultimately of a pool of carbon atoms with different atomic weights, mainly ^{12}C (98.9%) and ^{13}C (1.1%) (Farquhar et al., 1989). However, in these organisms carbon is generally depleted in ^{13}C relative to the carbon source, indicating a carbon fractionation in the photosynthetic incorporation of inorganic carbon to biomass. An important contribution comes from RUBISCO, the ultimate carboxylation enzyme in all photosynthetic organisms, which rely in dissolved CO_2 as the inorganic carbon source and discriminates against ^{13}C ranging from $\delta^{13}C$ = -29‰ in plants and eukaryotic algae to $\delta^{13}C$ = -21‰ in cyanobacteria. In aquatic organisms, departures from RUBISCO discrimination values can be due to both biochemical CCM mechanisms based on the activities of β-carboxylases or biophysical CCM based on specific membrane carbon transporters and the activity of carbonic anhydrase.

In our study, Alcochete samples present more enriched $\delta^{13}C$ values (-19.98 ± 0.86), suggesting the presence of active CCMs, by contrast to Trancão, where $\delta^{13}C$ values (-26.77 ± 0.38) can be explained by the higher local DIC concentration and concomitant absence of CCMs. Additionally, CCMs are polyphyletic and may be affected by several environmental factors such as temperature, photosynthetically active radiation, phosphorus, iron and nitrogen supply (Raven et al. 2008; 2011). Thus, we hypothesize that the increase in nitrogen supply at Alcochete conveyed by the lower C/N ratio and by the enriched $\delta^{15}N$ (more complex organic N molecular forms) also modulate/influence the CCM activity. However, differences in carbon isotope composition and photosynthetic capacity could also be related to differences in the species composition of the two studied MPB communities. Although both Trancão and Alcochete MPB communities are composed exclusively of diatoms, they differ in species composition and size-class distribution (Vieira et al., 2013b). In fact, the carbon

isotope composition of microalgae is the result of the complex interaction of several factors (water temperature, DIC, type of organism, growth rate and cell size and geometry, in addition to biochemical and biophysical CCMs), making difficult to assign the origin of the differences measured in natural communities such as Trancão and Alcochete.

When samples from both locations were supplemented with DIC, similar $rETR_{max}$ were observed, supporting the evidence of *in situ* DIC limitation of photosynthesis in natural MPB communities. In intertidal muddy sediments, MPB cells accumulate at the sediment surface during low tides during the photoperiod. During these periods of high photosynthetic activity, most of the MPB biomass is concentrated in the first hundreds of micrometers (De Brouwer and Stal, 2001; Kelly et al., 2001; Cartaxana et al., 2011) causing a local depletion of DIC in the photic layer. To our knowledge, these results provide the first direct experimental evidence for DIC limitation of photosynthesis in highly productive intertidal MPB communities.

Chapter 6

Effects of elevated temperature and CO_2 on intertidal microphytobenthos

Abstract

Microphytobenthos (MPB) are the main primary producers of many intertidal and shallow subtidal environments. Although these coastal ecosystems are particularly vulnerable to anthropogenic activities, little is known on the effects of climate change variables on the structure and productivity of MPB communities. In this study, the effects of elevated temperature and CO_2 on intertidal MPB biomass, species composition and photosynthetic performance were studied using a flow-through experimental life support system. Elevated temperature had a detrimental effect on MPB biomass and photosynthetic performance under both control and elevated CO_2. Furthermore, elevated temperature led to an increase of cyanobacteria and a change in the relative abundance of major benthic diatom species present in the MPB community. The most abundant motile epipelic species *Navicula spartinetensis* and *Gyrosigma acuminatum* were in part replaced by tychoplanktonic species (Minidiscus chilensis and Thalassiosira cf. pseudonana) and the motile epipelic *Nitzschia* cf. *aequorea* and *N*. cf. *aurariae*. Elevated CO_2 had a beneficial effect on MPB biomass, but only at the lower temperature. It is possible that elevated CO_2 alleviated local depletion of dissolved inorganic carbon resulting from high cell abundance at the sediment photic layer. No significant effect of elevated CO_2 was detected on the relative abundance of major groups of microalgae and benthic diatom species. The interactive effects of elevated temperature and CO_2 may have an overall detrimental impact on the structure and productivity of intertidal MPB, and eventually in related ecosystem services.

Introduction

Microphytobenthos (MPB) are phototrophic communities that constitute the main primary producers of intertidal and shallow subtidal ecosystems (MacIntyre et al., 1996; Underwood and Kromkamp, 1999). Usually diatom dominated, MPB mediate nutrient cycling, enhance benthic-pelagic coupling and act as efficient sediment stabilizers (Bellinger et al., 2009; Morris and Kromkamp, 2003). Although coastal ecosystems are particularly vulnerable to climate change, little is known on the effects of variables such as elevated temperature or CO_2 availability on MPB productivity and related ecosystem services.

Within specific ranges, increased temperature generally results in higher metabolic activity and thus increased growth rates. Accordingly, photosynthesis and productivity of cultured benthic diatoms (Morris and Kromkamp, 2003; Salleh and McMinn, 2011) and natural MPB communities (Blanchard et al., 1996; Vieira et al., 2013) have been shown to increase with transient high temperature. However, much less is known on the effect of temperature changes on MPB at longer time-scales. A gradual transition from a phototrophic to a heterotrophic-dominated benthic community with increasing temperature has been previously reported for intertidal and subtidal systems (Davis and McIntire, 1983; Hancke and Glud, 2004). Hicks et al. (2011) found a detrimental effect of higher temperatures on MPB biomass in a 7-day experiment.

Photosynthesis in marine diatoms is generally not limited by inorganic carbon availability due to the operation of carbon concentrating mechanisms (CCMs) (e.g. Giordano et al., 2005; Roberts et al., 2007). However, a few studies on diatoms as part of highly productive MPB biofilms suggest limitation of photosynthesis by inorganic carbon availability. Admiraal et al. (1982) found that the diffusion of inorganic carbon limited the productivity of dense unialgal mats of the diatom *Navicula salinarum*. Addition of HCO_3^- was also found to increase photosynthetic rates of MPB natural communities in subtidal sand (Cook and Roy, 2006) and in intertidal muddy sediments (Vieira et al., 2015). On the other hand, at a longer time-scale, Hicks et al. (2011) found no significant increase on MPB biomass in subtidal mesocosms under increased atmospheric CO_2 levels.

Several authors have stressed the importance of studying the combined effects of different environmental drivers on ecosystem functioning (e.g. Bulling et al., 2007). Recent studies have shown interactive negative effects of increased temperature and CO_2 in marine phytoplankton (e.g. Feng et al., 2009; Coelho-Camba et al., 2014). Elevated temperatures resulting from global climate change as low as 2–3°C can be expected to affect microalgal species differently, causing increased metabolic activity and growth of some species while pushing others beyond their temperature optima, thus changing species composition (Beardall and Raven, 2004). To our knowledge, only Hicks et al. (2011) addressed the interactive effects of elevated atmospheric CO_2 concentrations and temperature on MPB biomass, using a nontidal experimental mesocosms. In this work, the combined effects of elevated temperature and

CO_2 on MPB biomass, photosynthetic performance and species composition were studied on an intertidal system using a flow-through experimental life support system with a simulated tidal regime.

Methods

Sediment sampling and set-up

The sediment surface layer (approximately the first 2 cm) was collected during a summer low tide at Alcochete intertidal flats, Tagus estuary, Portugal (38°44'45''N, 08° 59'04''W). Sediment was transported in refrigerated containers to the laboratory, homegeneized and placed inside microcosms in a flow-through experimental life support system (ELSS), forming a layer of 6 cm.

Induction of MPB cell distribution within the sediment profile was achieved by exposing the sediment to an irradiance of 70 µmol photons m^{-2} s^{-1} for ca. 24 h. Establishment of the MPB surface biofilm was assessed by measuring the normalized difference vegetation index (NDVI, see below). Once the MPB surface biofilm was established, all microcosms were subjected to the initial conditions of temperature and pH (18°C, pH 8.0). After 24 h at these conditions, four different treatments were started and the experiment run for 11 days: 1) 18°C and pH 8.0; 2) 24°C and pH 8.0; 3) 18°C and pH 7.4; and 4) 24°C and pH 7.4. Four microcosms were used for each treatment (with a total of 16 microcosms being used in the whole experiment).

The temperatures were chosen within the summer variation range of the study site and corresponded to mean high tide (18°C) and mean diurnal low tide (24°C) sediment temperatures (Serôdio and Catarino, 1999). The pH of the sediment interstitial water was 8.0, while a pH drop of 0.6 units (pH 7.4) was chosen on the basis of the Intergovernmental Panel on Climate Changes (IPCC, 2014) maximum projections for the change in global ocean surface pH (~0.4 units) in 2100, together with possible increased acidification caused by upwelling of anthropogenic CO_2-enriched water in coastal systems (Feely et al., 2008).

Experimental life support system (ELSS)

A flow-through ELSS was used, as described in detail by Coelho et al. (2013). The ELSS consisted of 16 independent microcosms (glass tanks - 28 cm length x 25 cm height x 12.4 cm

width) with a maximum functional water volume of approximately 7 L (Appendix 1.). The ELSS was equipped with 4 full spectrum fluorescent tubes (AquaLight, T5/54 W/10000K, Bramsche, Germany) and set to 6 h light–18 h dark cycle with an irradiance at sediment surface of 70 µmol photons m^{-2} s^{-1}.

The ELSS was operated with one daily tide. Saltwater was prepared in two reservoirs (230 L each) by mixing freshwater purified by a reverse osmosis unit (Aqua-win RO-6080) with a commercially available marine salt mixture (Tropic Marin Pro Reef salt – Tropic Marine, Germany) to a final salinity of 30. The water for tidal cycles was prepared 24 h before use. To simulate high tide, saltwater was pumped from the respective reservoir using a submersible pump (Aquabee UP 3000) through an independent pipeline system of polyvinyl chloride (PVC) tubes into each microcosm. The saltwater flow rate was manually controlled by a PVC valve located above each microcosm. The saltwater input was stopped when the water layer reached ca. 15 cm. High tide started after 15 min of the onset of the dark period. To simulate low tide, outflow submersible pumps (Rena flow 400 C) were used in each microcosm, operated using digital timers. These pumps were positioned inside a PVC cylinder and protected with a mesh screen to avoid clogging. The water was discharged using a common outflow pipe. Low tide started 15 min before the period of light exposure.

The microcosms in the ELSS were partially submerged into two main water-bath tanks. One tank was set to 18°C, the water was continuously pumped by a canister filter pump (SunSun HW-302) through a cooler equipped with a thermostat (Teco TR10) with a flow rate of 1000 L h^{-1}. The other tank was equipped with two submersible 200 W heaters with thermostats (Rena Cal 200) set to increase water temperature to 24°C.

Water pH was manipulated by acidifying the water stocked in the saltwater reservoirs by bubbling CO_2 through a diffuser. The diffuser operated with a water pump (Aquabee UP 3000) to maximize CO_2 gas mixing in saltwater. CO_2 addition was controlled with a feedback system that included a combination of a pH electrode connected to a controller (V2 control pH controller, Tropical Marine Centre, Bristol, UK) and a pressure regulator with an integrated solenoid valve (V^2 pressure regulator pro, Tropical Marine Centre, UK). The digital display of the controller allowed visualization of actual pH in the saltwater reservoir and pH monitoring

with the pH electrode. The controller opened the solenoid valve whenever pH rose above the set value; CO_2 was then injected until water pH returned to the pre-set value.

MPB biomass

MPB biomass was estimated daily and non-intrusively in each microcosm by calculating NDVI. Daily measurements of spectral reflectance as well as Pulse Amplitude Modulated (PAM) fluorescence (see below) were done in all microscosms during low tide, starting after 90 min of light exposure to ensure that the sediment was in the same conditions regarding diatom migration and biofilm establishment. Reflectance spectra were measured over a 350–1000 nm bandwidth with a USB4000 (Ocean Optics, USA) with a VIS-NIR optical configuration connected to a 400 μm diameter fiber optic (QP400-2-VIS/NIR, Ocean Optics, USA). The light spectrum reflected from the sample was normalized to the spectrum reflected from a clean polystyrene plate. A reflectance spectrum measured in the dark was subtracted to both spectra to account for the dark current noise of the spectrometer. The fiber optic was positioned perpendicularly to the sediment surface and both sample and reference spectra were measured under a constant irradiance of 70 μmol photons m^{-2} s^{-1}. NDVI was calculated as (R750 − R675) / (R750 + R675), where R750, R675 and R636 represented the average diffusive reflectance in the intervals of 749.73–750.39 nm, 674.87–675.55 nm and 635.71–636.40 nm, respectively (Serôdio et al., 2009).

Additionally, MPB biomass was calculated using HPLC chlorophyll *a* (Chl *a*) analysis at the beginning (T0) and at the end of the experimental period (T11). Invasive sampling for Chl *a* determination was done because previous studies have indicated NDVI saturation for high MPB biomass (Serôdio et al., 2009; Méléder et al., 2003). Sampling for Chl *a* was performed after spectral reflectance and PAM fluorescence measurements. For Chl *a* analysis, one sediment minicore (diameter 1.1 cm) was collected per microcosm at the beginning of the experiment (T0) using a plastic corer. The sediment surface (0 – 2 mm) was pooled in groups of 4 to obtain 4 mixed sediment samples. At the end of the experiment (T11), three minicores were collected per microcosm and the sediment pooled to obtain a total of 16 samples, one per microcosm. Sediment samples were immediately frozen in liquid nitrogen and stored at −80°C. Before analysis, samples were freezedried and extracted with 95% cold buffered

methanol (2% ammonium acetate) for 15 min at −20°C, in the dark. Samples were sonicated (1210, Bransonic, USA) for 30 s at the beginning of the extraction period. Extracts were filtered (Fluoropore PTFE filter membranes, 0.2 µm pore size) and immediately injected in a high performance liquid chromatographer (HPLC; LC10AVP, Shimadzu, Japan) equipped with a photodiode array (SPD-M10AVP) detector (Cartaxana et al., 2006). Chromatographic separation was carried out using a C18 column for reverse phase chromatography (Supelcosil; 25 cm long; 4.6 mm in diameter; 5 µm particles) and a 35 min elution programme. The solvent gradient followed Kraay et al. (1992) with a flow rate of 0.6 mL min^{-1} and an injection volume of 100 µL. Chl *a* was identified from absorbance spectrum and retention time and concentrations calculated from the signals in the photodiode array detector. Calibration of the Chl *a* peak was performed using a commercial pigment standard from DHI (Institute for Water and Environment, Denmark).

MPB photosynthetic parameters

Measurement of MPB photosynthetic parameters were carried out in each microcosm using a Diving-PAM Fluorometer (Walz, Effeltrich, Germany). The distance between the fluorometer fiber optic and the surface of sample was kept constant at 2 mm during all measurements. Maximum quantum yield of photosystem (PS) II (F_v/F_m) was determined daily in each microcosm by calculating $(F_m – F_o)/F_m$, where F_m and F_o are, respectively, the maximum and the minimum fluorescence of dark adapted samples (Murchie and Lawson, 2013). F_v/F_m gives a robust indication of the maximum efficiency of photosynthesis. Dark adaptation period was restricted to 2 min to reduce the possibility of inducing downward vertical migration of the epipelic MPB (Jesus et al., 2006).

On specific days (T0, T6 and T11), rapid light response curves (RLC) were carried out in all microcosms to assess MPB photosynthetic activity over a wide range of ambient light intensities (Ralph and Gademann, 2005). For the construction of RLC, the samples were exposed to 8 intensities of actinic light increasing from 38 to 616 µmol photons m^{-2} s^{-1} (38, 55, 81, 122, 183, 262, 367 and 616 µmol photons m^{-2} s^{-1}). Each irradiance step was 10 s; the saturation pulse intensity had duration of 0.6 s and an intensity of 8,000 µmol photons m^{-2} s^{-1}. RLC were constructed by calculating, for each level of actinic light, the effective quantum

yield of PSII ($\Delta F/F_m'$) and the relative electron transport rate (*r*ETR) from the delivered actinic irradiance (E) by *r*ETR = E x $\Delta F/F_m'$ (Ralph and Gademann, 2005). The light response was characterized by fitting the model of Platt et al. (1980) to *r*ETR vs. E curves and by estimating the initial slope of the light curve α (light utilization coefficient), ETR_{max} (maximum *r*ETR) and E_k (light saturation parameter), where $E_k = ETR_{max} / \alpha$. The model was fitted iteratively using MS Excel Solver.

MPB community analysis

Surface sediment samples to determine the composition of the MPB community were collected as described for Chl *a* analysis and stored in a 2.5% glutaraldehyde solution at 4 °C. Cells were extracted from the sediment following an isopycnic separation technique using silica sol Ludox HS-40 that separates the organic material from mineral particles and is, thus, able to remove microorganisms (e.g. MPB) from the sediment. Cell counts of MPB were made in a Sedgwick-Rafter cell counting chamber (50 µL of each extract) on an Olympus BX50 optical microscope (Olympus Corporation, Tokyo, Japan) at a 400x magnification. Between 3 and 9 horizontal transects (1300-8500 individual cells) were made, the cells counted separated into major MPB taxonomical groups (i.e. diatoms, euglenids, dinoflagellates and cyanobacteria) and the relative percentage determined.

Diatom analysis was conducted after cleaning the diatom valves of organic material. A subsample of 750 µL of extract was oxidized with 5-7 mL of hydrogen peroxide (30%) at 90°C for at least 4 h. Permanent slides, mounted in Naphrax ™ (Northern Biological Supplies Ltd., Ipswich, UK), were made for each sample. Phase and differential interference contrast optical microscopy were used to identify and count diatoms at a magnification of 1,000x. For each slide, a minimum of 400 valves were counted and identified to the species level, following Ribeiro (2010) and references therein.

Statistical analysis

The existence of significant differences was tested using two-way repeated measurements ANOVA (NDVI, F_v/ F_m, and RLC parameters) or two-way ANOVA (Chl *a* and MPB major group relative abundance) for the effects of temperature (18 and 24°C) and pH (7.4 and 8.0). Multiple comparisons were performed using Tukey HSD. Bonferroni correction was applied

to p values of multiple tests on correlated variables (NDVI and Chl *a*; ETR_{max}, α and E_k; relative abundance of diatoms and cyanophytes). Statistical analyses were carried out using Statistica 10 (StatSoft Inc., USA).

Diatom community structure was analysed with nonparametric multivariate tools using PRIMER® 6 software package (PRIMER-E, Plymouth, UK). The species abundance matrix was previously standardized and root-transformed and used in all multivariate routines. Bray-Curtis coefficients (Bray and Curtis, 1957) were used to compute the similarity or dissimilarity distances between samples. A similarity-based ANOSIM permutation test, with a 2- way crossed layout (Clarke et al., 2008), was performed to test if there were any statistically differences between groups of samples, namely, between temperature or pH treatments. Classification analysis (CLUSTER), which uses hierarchical agglomerative clustering of the samples and group-average linking (Field et al., 1982), was also performed.

During the dendrogram construction statistical significance of every cluster node was tested by the SIMPROF routine (Clarke et al., 2008). The SIMPROF is an a posteriori permutation test of the null hypothesis that the set of samples below a given node does not show any multivariate structure, which are then represented by dashed lines. Species mainly responsible for possible differences between treatments were determined using SIMPER analysis (Clarke, 1993).

Results

MPB biomass

There was a significant effect of temperature on NDVI measured along the experimental time period ($F_{11, 132} = 28.172$, $p < 0.001$), but no significant effect of pH ($F_{11, 132} = 1.131$, $p = 0.686$; Figure 1). There was no significant interaction between the categorical factors (temperature and pH; $F_{11, 132} = 0.937$, $p = 1.000$; Figure 1). Between day 0 and 3, NDVI increased slightly in all treatments, followed by a decrease in the microcosms at 24°C, reaching values of ca. 0.2 after 11 days (Figure 1). At 18°C, NDVI was relatively constant throughout the experiment (ranging between 0.5 and 0.6).

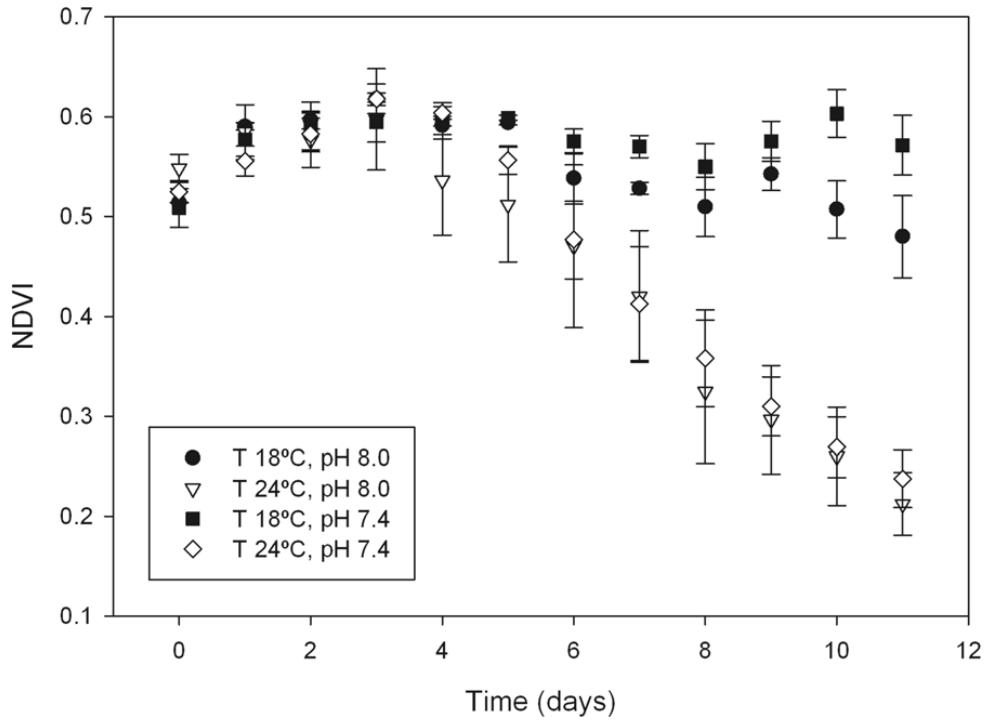

Figure 1. Microphytobenthos NDVI under control and elevated CO_2 and temperature. Changes in normalized difference vegetation index (NDVI, mean ± standard error, n = 4) of an intertidal sediment during an 11-day period under different temperatures and pH. T 18°C, pH 8.0: Temperature = 18°C, pH = 8.0; T 24°C, pH 8.0. Temperature = 24°C, pH = 8.0; T 18°C, pH 7.4.Temperature = 18°C, pH = 7.4; T 24°C, pH 7.4: Temperature = 24°C, pH = 7.4.

There was a significant interaction between temperature and pH on Chl *a* concentrations ($F_{1, 12}$ = 10.329, p = 0.015; Figure 2). Chl *a* concentrations were higher at 18°C than at 24°C, similar to what was observed with NDVI. On the other hand, at 18°C, Chl *a* concentrations were significantly higher at pH 7.4 than pH 8.0, reaching concentrations of 268 ± 53 µg g^{-1} (p = 0.014; Figure 2). No significant differences were observed between pH 7.4 and 8.0 at 24°C (p = 1.000; Figure 2).

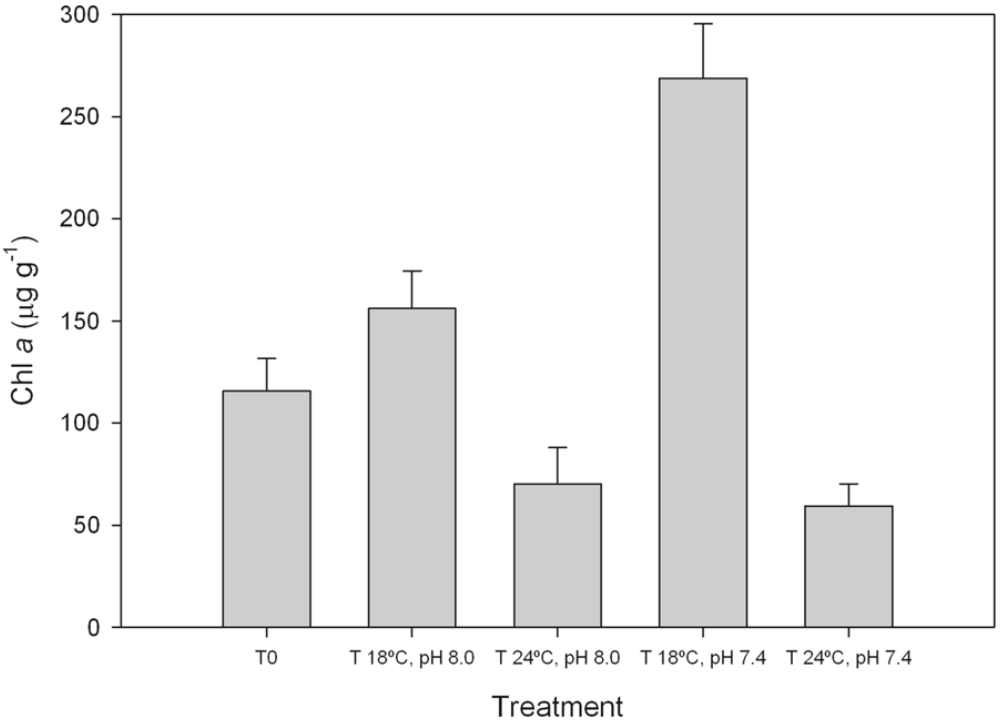

Figure 2. Microphytobenthos Chl *a* under control and elevated CO_2 and temperature. Chlorophyll *a* concentration (Chl *a*, mean ± standard error, n = 4) of an intertidal sediment (0–2 mm) at the beginning of the experiment (T0) and after 11 days under different temperatures and pH. T 18°C, pH 8.0: Temperature = 18°C, pH = 8.0; T 24°C, pH 8.0. Temperature = 24°C, pH = 8.0; T 18°C, pH 7.4. Temperature = 18°C, pH = 7.4; T 24°C, pH 7.4: Temperature = 24°C, pH = 7.4.

MPB photosynthetic parameters

There was a significant effect of temperature on maximum efficiency of PSII (F_v/F_m) measured along the experimental time period ($F_{11, 132} = 11.560$, $p < 0.001$), but no significant effect of pH ($F_{11, 132} = 0.170$, $p = 0.998$; Figure 3). At 18°C, F_v/F_m was relatively constant throughout the experiment (ca. 0.73), although a slight increase was observed between day 0 and 1 for all treatments. At 24°C, F_v/F_m decreased from day 7, reaching significantly lower values (<0.58) at the end of the experiment. There was a significant effect of both temperature ($F_{2, 24} = 21.824$, $p < 0.001$) and pH ($F_{2, 24} = 7.763$, $p = 0.008$) on ETR_{max} measured along the experimental time period (Figure 4A). After 6 days, photosynthetic electron transport capacity was significantly higher at 24°C and pH 7.4, when compared to other treatments (in all cases $p < 0.001$).

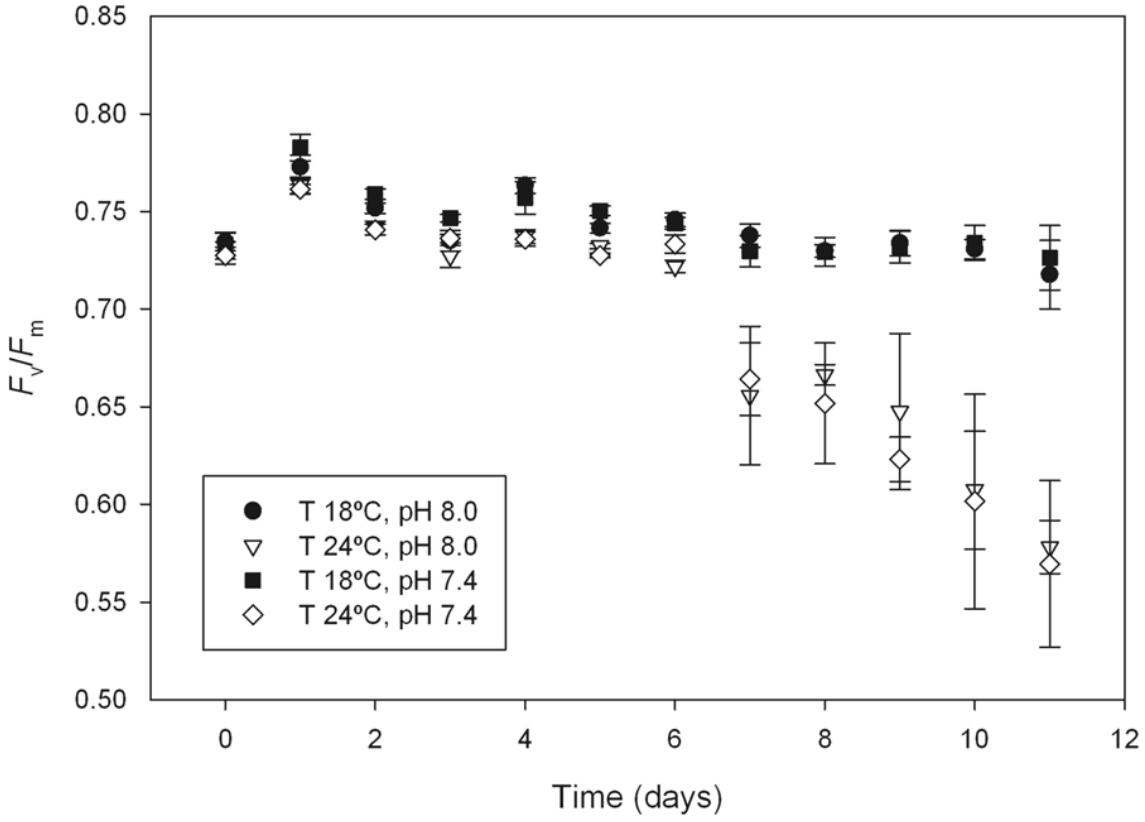

Figure 3. Microphytobenthos F_v/F_m under control and elevated CO_2 and temperature. Changes in maximum efficiency of photosystem (PS) II (Fv/Fm, mean ± standard error, n = 4) of an intertidal sediment during an 11-day period under different temperatures and pH. T 18°C, pH 8.0: Temperature = 18°C, pH = 8.0; T 24°C, pH 8.0. Temperature = 24°C, pH = 8.0; T 18°C, pH 7.4. Temperature = 18°C, pH = 7.4; T 24°C, pH 7.4.

At beginning (T0) or at the end of the experimental period (T11), differences in ETR_{max} were not significant. For α, there was a significant effect of temperature ($F_{2, 24}$ = 19.461, $p < 0.001$), but no significant effect of pH ($F_{2, 24}$ = 1.136, p = 1.000; Figure 4B). After 11 days, light utilization coefficient was significantly lower at 24°C than at 18°C ($p < 0.001$). Regarding E_k, there was a significant effect of temperature ($F_{2, 24}$ = 11.827, $p < 0.001$), but no significant effect of pH ($F_{2, 24}$ = 3.339, p = 0.158; Figure 4C), reflecting the trends observed for ETR_{max} and α. No significant interactions between the categorical factors (temperature and pH) were observed for any of the photosynthetic parameters analysed (lowest p = 0.669).

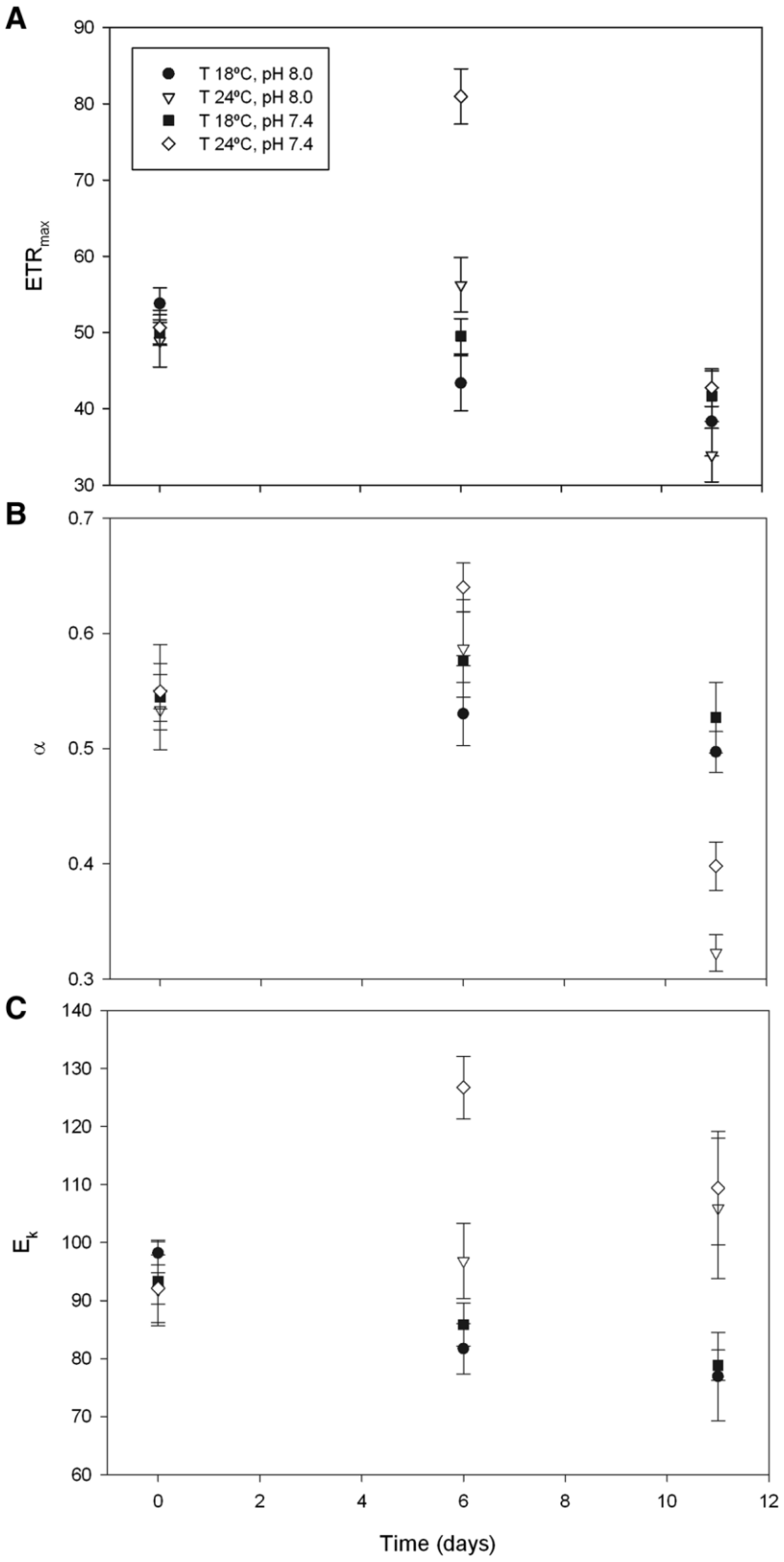

Figure 4. Microphytobenthos RLC parameters under control and elevated CO_2 and temperature. Changes in relative maximum electron transport rate (*r*ETR$_{max}$, A), light utilization coefficient (α, B) and light saturation parameter (E_k, C) (mean ± standard error, n = 4) of an intertidal sediment after 0, 6 and

11 days under different temperatures and pH. T 18°C, pH 8.0: Temperature = 18°C, pH = 8.0; T 24°C, pH 8.0. Temperature = 24°C, pH = 8.0; T 18°C, pH 7.4.Temperature = 18°C, pH = 7.4; T 24°C, pH 7.4: Temperature = 24°C, pH = 7.4.

MPB taxonomic composition

There was a significant effect of temperature on the relative abundance of MPB major groups ($F_{1, 12}$ = 16.035, p = 0.003 for diatoms and $F_{1, 12}$ = 16.296, p = 0.003 for cyanophytes; Figure 5), while pH had no significant effect ($F_{1, 12}$ = 0.348, p = 1.000 and $F_{1, 12}$ = 0.392, p = 1.000, respectively; Figure 5).

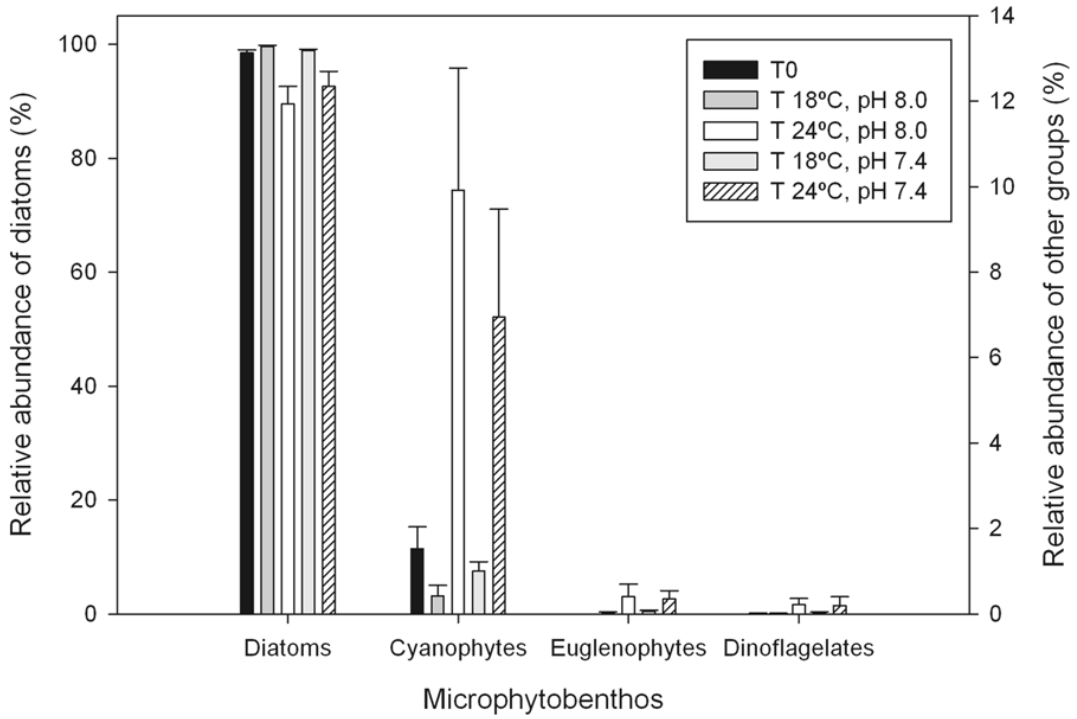

Figure 5. Relative abundance of major groups of microphytobenthos under control and elevated CO_2 and temperature. Relative abundance (%, mean ± standard error, n = 4) of major groups of microphytobenthos (diatoms, cyanobacteria, euglenophytes and dinoflagelates) of an intertidal sediment (0–2 mm) at the beginning of the experiment (T0) and after 11 days under different temperatures and pH. T 18°C, pH 8.0: Temperature = 18°C, pH = 8.0; T 24°C, pH 8.0.Temperature = 24 °C, pH = 8.0; T 18°C, pH 7.4.Temperature = 18°C, pH = 7.4; T 24°C, pH 7.4: Temperature = 24°C, pH = 7.4.

No significant interactions between the categorical factors (temperature and pH) were observed (lower p = 0.739). Although diatoms were the dominant group of the MPB community at the beginning and at end of all experimental treatments, diatom relative abundance was lower after 11 days under the higher temperature (99.2 ± 0.2% at 18°C compared to 91.0 ± 2.0% at 24°C). The decrease in diatoms at 24°C was associated with an increase in the relative abundance of cyanobacteria (0.70 ± 0.2% at 18°C and 8.40 ± 1.9% at 24°C). The contribution of euglenophytes and dinoflagelates to the MPB community was minor, representing in all cases less than 1% of relative abundance.

Concerning diatom assemblages, a total of 120 diatom taxa were identified (97 to the species level, see appendix 2), varying between 24 and 57 per sample. Significant differences in diatom assemblage structure were found between 24°C and 18°C (two-way crossed ANOSIM test: R = 0.667, p < 0.001), whereas differences between pH treatments were not significant (R = −0.063, p = 0.713). The CLUSTER analysis of the assemblage structure also showed that there were significant differences between the two incubation temperatures but not between pH (Figure 6), in spite of relatively high levels of similarity (i.e. between 60 and 80%). Samples from the microcosms at 24°C separated significantly from the microcosms at 18°C at 61.3% level of similarity (SIMPROF test: π = 2.24, p < 0.001). Samples collected at the beginning of the experiment (T0) separated significantly at 68.7% of level of similarity (SIMPROF test: π = 0.84, p = 0.019) from the samples collected at the end of the experimental period in the microcosms at 18°C. One of the samples of the 18°C group also separated significantly (SIMPROF test: π = 1.15, p = 0.002) from the rest early in the dendrogram, possible because it registered lower diversity and the highest relative abundance (68%) of *Navicula spartinetensis*. There was no subsequent significant multivariate pattern in the CLUSTER analysis (noted by the grey dotted lines in Figure 6).

Diatom assemblages were taxonomically similar (Apendix 2), with an average of 98% of cumulative relative abundance of shared species. Nevertheless, SIMPER analysis was able to detect slight differences in species relative abundance, responsible for the significant dissimilarities in assemblage structure between microcosm temperatures, as shown by ANOSIM and CLUSTER analysis. In this way, assemblages incubated at 18°C had higher abundances of *N. spartinetensis* and *Gyrosigma acuminatum*, whilst in assemblages at 24°C

these two motile epipelic species were in part replaced by tychoplanktonic species (i.e. *Minidiscus chilensis*, *Thalassiosira cf. pseudonana*) and the motile epipelic *Nitzschia* cf. *aequorea* and *N.* cf. *aurariae* (Appendix 2).

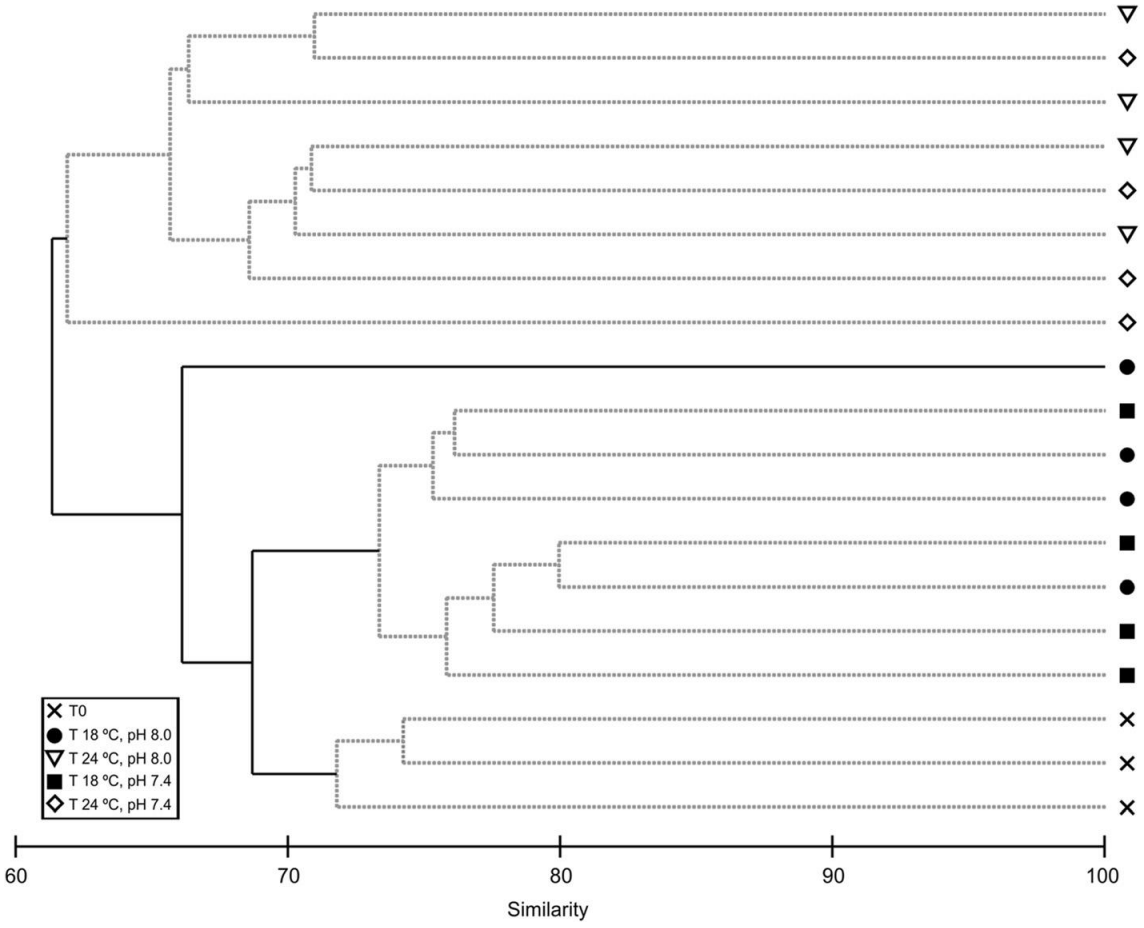

Figure 6. CLUSTER analysis of diatom assemblage structure under control and elevated CO_2 and temperature. Dendrogram for hierarchical clustering using group-average linking of Bray–Curtis similarities of diatom abundance of an intertidal sediment (0–2 mm) at the beginning of the experiment (T0) and after 11 days under different temperatures and pH. T 18°C, pH 8.0: Temperature = 18°C, pH = 8.0; T 24°C, pH 8.0. Temperature = 24°C, pH = 8.0; T 18°C, pH 7.4. Temperature = 18°C, pH = 7.4; T 24°C, pH 7.4: Temperature = 24°C, pH = 7.4. Dashed lines indicate groups of samples not separated (at $p < 0.05$) by SIMPROF.

Discussion

In the present 11-day study, elevated temperature promoted a detrimental effect on MPB biomass (using both NDVI and Chl *a* concentrations as proxies) and photosynthetic performance (through the quantification of maximum photosynthetic electron transport efficiency and light utilization coefficient by PAM fluorometry). This effect was recorded under both control and elevated CO_2. Using a non-tidal mesocosm system solely for 7 days, Hicks et al. (2011) also found lower MPB biomass at higher temperatures for a mudflat of the Ythan estuary in Scotland at three levels of atmospheric CO_2 concentrations. On the other hand, Torstensson et al. (2012) found that biomass and photosynthetic activity of the benthic/sea ice diatom *Navicula directa* were promoted by elevated temperature. However, the relevant temperatures tested in the latter 7-day laboratory study were 0.5 and 4.5°C. Intertidal MPB communities are exposed to extremely high temperature fluctuations in their natural environment. In the Tagus estuary, if emersion coincides with summer midday, the exposed dark-coloured mudflat sediment surface can reach temperatures above 30°C (Serôdio and Catarino, 1999), clearly exceeding the higher temperature tested in this study. On the other hand, sediment temperature drops to a mean temperature of 18°C during summer immersion periods (Serôdio and Catarino, 1999). Hence, MPB seem to be able to cope with extremely high temperature fluctuations and short periods of very high temperature exposure. On the other hand, this study indicates that there is a significant effect on the MPB community when a less pronounced but prolonged increase in sediment temperature is applied. It is legitimate to assume that the productive potential of MPB present in the temperate Tagus estuary intertidal system may be negatively impacted by higher temperatures in the future.

Elevated temperature had also significant effects on the composition of the MPB community, causing a change on the relative abundance of major groups of microalgae. While diatoms were dominant in all treatments, higher temperature led to an increase in the relative abundance of cyanobacteria. It has been previously observed that cyanobacteria can be favored over diatoms at higher temperatures in mixed benthic biofilms (Van der Grinten et al., 2005). Furthermore, higher temperature also affected the relative abundance of major benthic diatom species present in the MPB community. Temperature-driven changes in the dynamics of phototrophic and heterotrophic organisms of a typically mixed benthic

community are also expected to occur. Previous studies on diatom-dominated MPB of intertidal and subtidal systems showed that an increase in temperature stimulates more heterotrophy than photosynthetic activity, thus leading to a heterotrophic-dominated benthic community under elevated temperatures (Davis and McIntire, 1983; Hancke and Glud, 2004). Hence, a noticeable change in the structure of the MPB community of the Tagus estuary intertidal system can be expected to occur under higher temperatures promoted by climate change.

Elevated CO_2 and higher temperature led to a transient (day 6) increase in ETR_{max}, as rates of light-saturated photosynthesis are generally limited by carbon metabolism (namely fixation by ribulose-1,5-bisphosphate carboxylase/oxygenase, RUBISCO) (Davison, 1991). However, by the end of the experimental period, elevated CO_2 had a beneficial effect on MPB biomass only at the lower temperature tested and when considering Chl *a* as biomass proxy. No significant effects of CO_2 were detected on the relative abundance of major groups of microalgae and benthic diatom species. To maintain efficient photosynthetic rates under limited CO_2 supply, diatoms have developed high efficiency carbon concentrating mechanisms (CCMs) (e.g. Giordano et al., 2005; Roberts et al., 2007). As these mechanisms grant full saturation of RUBISCO catalytic centres it is generally assumed that diatom photosynthesis is not limited by dissolved inorganic carbon availability. Accordingly, Hicks et al. (2011) found no significant increase on MPB biomass of muddy intertidal sediments under increased CO_2 levels. Surprisingly, Torstensson et al. (2012) reported that *N. directa* was negatively affected by CO_2 enrichment, although the mechanism causing this effect was not identified. On the other hand, examining the colonisation of artificial substrata across a natural CO_2 gradient, Johnson et al. (2013) found that elevated CO_2 increased microphytobenthos biomass and induced diatom community shifts by promoting the growth of large pennate species. The latter authors argued that some diatoms could optimise resource allocation, benefiting from increasing CO_2 through a reduction in the energy costs of their CCMs.

Further challenging the notion of CO_2-insentitive photosynthesis in diatoms, Admiraal et al. (1982) provided indirect experimental evidence of inorganic carbon limitation in benthic diatom mats cultured in the laboratory. In $_{14}C$ tracer column experiments, Cook and Roy (2006) also found that increased rates of pore-water advection or addition of HCO_3^- increased

photosynthesis to similar rates in MPB of subtidal sandy sediments. Again, the supply of HCO_3^- was found to increase photosynthetic rates of highly productive MPB natural communities of intertidal muddy sediments (Vieira et al., 2016).

The beneficial effect of elevated CO_2 on MPB biomass at the lower temperature tested in our study suggests that carbon may have become a limiting resource for the MPB community. Upward migration of diatom cells to the sediment surface occurs in this benthic community during diurnal low tides, leading to the formation of an extremely dense biofilm in a relatively thin photic layer (the first hundreds of micrometers) (Cartaxana et al., 2011). In this crowded community, carbon may be a limiting resource even for organisms with high efficiency CCMs.

Conclusions

As MPB are the main primary producers of many intertidal and shallow subtidal environments, changes in MPB biomass will certainly impact the trophodynamics of these systems. Nonetheless, very few studies have considered the interactive effects of climate change variables on MPB communities (Hicks et al., 2011). There are obvious limitations in providing realistic interpretations of natural ecosystem response by using artificial systems such as the one used in this study. For example, longer-term increased temperature could favor selection and growth of high-temperature adapted MPB species that could partially modulate the observed negative impact on biomass and productivity. Nevertheless, small-scale experiments in microcosms or mesocosms can provide valuable insights on how complex ecosystems will cope with climate change (Benton et al., 2007). In this work, elevated temperatures under both present day and increased CO_2 led to a reduction of MPB biomass and photosynthetic performance, an increase of cyanophytes and a change in the relative abundance of major benthic diatom species present. Overall, it suggests that the interactive effects of studied parameters could have a detrimental impact on the structure and productivity of intertidal MPB, and eventually in related ecosystem services.

.

Chapter 7

General Discussion

Technical advances in the study of MPB: Laser induced fluorescence and pulse amplitude modulated fluorescence imaging

Remote sensing techniques use optical properties of sediments and biofilms to make inferences about the distribution and productivity of benthic photoautotrophs, without interfering with the sediment surface (Paterson et al., 1998). Hence, the application of these techniques to the study of MPB has increased significantly in recent years (Serôdio et al., 1997; Kromkamp et al., 1998; Paterson et al., 1998; Serôdio et al., 2001; Honeywill et al., 2002; Perkins et al., 2002; Serôdio, 2003; Stephens et al., 2003; Forster and Kromkamp, 2004; Murphy et al., 2004; Serôdio, 2004; Forster and Jesus, 2005; Murphy et al., 2005). Pulse amplitude modulated (PAM) fluorometry and spectral reflectance are the optical techniques most commonly used in intertidal MPB communities. In this work, we have successfully applied laser induced fluorescence (LIF) **(chapter 2)** to the study of vertical migrations of MPB epipelic communities.

The MPB biomass was estimated non-destructively with LIF by establishing a direct relationship between ln-transformed data of peak area (Chl fluorescence emission spectra of MPB communities) and the biomass proxies: normalized difference vegetation index (NDVI) and phytobenthos index (PI). Surface microalgal biomass accumulation on mud sediments caused changes in the characteristics of the fluorescence peak, namely a shift to longer wavelengths of the red emission maximum and the increase of the emission shoulder at the far-red region. Using LIF we were able to relate the vertical movements of benthic epipelic diatoms to changing irradiance levels. Rapid downward diatom movement was observed upon exposure to 1200 µmol photons m^{-2} s^{-1}, followed by upward migration when light levels were reduced to 70 µmol photons m^{-2} s^{-1}. These results confirmed that diatoms exhibit behavioural photoprotection by avoiding photoinhibitory light levels (Admiraal, 1984, Kromkamp et al., 1998, Perkins et al., 2001, 2010; Serôdio et al., 2006). The use of LIF has advantages over other remote sensing techniques for the study of intertidal MPB because it uses its own illumination source to actively excite fluorescence. On the contrary, spectral reflectance is a passive method of remote sensing that requires stable and uniform illumination, which is usually not the case under overcast and partly cloudy conditions. Results obtained with hand-held LIF instruments in higher plants have shown that this technique can be used for remote sensing under a diversity of light conditions, including full darkness, at dawn and dusk and under rapidly changing light environments (Richards et al., 2003). Recently, LIF was applied to assess the species diversity

of macroalgae in communities inhabiting estuarine intertidal areas. The characteristics of LIF emission spectra were determined by differences in the main fluorescing pigments - phycoerythrin, phycocyanin and chlorophyll *a* (Chl *a*) of different macroalgae (Gameiro et al., 2015), allowing species sorting. Likewise, LIF is a promising technique for the medium or long-range remote sensing of intertidal MPB communities.

Imaging-PAM fluorometry **(chapter 3)** revealed to be a particularly useful tool in determining spatial heterogeneity of MPB biomass and photophysiology across the sediment surface. Nevertheless, the differences we observed between the results of conventional and Imaging-PAM fluorometry advises caution when making quantitative assessments of MPB photosynthetic activities. First, imaging systems require higher intensity of measuring light, due the use of CCD cameras that use integration times much longer than the time required by photodiodes and phototubes used in conventional PAM. Second, the heating effect caused by saturating pulses on the LED array may cause an underestimation of $\Delta F/F_m'$ in the imaging systems. Finally, in imaging systems providing homogenous high photon irradiances in relatively large areas turned to be a significant technical challenge. The level of discrepancy between conventional and imaging systems was particularly relevant for MPB of muddy sediments. This can be partially explained by differences in the thickness of the photosynthetic layer and in the depth-integration of the fluorescence signal. Additionally, the presence of cyanobacteria in MPB assemblages requires caution in the interpretation of the fluorescence signals and may render different results with red and blue light excitation fluorometers. In fact, whereas in plants, green algae and diatoms fluorescence emission can be induced by either red or blue light excitation, in cyanobacteria blue light is mostly ineffective in variable fluorescence induction, although some basal (F_o) fluorescence is still observed (Schubert et al., 1989), leading to a significant decrease of the measured quantum yield. On one hand, these findings highlight the caution needed when interpreting Chl fluorescence data of MPB. On the other hand, they contribute to establish the safe limits within which the potential of Imaging-PAM techniques to study spatial heterogeneity of photosynthesizing surfaces may be fully explored.

Impact of the climate change variables "temperature" and "carbon" on the photosynthesis of MPB

Due to climate change, conditions in coastal and estuarine ecosystems are predictable to change dramatically. Studies on the effects of climate change on diatom diversity and productivity are scarce, especially for benthic habitats, and therefore little is known about the interactive effects of climate change variables (increase in temperature and inorganic carbon availability) on the structure and productivity of MPB communities. Nevertheless, variations in MPB biomass will impact the dynamics of estuarine and coastal habitats and, consequently, understanding the effect of changes in temperature and carbon on photosynthesis and on the primary productivity of estuarine intertidal MPB communities gains particular relevance.

There are a few studies on the photosynthetic response of benthic diatoms to short-term changes in temperature (e.g. Morris and Kromkamp, 2003; Hancke et al., 2008). Intertidal sediment temperature fluctuations occur on long (seasonal) and short (daily and hourly) time scales, depending on factors such as meteorological conditions, time of day and tidal inundation. In summer, intertidal sediment temperature can easily change 10-15^{o}C during an emersion period, reaching values higher than 35^{o}C at midday (Blanchard et al., 1997; Serôdio and Catarino, 1999). In our study, **(chapter 4**) the two MPB communities of the Tagus estuary show increased photosynthetic capacities (ETR_{max}) with temperature in the 15-35^{o}C range and a decrease at 42^{o}C. The estimated optimum temperature was between 34 and 35^{o}C and was higher than those previously reported for benthic diatom cultures (Morris and Kromkamp, 2003; Salleh and McMinn, 2011) and MPB suspensions (Blanchard et al., 1997). Photosynthetic efficiencies at limiting irradiance (α) of the two studied MPB communities were not affected by temperature in the 15-35^{o}C range, while decreasing markedly at 42^{o}C. The two studied MPB communities have differences in the diatom species composition and in the measured photosynthetic parameters. The Trancão MPB community was dominated by smaller diatoms, particularly *Navicula* cf. *phyllepta*, whereas the Alcochete community showed a more even distribution of small, medium and large-size diatoms and was mainly composed by a combination of species of the genera *Navicula, Thalassiosira and Gyrosigma.* The different diatom taxa within the same biofilm may respond differently to temperature. The Trancão MPB community had higher photosynthetic capacity (higher ETR_{max}), was photoacclimated to higher irradiances (higher E_k) and had lower photosynthetic efficiency at limiting

irradiances (lower α) than Alcochete community. So, the different size class distribution could explain the higher maximum photosynthetic rates, where small cells are usually more active due to larger surface to volume ratios (Taguchi, 1976). The diatom taxa present in MPB communities can exploit the increased temperature in summer low tide emersion periods, increasing MPB productivity. Yet, when a longer-term (11-day) effect of elevated temperature (24°C) was studied on a MPB community, a detrimental influence on MPB biomass and photosynthetic performance under both control (pH=8.0) and elevated CO_2 (pH=7.4) was found (chapter 6). This is in agreement with the results obtained by Hicks et al. (2011) using a non-tidal mesocosm system for 7 days, where higher temperatures decreased the MPB biomass of a mudflat from the Ythan estuary, in Scotland, at three levels of inorganic carbon availability. On the other hand, long-term higher temperature led to an increase in the relative abundance of cyanobacteria and caused changes on the relative abundance of major benthic diatoms **(chapter 6)**.

Differences in ETR_{max} between Trancão and Alcochete MPB may also be related to different carbon availabilities at the sampling sites. It has been suggested that DIC limitation may occur in natural MPB communities at times of high productivity (Cook and Roy, 2006) but, for the first time, we provided a direct experimental evidence of such inorganic carbon limitation **(chapter 5**). In fact, we found a marking contrast on the effect of DIC on MPB suspensions and MPB biofilms. The net photosynthetic rate of MPB suspensions reached saturation at a DIC concentration 1-1.5 mM, lower than the concentrations found in the interstitial water of the top 5 mm sediment layer (3.53 mM in Trancão and 1.87 mM in Alcochete), suggesting the absence of DIC limitation on photosynthesis. However, when we added DIC to intact MPB biofilms a different response was achieved. The addition of DIC to the two MPB communities of the Tagus estuary caused, in both communities, an increase in the photosynthetic capacity, when compared to control, non DIC-enriched MPB, demonstrating DIC limitation of MPB photosynthesis. This limitation may be accounted by the accumulation of MPB cells at the surface of intertidal muddy sediments during diurnal low tides. In fact, during these periods of high photosynthetic activity, most of the MPB biomass is concentrated in the top hundreds micrometers (De Brouwer and Stal, 2001; Kelly et al., 2001; Cartaxana et al., 2011) causing a local depletion of DIC in the photic layer. We also found that the MPB community from Alcochete showed lower photosynthetic capacity ($rETR_{max}$) and higher photoinhibition than Trancão, in control sediment samples, and a more pronounced increase of the photosynthetic

electron transport capacity with the addition of DIC. These results suggest a larger limitation by DIC in the Alcochete MPB community, which is in accordance with the lower interstitial DIC concentration in this location. On the other hand, carbon isotopic discrimination at the Alcochete MPB community indicated the presence of active carbon concentrating mechanisms (CCMs). The Alcochete samples present more enriched δ13C values (-19.98 ± 0.86), by opposition to the Trancão, where δ13C values (-26.77 ± 0.38) can be explained by the higher local DIC concentration and reduced CCMs activity. In Alcochete MPB communities dissolved inorganic carbon is more abundant and therefore it is unnecessary to activate costly energy consuming mechanisms. The longer-term effect of elevated DIC (pH=7.4, T=18°C) had a beneficial effect on MPB biomass (chapter 6). This suggests that carbon may have become a limiting resource for the MPB community, as was in fact shown in the short-term carbon enrichment experiments.

There are complex interactions between the effects of elevated temperature and carbon in MPB biomass and photosynthetic performance. The studies about climate change variables on MPB communities are few (Hicks et al., 2011), so, small-scale experiments in microcosms or mesocosms can provide valuable insights on how complex ecosystems will cope with climate change (Benton et al., 2007). Nevertheless, there are some limitations in providing realistic interpretation of natural ecosystem response using artificial systems. For example, longer-term increased temperature could favor selection and growth of high-temperature adapted MPB species that could partially modulate the observed negative impact on biomass and productivity.

In this work (**chapter 6),** elevated temperatures under both present day and increased CO_2 led to a reduction of MPB biomass, an increase of cyanophytes and a change in the relative abundance of major benthic diatom species. This suggests that the interactive effects of climate change variables may have a detrimental impact on the structure and productivity of intertidal MPB, and eventually in related ecosystem services.

Chapter 8

References

Admiraal W (1977) Influence of light and temperature on the growth rate of estuarine benthic diatoms in culture. Marine Biology 39:1-9.

Admiraal W (1984) The ecology of estuarine sediment-inhabiting diatoms. In: Round FE (ed.). In: Chapman DJ (ed.), Progress in Phycological Research Biopress Bristol. 3:269-322.

Admiraal W, Peletier H, Zomer H (1982) Observations and experiments on the population-dynamics of epipelic diatoms from an estuarine mudflat. Estuarine Coastal and Shelf Science 14:471-487.

Anderson B, Buah-Bassuah P, Tetteh J (2004) Using violet laser-induced chlorophyll fluorescence emission spectra for crop yield assessment of cowpea (*Vigna unguiculata* (L) Walp) varieties. Measurement Science and Technology 15:1255-1265.

Badger MR, Price GD (1998) CO_2 concentrating mechanisms in cyanobacteria: molecular components, their diversity and evolution. Journal of Experimental Botany 54:609-622.

Badger MR, Andrews TJ, Whitney SM, Ludwig M, Yellowlees DC, Leggat W, Price GD (1998) The diversity and coevolution of RubisCo plastids pyrenoids and chloroplast-based CO_2-concentrating mechanisms in algae. Canadian Journal of Botany 76:1052-1071.

Barbini R, Colao F, Fantoni R, Micheli C, Palucci A, Ribezzo S (1998) Design and application of a lidar fluorescence system for remote monitoring of phytoplankton ICES Journal of Marine Science 55:793-802.

Barillé L, Méléder V, Combe JP, Launeau P, Rincé Y, Carrère V, Morançais M (2007) Comparative analysis of field and laboratory spectral reflectances of benthic diatoms with a modified Gaussian model approach. Journal of Experimental Marine Biology Ecology 343: 197-209.

Barranguet C, Kromkamp J (2000) Estimating primary production rates from photosynthetic electron transport in estuarine microphytobenthos. Marine Ecology Progress Series 204:39-52.

Barranguet C, Kromkamp J, Peene J (1998) Factors controlling primary production and photosynthetic characteristics of intertidal microphytobenthos. Marine Ecology Progress Series 173:117-126.

Beardall J, Raven JA (2004) The potential effects of global climate change on macroalgal photosynthesis, growth and ecology. Phycologia 43:26-40.

Beer S, Björk M (2000) Measuring rates of photosynthesis by pulse amplitude modulated (PAM) fluorometry. Aquatic Botany 66:69-76.

Beer S, Larsson C, Poryan O, Axelsson L (2000) Photosynthetic rates of *Ulva* (Chlorophyta) measured by pulse amplitude modulated (PAM) fluorometry. European Journal of Phycology 35: 69-74.

Behrenfeld MJ, Prasil O, Babin M and Bruyant F (2004) In search of a physiological basis for covariations in light limited and light saturated photosynthesis. Journal of Phycology 40:4-25.

Bellinger BJ, Underwood GJC, Ziegler SE, Gretz MR (2009) Significance of diatom-derived polymers in carbon flow dynamics within estuarine biofilms determined through isotopic enrichment. Aquatic Microbial Ecology 55:169-187.

Benton TG, Solan M, Travis J, Salt SM (2007) Microcosm experiments can inform global ecological problems. Trends in Ecology and Evolution 22:516-521.

Blanchard GF, Guarini JM, Gros P, Richard P (1997) Seasonal effects on the relationship between the photosynthetic capacity of intertidal microphytobenthos and temperature. Journal of Phycology 33:723-728.

Blanchard GF, Guarini JM, Richard P, Gros P, Mornet F (1996) Quantifying the short- term temperature effect on light-saturated photosynthesis of intertidal microphytobenthos. Marine Ecology Progress Series 134:309-313.

Bray JR, Curtis JT (1957) An ordination of the upland forest communities of Southern Wisconsin. Ecological Monographs 27:326-349.

Brotas V, Catarino F (1995) Microphytobenthos primary production of Tagus estuary intertidal flats (Portugal). Netherlands Journal of Aquatic Ecology. 29:333-339.

Bryant D (1994) The Molecular Biology of Cyanobacteria. Kluwer Academic, Netherlands.

Buffan-Dubau E, Carman KR (2000) Diel feeding behavior of meiofauna and their relationships with microalgal resources. Limnology and Oceanography 45:381-395.

Bulling MT, Hicks N, Murray L, Paterson DM, Raffaelli D, White PCL, Solan M(2010) Marine biodiversity-ecosystem functions under uncertain environmental futures. Philosophical Transactions of the Royal Society B 365:2107-2116.

Burkhardt S, Amoroso G, Riebesell U, Sültemeyer D (2001) CO_2 and HCO_3 uptake in marine diatoms acclimated to different CO_2 concentrations. Limnology and Oceanography 46:1378-1391.

Buschmann C (2007) Variability and application of the chlorophyll fluorescence emission ratio red/far-red of leaves. Photosynthesis Research 92:261-271.

Campbell, D, Hurry V, Clarke A, Gustafsson P, Öquist G (1998) Chlorophyll fluorescence analysis of cyanobacterial photosynthesis and acclimation. Microbiology and Molecular Biology Reviews 62:667-683.

Caperon J, Smith DF (1978) Photosynthetic rates of marine algae as a function of inorganic carbon concentration. Limnology and Oceanography 23:704-708.

Carr H, Bjork M (2003) A methodological comparison of photosynthetic oxygen evolution and estimated electron transport rate in tropical *Ulva* (Chlorophyceae) species under different light and inorganic carbon conditions. Journal of Phycology 39:1125-1131.

Cartaxana P, Serôdio J (2008) Inhibiting diatom motility: a new tool for the study of the photophysiology of intertidal microphytobenthic biofilms. Limnology and Oceanography Methods 6:466-476.

Cartaxana P, Ruivo M, Hubas C, Davidson I, Serôdio J, Jesus B (2011) Physiological versus behavioural photoprotection in intertidal epipelic and epipsamic benthic diatom communities. Journal of Experimental Marine Biology Ecology 405:120-127.

Cartaxana P, Vieira S, Ribeiro L, Rocha RJM, Cruz S, Calado R, Marques da Silva J (2015) Effects of elevated temperature and CO_2 on intertidal microphytobenthos. BMC Ecology 15:10.

Clarke KR (1993) Non-parametric multivariate analyses of changes in community structure. Australian Journal of Ecology 18:117-143.

Clarke KR, Somerfield PJ, Gorley RN (2008) Testing of null hypotheses in exploratory community analyses: similarity profiles and biota-environment linkage. Journal of Experimental Marine Biology and Ecology 366:56-69.

Coelho FJRC, Rocha RJM, Pires ACC, Ladeiro B, Castanheira JM, Costa R (2013) Development and validation of an experimental life support system for assessing the effects of global climate change and environmental contamination on estuarine and coastal marine benthic communities. Global Change Biology 19:2584-2595.

Coello-Camba A, Agustí S, Holding J, Arrieta JM, Duarte CM (2014) Interactive effect of temperature and CO_2 increase in Arctic phytoplankton. Frontiers in Marine Science 1:49.

Consalvey M, Jesus B, Perkins RG, Brotas V, Underwood GJC, Paterson DM (2004) Monitoring migration and measuring biomass in benthic biofilms: the effects of dark/far-red adaptation and vertical migration on fluorescence measurements. Photosynthesis Research 81:91-101.

Consalvey M, Paterson DM, Underwood GJC (2004) The ups and downs of life in a benthic biofilm: migration of benthic diatoms. Diatom Research 19:181-202.

Constanza R, Arge R, Groot R, Farber S, Grasso M, Hannon B, Limburg K, Naeem S, O'Neill R, Paruelo J, Raskin R, Sutton P, Belt M (1997) The value of the world's ecosystems services and natural capital. Nature 387: 253-260.

Cook PLM, Roy H (2006) Advective relief of CO_2 limitation in microphytobenthos in highly productive sandy sediments. Limnology and Oceanography 51:1594-1601.

Davis MW, McIntire CD (1983) Effects of physical gradients on the production dynamics of sediment-associated algae. Marine Ecology Progress Series 13:103-14.

Davison IR (1991) Environmental effects on algal photosynthesis: temperature. Journal of Phycology 27:2-8.

De Brouwer JFC, Stal LJ (2001) Short-term dynamics in microphytobenthos distribution and associated extracellular carbohydrates in surface sediments of an intertidal mudflat. Marine Ecology Progress Series 218:33-44.

De Jonge VN, de Jong DJ (2002) 'Global change' impact of inter-annual variation in water discharge as a driving factor to dredging and spoil disposal in the River Rhine system and of turbidity in the Wadden Sea. Estuarine Coast and Shelf Science 55:969-991.

Decho AW (1990) Microbial exopolymer secretions in ocean environments: their role(s) in food webs and marine processes. Oceanography Marine Biology Annual Review 28:73-153.

Defew L, Mair J and Guzman H (2004) An assessment of metal contamination in mangrove sediments and leaves from Punta Mala Bay, Pacific Panama. Marine Pollution Bulletin 50:547-552.

Delgado M, de Jonge VN, Peletier H (1991) Sediment grain size effect on benthic microalgal biomass in shallow aquatic ecosystems. Marine Biology 108:321-328.

Drews G (1985) Structure and functional organization of light-harvesting complexes and photochemical reaction centers in membranes of phototrophic bacteria. Microbiological Reviews 49:59-70.

Eaton JW, Moss B (1966) The estimation of numbers and pigment content in epipelic algal populations. Limnology and Oceanography 11:584-595.

Falkowski PG (1994) The role of phytoplanckton photosynthesis in global biogeochemical cycles. Photosynthesis Research 39:235-258.

Falkowski PG, Raven JA (1997) Aquatic photosynthesis. Blackwell Science, Malden, MA.
Farquhar GD, Ehleringer JR, Hubick KT (1989) Carbon isotope discrimination and photosynthesis. Annual Review of Plant Physiology and Plant Molecular Biology 40:503-537.

Feely RA, Sabine CL, Hernandez-Ayon JM, Ianson D, Hales B (2008) Evidence for upwelling of corrosive “acidified” water onto the continental shelf. Science 320:1490-2.

Feng Y, Hare CE, Leblanc K, Rose JM, Zhang Y, DiTullio GR, Lee PA, Wilhelm SW, Rowe JM, Sun J, Memcek M, Gueguen C, Passow U, Benner I, Hutchins DA (2009) Effects of increased pCO_2 and temperature on the North Atlantic spring bloom. I. The phytoplankton community and biogeochemical response. Marine Ecology Progress Series 388:13-25.

Field JG, Clarke KR, Warwick RM (1982) A practical strategy for analyzing multispecies distribution patterns. Marine Ecology Progress and Series 8:37-52.

Forster RM, Jesus B (2006) Field spectroscopy of estuarine intertidal sediments. International Journal of Remote Sensing 27:3657-3669.

Forster, R. M. and J. C. Kromkamp (2004) Modelling the effects of chlorophyll fluorescence from subsurface layers on photosynthetic efficiency measurements in microphytobenthic algae. Marine Ecology Progress and Series 284:9-22.

Franck F, Juneau P, Popovic R (2002) Resolution of the photosystem I and photosystem II contributions to chlorophyll fluorescence of intact leaves at room temperature. Biochemical et Biophysica Acta 1556:239-246.

Fréchette M and Bourget E (1985) Food-limited growth of *Mytilus edulis L*. in relation to the benthic boundary layer. Canadian Journal of Fisheries and Aquatic Sciences 42:1166-1170.

Gademann R, Kühl M, Larkum AWD (2005) Coral photobiology studied with a new imaging pulse amplitude modulated fluorometer. Journal of Phycology 41:335-342.

Gameiro C, Cartaxana P, Brotas V (2007) Environmental drivers of phytoplankton distribution and composition in Tagus estuary, Portugal. Estuarine, Coastal and Shelf Science 75:21-34.

Gameiro C, Utkin AB, Cartaxana P (2015) Characterisation of estuarine intertidal macroalgae by laser-induced fluorescence. Estuarine Cosstal, Shelf Science 167:119-124.

Genty B, Briantais J, Baker NR (1989) The relationship between the quantum yield of photosynthetic electron transport and quenching of chlorophyll fluorescence Biochimica et Biophysica Acta 990:87-92.

Gévaert F, Créach A, Davoult D, Migné A, LeVavasseur G, Arzel P, Holl A-C, Lemoine Y (2003) *Laminaria saccharina* photosynthesis measured in situ: photoinhibition and xanthophyll cycle during a tidal cycle. Marine Ecology Progress Series 247:43-50.

Gimmler H, Slovik S (1995) The mode of uptake of dissolved inorganic carbon in the extremely acid resistant green algae *Dunaliella acidophila*. Plant Physiology and Biochemistry 33:655-664.

Giordano M, Beardall J, Raven JA (2005) CO_2 concentrating mechanisms in algae: Mechanisms environmental modulation and evolution. Annual Review in Plant Biology 56:99-131.

Gitelson AA, Bushmann C, Lichtenthaler HK (1998) Leaf chlorophyll fluorescence corrected for re-absorption by means of absorption and reflectance measurements. Journal of Plant Physiology 152:283-296.

Govindjee (1995) Sixty-three years since Kautsky: chlorophyll *a* fluorescence. Australian Journal of Plant Physiology 22:131-160.

Guarini JM, Blanchard G, Gros Ph, Harrison SJ (1997) Modeling the mud surface temperature on intertidal flats to investigate the spatio-temporal dynamics of the benthic microalgal photosynthetic capacity. Marine Ecology Progress Series 153:25-36.

Hancke K, Glud RN (2004) Temperature effects on respiration and photosynthesis in three diatom-dominated benthic communities. Aquatic Microbial Ecology 37:265-281.

Harrison SJ, Phizacklea AP (1987) Vertical temperature gradients in muddy intertidal sediments in the Forth estuary, Scotland. Limnology and Oceanography 32:954-963.

Hayes JM (1993) Factors controlling ^{13}C contents of sedimentary organic compounds: Principles and evidence. Marine Geology 113:111-125.

Hicks N, Bulling MT, Solan M, Raffaelli D, White PCL, Paterson DM (2011) Impact of biodiversity-climate futures on primary production and metabolism in a model benthic estuarine system. BMC Ecology 11:7.

Hill R, Schreiber U, Gademann R, Larkum AW D, Kühl M, Ralph PJ (2004) Spatial heterogeneity of photosynthesis and the effect of temperature-induced bleaching conditions in three species of corals. Marine Biology 144:633-640.

Hillebrand C, Dürselen CD, Kirschtel D, Pollingher U, Zohary T (1999) Biovolume calculation for pelagic and benthic microalgae. Journal of Phycology 35:324-405.

Honeywill C, Paterson DM, Hagerthey SE (2002) Instant determination of microphytobenthic biomass using fluorescence. European Journal of Phycology 37:485-492.

Hubas C, Davoult D, Cariou T, Artigas LF (2006) Factors controlling benthic metabolism during low tide along a granulometric gradient in an intertidal bay (Roscoff Aber Bay, France). Marine Ecology Progress Series 316:53-68.

Huggett J, Griffiths CL (1986) Some relationships between elevation, physicochemical variables and biota of intertidal rock pools. Marine Ecology Progress Series 29:189-197.

Jeffrey SW, Humphrey GF (1975) New spectrophotometric equations for determining chlorophylls a, b, c1, and c2 in higher plants, algae and natural phytoplankton. Biochemie und Physiologie der Pflanzen 167:191-194.

Jesus B, Brotas V, Marani M, Paterson DM (2005) Spatial dynamics of microphytobenthos determined by PAM fluorescence. Estuarine, Coastal and Shelf Science. 65:30-42.

Jesus B, Brotas V, Ribeiro L, Mendes CR, Cartaxana P, Paterson DM (2009) Adaptations of microphytobenthos assemblages to sediment type and tidal position. Continental Shelf Research 29:1624-1634.

Jesus B, Mendes C, Brotas V, Paterson DM (2006a) Effect of sediment type on microphytobenthos vertical distribution: modelling the productive biomass and improving ground truth measurements. Journal of Experimental Marine Biology and Ecology 332:60-74.

Jesus B, Perkins RG, Consalvey M, Brotas V, Paterson DM (2006b) Effects of vertical migrations by benthic microalgae on fluorescence measurements of photophysiology. Journal of Experimental Marine Biology and Ecology 315:55-66.

Johnson VR, Brownlee C, Rickaby REM, Graziano M, Milazzo M, Hall-Spencer JM (2013) Responses of marine benthic microalgae to elevated CO_2. Marine Biology 160:1813-1824.

Johnston AM, Raven JA (1996) Inorganic carbon accumulation by the marine diatom Phaeodactylum *tricornutum*. European Journal of Phycology 31:285-290.

Kelly GJ, Latzko E (2006) Photosynthesis: Carbon Metabolism – Twenty Years of Following Carbon Cycles in Photosynthetic Cells. In: Thirty Years of Photosynthesis (G Kelly and E Latzko eds.), 210-236, Springer-Verlag Berlin Hiedelberg.

Kelly JA, Honeywill C, Paterson DM (2001) Microscale analysis of chlorophyll-*a* in cohesive intertidal sediments: the implications of microphytobenthos distribution. Journal of Marine Biological Association of the United Kingdom 81:151-162.

Kieleck C, Bousquet B, Le Brun G, Cariou J, Lotrian J (2001) Laser induced fluorescence imaging: application to groups of macroalgae identification. Journal of Physics D: Applied Physics 34: 2561-2571.

Kingston MB (1999) Wave effects on the vertical migration of two benthic microalgae: *Hantzschia virgata* var. *intermedia* and *Euglena proxima*. Estuaries 22:81-91.

Kolber Z, Klimov D, Ananyev G, Rascher U, Berry J, Osmond B (2005) Measuring photosynthetic parameters at a distance: laser induced fluorescence transient (LIFT) method for remote measurements of photosynthesis in terrestrial vegetation. Photosynthesis Research 84:121-129.

Kolber ZS, Falkowski PG (1993) Use of active fluorescence to estimate phytoplankton photosynthesis in situ. Limnology and Oceanography 38:1646-1665.

Kraay GW, Zapata M, Veldhuis M (1992) Separation of chlorophylls c_1, c_2, and c_3 of marine phytoplankton by reversed-phase-C18-high-performance liquid chromatography. Journal of Phycology. 28:708-712.

Kromkamp J, Barranguet C, Peene J (1998) Determination of microphytobenthos PSII quantum efficiency and photosynthetic activity by means of variable chlorophyll fluorescence. Marine Ecology Progress Series 162:45-55.

Kromkamp JC, Forster RM (2003) The use of fluorescence measurements in aquatic ecosystems: differences between multiple and single turnover measuring protocols and suggested terminology. European Journal of Phycology 38:103-112.

Kromkamp JC, Morris EP, Forster RM, Honeywill C, Hagerthey S, Paterson DM (2006) Relationship of intertidal surface sediment chlorophyll concentration to hyperspectral reflectance and chlorophyll fluorescence. Estuaries and Coasts 29:183-196.

Kühl M, Jorgensen B (1994) The light-field of microbenthic communities radiance distribution and microscale optics of sandy coastal sediments. Limnology and Oceanography 39:1368-1398.

Li P, Cheng L, Gao H, Jiang C, Peng T (2009) Heterogeneous behavior of PS II in soybean (Glycine max) leaves with identical PSII photochemistry efficiency under different high temperature treatments. Journal of Plant Physiology 166:1607-1615.

Lichtenthaler HK, Rinderle U (1988) The role of chlorophyll fluorescence in the detection of stress conditions in plants. Critical Reviews in Analytical Chemistry 19:29-85.

MacIntyre HL, Lawrenz E, Richardson TL (2010) Taxonomic discrimination of phytoplankton by spectral fluorescence. In: Suggett DJ, Prá$il O, Borowitzka MA (eds) Chlorophyll *a* fluorescence in aquatic sciences: methods and applications. Springer, Dordrecht, p 129-169.

MacIntyre HL, Geider RJ, Miller DC (1996) Microphytobenthos: the ecological role of the 'Secret Garden' of unvegetated, shallow-water marine habitats. I. Distribution, abundance and primary production. Estuaries 19:186-201.

Matsuda Y, Hara T, Colman B (2001) Regulation of the induction of bicarbonate uptake by dissolved CO_2 in marine diatom *Phaeodactylum tricornutum*. Plant, Cell and Environment 24:611-620.

Matsuda Y, Satoh K, Harada H, Satoh D, Hiraoka Y, Hara T (2002) Regulation of the expressions of HCO_3 uptake and intracellular carbonic anhydrase in response to CO_2 concentration in the marine diatom *Phaeodactylum* sp. Functional Plant Biology 29:261-270.

McMurtrey JE III, Chappelle EW, Kim MS, Meisinger JJ, Corp LA (1994) Distinguishing nitrogen fertilization levels in field corn *(Zea mays* L.) with actively induced fluorescence and passive reflectance measurements. Remote Sensing of Environment 47:36-44.

Méléder V, Barillé L, Launeau P, Carrère V, Rincé Y (2003) Spectrometric constraint in analysis of benthic diatom biomass using monospecific cultures. Remote Sensing of Environment 88:386-400.

Meng Q, Siebke K, Lippert P, Baur B, Mukherjee U, Weis E (2001) Sink-source transition in tobacoo leaves visualized using chlorophyll fluorescence imaging. New Phytologist 151:585-596.

Meyer M, Griffiths H (2013) Origins and diversity of eukaryotic CO_2-concentrating mechanisms: lessons for the future. Journal of Experimental Botany 64:769-786.

Meyercordt J, Meyer-Reil LA (1999) Primary production of benthic microalgae in two shallow coastal lagoons of different trophic status in the southern Baltic Sea. Marine Ecology Progress Series 178:179-191.

Middleburg JJ, Barranguet C, Boschker HTS, Herman PMJ, Moens T, Heip CHR (2000) The fate of intertidal microphytobenthos carbon: an in situ ^{13}C-labeling study. Limnology and Oceanography 45:1224-1234.

Millero FJ, Pierrot D, Lee K, Wanninkhof R, Feely RA, Sabine CL, Key RM (2002) Dissociation constants for carbonic acid determined from field measurements. Deep Sea Research I: Oceanography Research 49:1705-1723.

Montagna PA, Blanchard GF, Dinet A (1995) Effect of production and biomass of intertidal microphytobenthos on meiofaunal grazing rates. Journal of Experimental Marine Biology and Ecology 185:149-165.

Mook WG, Bommerson JC, Staverman WH (1974) Carbon isotope fractionation between dissolved bicarbonate and gaseous carbon dioxide. Earth and Planetary Science Letters 22:169-176.

Morris EP, Kromkamp JC (2003) Influence of temperature on the relationship between oxygen- and fluorescence-based estimates of photosynthetic parameters in a marine benthic diatom. European Journal of Phycology 38:133-142.

Murchie EH, Lawson T (2013) Chlorophyll fluorescence analysis: a guide to good practice and understanding some new applications. Journal of Experimental Botany 64:3983-3998.

Murphy RJ, Tolhurst TJ, Chapman MG, Underwood AJ (2004) Estimation of surface chlorophyll on an exposed mudflat using digital colour infrared (CIR) photography. Estuarine Coastal and Shelf Science 59: 625-638.

Murphy RJ, Tolhurst TJ, Chapman MG, Underwood AJ (2005) Remote-sensing of benthic chlorophyll: should ground truth data be expressed in units of area or mass? Journal of experimental Marine Biology and Ecology 316:69-77.

Murphy RJ, Underwood AJ, Tolhurst TJ, Chapman MG (2008) Field-based remote-sensing for experimental intertidal ecology: case studies using hyperspatial and hyperspectral data for New South Wales (Australia). Remote Sensing of Environment 112:3353-3365.

Nedbal L, Soukupova J, Kaftan D, Whitmarsh J, Trilek M (2000) Kinetic imaging of chlorophyll fluorescence using modulated light. Photosynthesis Research 66:25-34.

Nielsen HD and SL Nielsen (2008) Evaluation of imaging and conventional PAM as a measure of photosynthesis in thin- and thick-leaved marine macroalgae. Aquatic Biology 3:121-131.

Nimer NA, Iglesias-Rodriguez MD, Merrett MJ (1997) Bicarbonate utilization by marine phytoplankton species. Journal of Phycology 33:625-631.

Niyogi KK (1999) Photoprotection revisited: genetic and molecular approaches. Annual Review Plant Physiology and Plant Molecular Biology 50:333-59.

Omasa K, KL Shimazaki, I Aiga, W Larcher and M Onoe (1987) Image analysis of chlorophyll fluorescence transients for diagnosing the photosynthetic system of attached leaves. Plant Physiology 84:748-752.

Oppenheim DR (1988) The distribution of epipelic diatoms along an intertidal shore in relation to principal physical gradients. Botanica Marina 31:65-72.

Oxborough K (2004) Imaging of chlorophyll *a* fluorescence: Theoretical and practical aspects of an emerging technique for the monitoring of photosynthetic performance. Journal of Experimental Botany 55:1195-1205.

Oxborough K, Baker NR (1997) An instrument capable of imaging chlorophyll *a* fluorescence from intact leaves at very low irradiance and at cellular and subcellular levels of organization. Plant, Cell and Environment 20:1473-1483.

Oxborough K, Hanlon ARM, Underwood GJC, Baker NR (2000) In vivo estimation of the Photosystem II photochemical efficiency of individual microphytobenthic cells using

high-resolution imaging of chlorophyll *a* fluorescence. Limnology and Oceanography 45:1420-1425.

Paterson DM (1989) Short-term changes in the erodibility of intertidal cohesive sediments related to the migratory behavior of epipelic diatoms. Limnology and Oceanography 34:223-234.

Paterson DM, Wiltshire KH, Miles A, Backburn J, Davidson I, Yates MG, McGorty S, Eastwood JA (1998) Microbiological mediation of spectral reflectance from intertidal cohesive sediments- Limnology and Oceanography 43: 1207-1221.

Paterson DM, Black KS (1999) Water flow, sediment dynamics and benthic biology. Advances in Ecological Research 29:155-194.

Perkins RG, Kromkamp JC, Serôdio J, Lavaud J, Jesus B, Mouget JL, Lefebvre S , Forster RM (2010) The application of variable chlorophyll fluorescence to microphytobenthic biofilms. In Chlorophyll *a* Fluorescence in Aquatic Sciences: Methods and Applications (Edited by D. J. Suggett, O. Prášil and M. A. Borowitzka), pp. 237-275. Springer, Dordrecht.

Perkins RG, Lavaud J, Serôdio J, Mouget JL, Cartaxana P, Rosa P, Barille L, Brotas V, Jesus BM (2010) Vertical cell movement is a primary response of intertidal benthic biofilms to increasing light dose. Marine Ecology Progress Series 416:93-103.

Perkins RG, Oxborough K, Hanlon ARM, Underwood GJC, Baker NR (2002) Can chlorophyll fluorescence be used to estimate the rate of photosynthetic electron transport within microphytobenthic biofilms? Marine Ecology Progress Series 228:247-56.

Perkins RG, Underwood GJC, Brotas V, Snow GC, Jesus B, Ribeiro L (2001) Responses of microphytobenthos to light: primary production and carbohydrate allocation over an emersion period. Marine Ecology Progress Series 223:101-112.

Perkins RG, Mouget JL, Lefebvre S, Lavaud J (2006) Light response curve methodology and possible implications in the application of chlorophyll fluorescence to benthic diatoms. Marine Biology 149:703-712.

Pieruschka R, Klimov D, Kolber Z, Berry JA (2010) Monitoring of cold and light stress impact on photosynthesis by using laser induced fluorescence transient (LIFT) approach. Functional Plant Biology 37:395-402.

Pinckney J, Sandulli R (1990) Spatial autocorrelation analysis of meiofaunal and microalgal populations on an intertidal sandflat: scale linkage between consumers and resources. Estuarine, Coastal and Shelf Science 30: 341-353.

Pinckney JL, Zingmark RG (1993) Modeling the annual production of intertidal benthic microalgae in estuarine ecosystems. Journal of Phycology 29:396-407.

Platt T, Gallegos CL, Harrison WG (1980) Photoinhibition of photosynthesis in natural assemblages of marine phytoplankton. Journal of Marine Research 38:687-701.

Pomeroy LR (1959) Algal productivity in salt marshes of Georgia. Limnology and Oceanography 4: 386-397.

Pörtner HO, Karl DM, Boyd PW, Cheung WWL, Lluch-Cota SE, Nojiri Y, et al. Ocean systems. In: Field CB, Barros VR, Dokken DJ, Mach KJ, Mastrandrea MD, Bilir TE, Chatterjee M, Ebi KL, Estrada YO, Genova RC, Girma B, Kissel ES, Levy AN, MacCracken S, Mastrandrea PR, White LL, editors (2014). Climate Change 2014: Impacts, Adaptation, and Vulnerability. Part A: Global and Sectoral Aspects. Contribution of Working Group II to the Fifth Assessment Report of the Intergovernmental Panel on Climate Change. Cambridge, United Kingdom and New York, NY, USA: Cambridge University Press; p. 411–484.

Pyszniac AM, Gibbs SP (1992) Immunocytochemical localization of photosystem I and the fucoxanthin-chlorophyll *a*/*c* light-harvesting complex in the diatom *Phaeodactylum tricornutum*. Protoplasma 166:208-217.

Ralph PJ, Gademann R (2005) Rapid light curves: A powerful tool to assess photosynthetic activity. Aquatic Botany 82:222-37.

Ralph PJ, Gademann R, Dennison WC (1998) In situ seagrass photosynthesis measured using a submersible, pulse-amplitude modulated fluorometer. Marine Biology 132:367-373.

Raven JA, Cockell CS, De La Rocha CL (2008) The evolution of inorganic carbon concentrating mechanisms in photosynthesis. Philosophical Transactions of the Royal Society B 363:2641-2650.

Raven JA, Falkowski PG (1999) Oceanic sinks for atmospheric CO_2. Plant, Cell and Environment 22:741-755.

Raven JA, Giordano M, Beardall J, Maberly SC (2011) Algal and aquatic plant carbon concentrating mechanisms in relation to environmental change. Photosynthesis Research 109:1-16.

Raven JA, Giordano M, Beardall J, Maberly SC (2012) Algal evolution in relation to atmospheric CO_2: carboxylases, carbon-concentrating mechanisms and carbon oxidation cycles. Philosophical Transactions of the Royal Society B. 367:493-507.

Raven JA, Johnston AM (1991) Mechanisms of inorganic-carbon acquisition in marine phytoplankton and their implications for the use of other resources. Limnology and Oceanography 36:1701-1714.

Redlinger T, Grantt E (1983) Molecular menbranes of Prophyridium cruentum. An analysis of chlorophyll-protein complex and heme-binding proteins. Plant Physiology 73:36-40.

Reinfelder JR (2011) Carbon concentrating mechanisms in eukaryotic marine phytoplankton. Annual Review of Marine Science 3:291-315.

Reinfelder JR, Kraepiel AML, Morel FMM (2000) Unicellular C_4 photosynthesis in marine diatom. Nature 407:996-999.

Reinfelder JR, Milligan AJ, Morel FMM (2004) The role of the C_4 pathway in carbon accumulation and fixation in a marine diatom. Plant Physiology 135:2106-2111.

Ribeiro L (2010) Intertidal benthic diatoms of the Tagus estuary: taxonomic composition and spatial-temporal variation. PhD Dissertation, University of Lisbon, Portugal. http://repositorio.ul.pt/handle/10451/2330.

Richards JT, Schuerger AC, Capelle G, Guikema JA (2003) Laser-induced fluorescence spectroscopy of dark and light-adapted bean (*Phaseolus vulgaris L*.) and wheat (*Triticum aestivum L*.) plants grown under three irradiance levels and subjected to fluctuating lighting conditions. Remote Sensing of Environment 84:323-341.

Roberts K, Granum E, Leegood RC, Raven JA (2007a) C_3 and C_4 pathways of photosynthetic carbon assimilation in marine diatoms are under genetic, not environmental, control. Plant Physiology 145:230-235.

Roberts K, Granum E, Leegood RC, Raven JA (2007b) Carbon acquisition by diatoms. Photosynthesis Research 93:79-88.

Rosema A, Snel JFH, Zahn H, Buurmeijer WF, van Hove LWA (1998) The relation between laser-induced chlorophyll fluorescence and photosynthesis. Remote Sensing of Environment 65:143-154.

Rotatore C, Colman C, Kuzma M (1995) The active uptake of carbon dioxide by the marine diatoms *Phaeodactylum tricornutum* and *Cyclotella sp*. Plant, Cell and Environment 18:913-918.

Round FE, Palmer JD (1966) Persistent, vertical-migration rhythms in benthic microflora II. Field and laboratory studies on diatoms from the banks of the River Avon. Journal of the Marine Biological Association of the United Kingdom 46:191–214.

Rouse JW, Haas RH Jr, Schell JA, Deering DW (1973) Monitoring vegetation systems in the Great Plains with ERTS. Proceedings of the 3rd ERTS (Earth Resources Technology Satellite) Symposium, NASA SP-351, Vol 1. National Aeronautics and Space Administration, Washington, DC, p 309–317.

Ruban AV, Lavaud J, Rousseau B, Guglielmi G, Horton P, Etienne AL (2004) The super-excess energy dissipation in diatom algae: comparative analysis with higher plants. Photosynthesis Research 82: 65-175.

Saburova MA, Polikarpov IG (2003) Diatom activity within soft sediments: behavioural and physiological processes. Marine Ecology Progress Series 251:115-126.

Salleh S, McMinn A (2011). The effects of temperature on the photosynthetic parameters and recovery of two temperate benthic microalgae, *Amphora* cf. *coffeaeformis* and *Cocconeis* cf. *sublittoralis* (Bacillariophyceae). Journal of Phycology 47:1413-1424.

Schlensog M and Schroeter B (2001) A new method for the accurate in situ monitoring of chlorophyll *a* fluorescence in lichens and bryophytes. The Lichenologist 33:443-452.

Scholes JD, Rolfe SA (1996) Photosynthesis in localized regions of oat leaves infected with crown rust (*Puccinia coronata*): Quantitative imaging of chlorophyll fluorescence. Planta 199:573-582.

Schreiber U (1986) Detection of rapid induction kinetics with a new type of high-frequency modulated chlorophyll fluorometer. Photosynthesis Research 9:261-272.

Schreiber U, Schliwa U, Bilger W (1986) Continuous recording of photochemical and nonphotochemical chlorophyll fluorescence quenching with a new type of modulation fluorometer. Photosynthesis Research 10:51-62.

Schubert H, Schiewer U, Tschierner E (1989) Fluorescence characteristics of cyanobacteria (blue–green algae). Journal of Plankton Research 11:353-359.

Schuerger AC, Capelle GA, Di Benedetto JA, Mao C, Thai CM, Evans MD, Richards JT, Blank TA, Stryjewski EC (2003) Comparison of two hyperspectral imaging and two laser-induced fluorescence instruments for the detection of zinc stress and chlorophyll concentration in Bahia grass (*Paspalum notatum* Flugge). Remote Sensing of Environment 84:572-588.

Serôdio J (2004) Analysis of variable chlorophyll fluorescence in microphytobenthos assemblages: Implications of the use of depth integrated measurements. Aquatic Microbial Ecology 36:137-152.

Serôdio J, Cartaxana P, Coelho H, Vieira S (2009) Effects of chlorophyll fluorescence on the estimation of microphytobenthos biomass using spectral reflectance indices. Remote Sensing of Environment 113:1760-1768.

Serôdio J, Catarino F (1999) Fortnightly light and temperature variability in estuarine intertidal sediments and implications for microphytobenthos primary productivity. Aquatic Ecology 33:235-241.

Serôdio J, Catarino F (2000) Modelling the primary productivity of intertidal microphytobenthos: time scales of variability and effects of migratory rhythms. Marine Ecology Progress Series 192:13-30.

Serôdio J, Coelho H, Vieira S, Cruz S (2006) Microphytobenthos vertical migratory photoresponse as characterised by light-response curves of surface biomass. Estuarine, Coastal and Shelf Science 68:547-556.

Serôdio J, Marques da Silva J, Catarino F (1997) Nondestructive tracing of migratory rhythms of intertidal benthic microalgae using in vivo chlorophyll *a* fluorescence. Journal of Phycology 33:542-553.

Serôdio J, Marques da Silva J, Catarino F (2001). Use of in vivo chlorophyll *a* fluorescence to quantify short-term variations in the productive biomass of intertidal microphytobenthos. Marine Ecology Progress Series 218:45-61.

Serôdio J, Vieira S, and Cruz S (2008) Photosynthetic activity, photoprotection and photoinhibition in intertidal microphytobenthos as studied in situ using variable chlorophyll fluorescence. Continental Shelf Research 28:1363-1375.

Serôdio J, Vieira S, Cruz S, Barroso F (2005) Short-term variability in the photosynthetic activity of microphytobenthos as detected by measuring rapid light curves using variable fluorescence. Marine Biology 146:903-914.

Serôdio J, Vieira S, Barros F (2007) Relationship of variable chlorophyll fluorescence indices to photosynthetic rates in microphytobenthos. Aquatic Microbial Ecology 49:71–85.

Souffreau C, Vanormelingen P, Verleyen E, Sabbe K, Vyverman W (2010) Tolerance of benthic diatoms from temperate aquatic and terrestrial habitats to experimental desiccation and temperature stress. Phycologia 49:309-324.

Stephens FC, Louchard EM, Reid P, Maffionr RA (2003) Effects of microalgal communities on reflectance spectra of carbonate sediments in subtidal optically shallow marine environments. Limnology and Oceanography 48:535–546.

Subhash N, Mohanan CN (1997) Curve-fit analysis of chlorophyll fluorescence spectra: application to nutrient stress detection in sunflower. Remote Sensing of Environment 60:347-356.

Sullivan MJ, Moncrieff CA (1988) A multivariate analysis of diatom community structure and distribution in a Mississippi salt marsh. Botanica Marina 31: 93-99.

Sundbäck K, Miles A, Goransson E (2000) Nitrogen fluxes, denitrification and the role of microphytobenthos in microtidal shallow-water sediments: an annual study. Marine Ecology Progress Series 200:59-76.

Sutherland TF, Amos CL, Grant J (1998) The effect of buoyant biofilms on the erodibility of sublittoral sediments of a temperate microtidal estuary. Limnology and Oceanography 43:225-235.

Taguchi S (1976) Relation between photosynthesis and cell size of marine diatoms. Journal of Phycology 12:185-189.

Torstensson A, Chierici M, Wulff A (2012) The influence of increased temperature and carbon dioxide levels on the benthic/sea ice diatom *Navicula directa*. Polar Biology 35:205-214.

Tortell PD, Reinfelder JR, Morel FMM (1997) Active uptake of bicarbonate by diatoms. Nature 390:243-244.

Turpin DH, Layzell DB, Elrifi IR (1985) Modeling the C Economy of *Anabaena flosaquae*: estimates of establishment maintenance and active costs associated with growth on NH_3, NO_2 and N_2. Plant Physiology 78:746-752.

Underwood GJC (1994) Seasonal and spatial variation in epipelic diatom assemblages in the Severn estuary. Diatom Research 9:451-472.

Underwood GJC, Kromkamp J (1999) Primary production by phytoplankton and microphytobenthos in estuaries. Advances in Ecological Research 29:93-153.

Underwood GJC, Paterson DM (2003) The importance of extracellular carbohydrate production by marine epipelic diatoms. Advances in Botanical Research 40:183-240.

Underwood GJC, RG Perkins, MC Consalvey, ARM Hanlon, K Oxborough, NR Baker and DM Paterson (2005) Patterns in microphytobenthic primary productivity: Species-specific variation in migratory rhythms and photosynthetic efficiency in mixed-species biofilms. Limnology and Oceanography 50:755-767.

Underwood GJC (2005) Microalgal (microphytobenthic) biofilms in shallow coastal waters: how important are species? Proceedings of the California Academy of Sciences 56:162-169.

Van der Grinten E, Simis S, Barranguet C, Admiraal W (2004) Dominance of diatoms over cyanobacterial species in nitrogen-limited biofilms. Archiv für Hydrobiologie 161:98-111.

Van der Grinten E, Simis S, Barranguet C, Admiraal W (2005) Temperature and light dependent performance of the cyanobacterium *Leptolyngbya foveolarum* and the diatom *Nitzschia perminuta* in mixed biofilms. Hydobiologia 548:267-278.

Vanelslander B, Créach V, Vanormelingen P, Ernst A, Chepurnov VA, Sahan E, Muyzer G, Stal LJ, Vyverman W, Sabbe K (2009) Ecological differentiation between sympatric

pseudocryptic species in the estuarine benthic diatom *Navicula phyllepta* (Bacillariophyceae). Journal of Phycology 45:1278-1289.

Vieira S, Ribeiro L, Jesus B, Cartaxana P, Marques da Silva J (2013a) Photosynthesis assessment in microphytobenthos using conventional and imaging pulse amplitude modulation fluorometry. Photochemistry and Photobiology 89:97-102.

Vieira S, Ribeiro L, Marques da Silva J Cartaxana P (2013b) Effects of short-term changes in sediment temperature on the photosynthesis of two intertidal microphytobenthos communities. Estuarine, Coastal and Shelf Science 119:112-118.

Vieira S, Utkin A, Lavrov A, Santos NM, Vilar R, Marques da Silva J, Cartaxana P (2011) Effects of intertidal microphytobenthos migration on biomass determination via laser-induced fluorescence. Marine Ecology Progress Series 432:45-52.

Vieira S, Cartaxana P, Máguas C, Marques da Silva J (2016) Photosynthesis in estuarine intertidal microphytobenthos is limited by inorganic carbon availability. Photosynthesis Research (in press) DOI 10.1007/s11120-015-0203-0.

Villareal TA, Morton SL (2002) Use of cell-specific PAM-fluorometry to characterize host shading in the epiphytic dinoflagellate *Gambierdiscus toxicus*. Marine Ecology 23:127-140.

Vogelmann T, Han T (2000) Measurement of gradients of absorbed light in spinach leaves from chlorophyll fluorescence profiles. Plant, Cell and Environment 23:1303-1311.

Yallop ML (1994) Survey of Servern estuary. In Bioestabilisation of sediments. W.E. Krumbun et al. (eds). Oldenburg. 279-326.

Young AJ, Phillip D, Ruban AV, Horton P, Frank HA (1997) The xanthophyll cycle and carotenoid-mediated dissipation of excess excitation energy in photosynthesis. Pure and Applied Chemistry 69:2125-2130.

Appendix 1. Experimental life support system (ELSS). Photographs of the flow-through experimental life support system (ELSS) used in this study. General view of the ELSS (A); Approximation showing two microcosms with the sediment surface cover by MPB and the pipe system for tidal water in and outflow (B). For more details see Coelho et al. (2013).

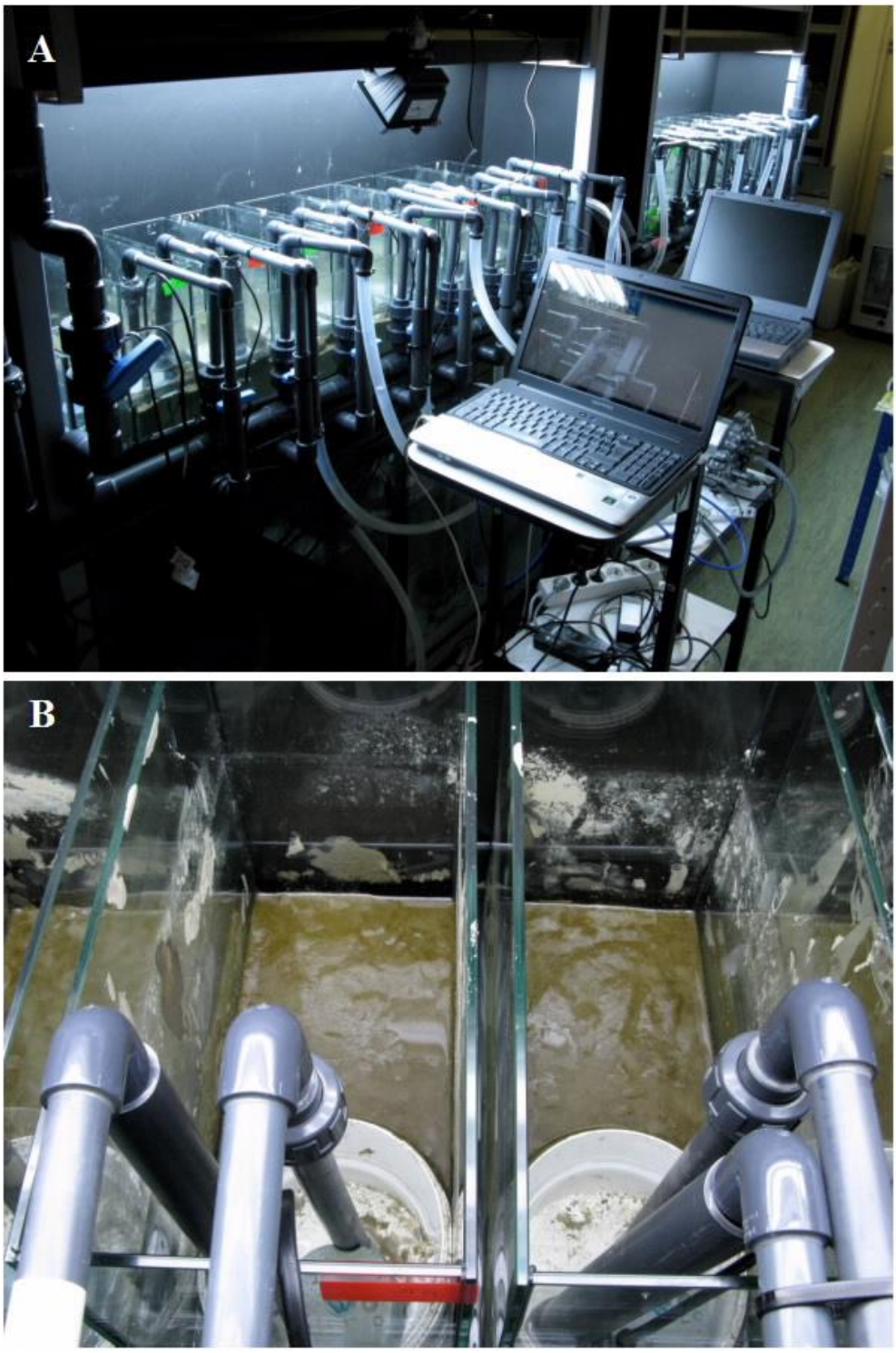

Appendix 2. Species composition and relative abundance of microphytobenthic diatoms under control and elevated CO_2 and temperature. Diatom composition and relative abundance (%, mean ± standard error, n=4) of a Tagus estuary intertidal microphytobenthic community at the beginning of the experiment (T0) and after 11 days under different temperatures and pH. T 18 °C pH 8.0: Temperature = 18°C, pH = 8.0; T 24°C pH 8.0.Temperature = 24°C, pH = 8.0; T 18 °C pH 7.4.Temperature = 18°C, pH = 7.4; T 24°C pH 7.4: Temperature = 24°C, pH=7.4.

Species	T0	T 18ºC pH 8.0	T 18ºC pH 7.4	T 24ºC pH 8.0	T 24ºC pH 7.4
Achnanthes lemmermannii var. *obtusa* Hustedt			0.04 (0.04)		
Achnanthes s.l. sp.1					0.11 (0.11)
Achnanthes s.l. sp.2		0.04 (0.04)			0.20 (0.13)
Achnanthidium minutissimum (Kützing) Czarnecki			0.16 (0.16)	0.10 (0.10)	0.05 (0.05)
Actinocyclus normanii (Gregory) Hustedt	0.08 (0.08)	0.04 (0.04)	0.10 (0.10)	0.16 (0.10)	0.09 (0.09)
Amphora arenicola Grunow in Cleve			0.04 (0.04)		
Amphora cf. *helenensis* Giffen					0.05 (0.05)
Amphora cf. *micrometra* Giffen		0.13 (0.13)	0.18 (0.18)		
Amphora cf. *pediculus* (Kützing) Grunow in Schmidt et al.	0.08 (0.08)	0.13 (0.08)	0.10 (0.10)	0.20 (0.11)	0.37 (0.32)
Amphora cf. *subacutiuscula* Schoeman	0.31 (0.20)	0.27 (0.14)	0.32 (0.13)	0.72 (0.41)	0.33 (0.22)
Amphora cf. *tenuissima* Hustedt				0.43 (0.16)	0.29 (0.16)
Aulacoseira granulata (Ehrenberg) Simonsen	0.24 (0.24)			0.11 (0.11)	
Aulacoseira islandica (O. Müller) Simonsen			0.12 (0.12)		
Aulacoseira subartica (O. Müller) Haworth				0.10 (0.06)	
Berkeleya rutilans (Trentepohl ex Roth) Grunow				0.05 (0.05)	
Biremis lucens (Hustedt) Sabbe Witkowski & Vyverman		0.09 (0.06)		0.30 (0.17)	0.15 (0.09)
Catenula adhaerens (Mereschkowsky) Mereschkowsky		0.04 (0.04)		0.24 (0.24)	0.14 (0.14)
Catenula sp.1				0.05 (0.05)	0.09 (0.09)
Catenula sp.2					0.09 (0.09)
Climaconeis fasciculata (Grunow ex Cleve) Cox		0.03 (0.03)			0.09 (0.05)
Cocconeiopsis breviata (Hustedt) Witkowski. Lange-Bertalot & Metzeltin	0.08 (0.08)	0.06 (0.06)		0.21 (0.09)	0.14 (0.14)
Cocconeis cf. *placentula* Ehrenberg			0.04 (0.04)	0.05 (0.05)	0.05 (0.05)
Cocconeis hauniensis Witkowski emend. Witkowski		0.13 (0.05)		0.14 (0.09)	0.19 (0.19)
Cocconeis pelta Schmidt			0.04 (0.04)	0.10 (0.10)	0.09 (0.05)
Cocconeis peltoides Hustedt				0.19 (0.19)	0.14 (0.14)
Cocconeis scutellum Ehrenberg var. *parva* (Grunow) Cleve in Van Heurck					0.05 (0.05)
Coscinodiscus radiatus Ehrenberg			0.05 (0.05)		
Cyclotella atomus Hustedt					0.09 (0.09)
Cyclotella meneghiniana Kützing	0.08 (0.08)	0.10 (0.06)	0.09 (0.05)		0.14 (0.09)
Cymatosira belgica Grunow in Van Heurck		0.18 (0.10)			0.56 (0.56)
Neodelphineis pelagica Takano		0.04 (0.04)			
Dickieia sp.1	0.15 (0.27)				
Diploneis didyma (Ehrenberg) Cleve	0.08 (0.14)		0.06 (0.06)		
Eolimna minima (Grunow in Van Heurck) Lange-Bertalot				0.05 (0.05)	
Fallacia cf. *teneroides* (Hustedt) Mann					0.09 (0.09)
Fallacia florinae (Moeller) Witkowski	0.08 (0.13)	0.03 (0.03)	0.04 (0.04)	0.19 (0.13)	0.19 (0.19)
Fallacia oculiformis (Hustedt) Mann				0.19 (0.13)	
Frustulia interposita (Lewis) De Toni	0.78 (0.58)	1.39 (0.25)	1.51 (0.35)	0.93 (0.29)	1.63 (0.61)

Gyrosigma acuminatum (Kützing) Rabenhorst	8.88 (3.72)	5.69 (0.84)	5.63 (0.35)	2.09 (0.47)	3.29 (0.52)
Gyrosigma fasciola (Ehrenberg) Griffith & Henfrey	0.31 (0.35)	0.04 (0.04)	0.44 (0.24)	0.20 (0.11)	0.18 (0.11)
Gyrosigma cf. *limosum* Sterrenburg & Underwood	6.04 (1.12)	1.36 (0.54)	1.42 (0.20)	1.27 (0.30)	2.89 (0.85)
Gyrosigma scalproides (Rabenhorst) Cleve		0.04 (0.04)			
Gyrosigma sp.1	1.17 (0.81)	1.60 (0.26)	0.73 (0.19)	0.97 (0.35)	0.61 (0.15)
Halamphora cf. *abuensis* (Foged) Levkov				0.19 (0.13)	
Halamphora sp.1			0.05 (0.05)	0.05 (0.05)	0.05 (0.05)
Hippodonta caotica Witkowski. Lange-Bertalot & Metzeltin	0.08 (0.13)	0.07 (0.04)		0.05 (0.05)	0.04 (0.04)
Luticola mutica (Kützing) Mann.		0.04 (0.04)			
Minidiscus chilensis Rivera in Rivera & Koch	6.53 (3.38)	6.22 (1.25)	5.31 (1.66)	12.64 (2.89)	15.69 (1.34)
Navicula abscondita Hustedt					0.05 (0.05)
Navicula cf. *aleksandrae* Lange-Bertalot. Bogaczewicz-Adamczak & Witkowski	0.08 (0.13)				0.41 (0.15)
Navicula arenaria Donkin				0.09 (0.09)	
Navicula bozenae Lange-Bertalot. Witkowski & Zgrundo		0.21 (0.21)	0.16 (0.10)	0.23 (0.17)	0.14 (0.09)
Navicula diserta Hustedt		0.12 (0.08)	0.17 (0.11)	0.05 (0.05)	0.19 (0.13)
Navicula flagellifera Hustedt				0.05 (0.05)	
Navicula gregaria Donkin m.1	10.98 (0.54)	5.26 (0.51)	5.96 (0.63)	7.21 (1.77)	6.25 (1.30)
Navicula cf. *microdigitoradiata* Lange-Bertalot			0.14 (0.14)	0.09 (0.05)	
Navicula cf. *mollis* (W. Smith) Cleve					0.10 (0.06)
Navicula paeninsulae Cholnoky		0.04 (0.04)			0.05 (0.05)
Navicula pargemina Underwood & Yallop	0.15 (0.27)	0.46 (0.16)	0.20 (0.15)	2.14 (0.85)	0.67 (0.53)
Navicula cf. *phyllepta* Kützing	8.22 (3.44)	6.20 (0.87)	5.65 (0.87)	12.28 (1.74)	10.67 (2.02)
Navicula platyventris Meister				0.05 (0.05)	
Navicula ponticula Giffen		0.04 (0.04)			
Navicula salinarum Grunow					0.23 (0.23)
Navicula cf. *salinicola* Hustedt	0.16 (0.28)				
Navicula recens (Lange-Bertalot) Lange-Bertalot	0.15 (0.27)	0.06 (0.06)	0.04 (0.04)	0.10 (0.06)	0.05 (0.05)
Navicula spartinetensis Sullivan & Reimer	37.33 (7.18)	51.66 (2.04)	55.02 (2.04)	23.09 (5.89)	20.85 (3.85)
Navicula viminoides Giffen					0.23 (0.23)
Navicula sp.3	0.31 (0.35)	0.50 (0.15)	0.44 (0.20)		
Nitzschia cf. *aequorea* Hustedt	3.90 (1.45)	6.55 (0.81)	6.85 (2.17)	9.55 (3.79)	10.90 (2.85)
Nitzschia cf. *aurariae* Cholnoky	2.35 (1.72)	0.76 (0.31)	0.57 (0.24)	7.58 (3.65)	4.21 (0.85)
Nitzschia cf. *dissipata* (Kützing) Grunow	0.93 (0.26)		0.22 (0.17)	0.55 (0.21)	0.44 (0.10)
Nitzschia cf. *distans* Gregory	0.08 (0.13)	0.68 (0.26)	0.56 (0.23)	0.05 (0.05)	0.13 (0.13)
Nitzschia cf. *parvula* W. Smith non Lewis	0.70 (0.41)	0.14 (0.09)	0.47 (0.27)	0.57 (0.23)	0.66 (0.39)
Nitzschia frustulum (Kützing) Grunow in Cleve & Grunow	0.23 (0.23)	0.38 (0.19)	0.17 (0.11)	0.58 (0.25)	0.48 (0.18)
Nitzschia navicularis (Brébisson) Grunow		0.06 (0.06)			
Nitzschia sigma (Kützing) W. Smith	0.23 (0.01)	0.20 (0.08)	0.52 (0.14)	0.34 (0.16)	1.26 (0.50)
Nitzschia cf. *tubicola* Grunow in Cleve & Grunow			0.05 (0.05)		
Nitzschia valdestriata Aleem & Hustedt		0.15 (0.11)	0.05 (0.05)	0.29 (0.12)	0.11 (0.11)
Nitzschia sp.1				0.05 (0.05)	
Nitzschia sp.4	0.31 (0.35)			0.05 (0.05)	0.16 (0.10)
Nitzschia sp.5		0.23 (0.11)	0.04 (0.04)		
Nitzschia sp.6		0.16 (0.12)	0.32 (0.13)	0.59 (0.29)	0.28 (0.16)
Nitzschia sp.7				0.05 (0.05)	
Nitzschia sp.8			0.10 (0.06)	0.19 (0.11)	
Nitzschia sp.9					0.05 (0.05)
Nitzschia sp.10					0.16 (0.16)
Nitzschia sp.11	0.47 (0.48)	0.13 (0.13)		1.07 (0.36)	

Nitzschia sp.12		0.21 (0.21)	0.06 (0.06)		0.26 (0.26)
Opephora guenter-grassii (Witkowski & Lange-Bertalot) Sabbe & Vyverman				0.10 (0.10)	
Opephora sp.1				0.05 (0.05)	
Parlibellus berkeleyi (Kützing) Cox			0.10 (0.06)		
Petrodictyon gemma (Ehrenberg) Mann in Round. Crawford & Mann	0.30 (0.26)	0.36 (0.15)	0.10 (0.10)	0.35 (0.10)	0.05 (0.05)
Pierrecomperia catenuloides Sabbe. Vyverman & Ribeiro		0.08 (0.08)	0.05 (0.05)	0.09 (0.09)	
Plagiogrammopsis minima (Salah) Sabbe & Witkowski	0.16 (0.28)	0.89 (0.36)	0.57 (0.32)	1.37 (0.33)	2.02 (0.23)
Plagiotropis vanheurckii Grunow in Van Heurck	3.96 (0.58)	2.12 (0.27)	1.13 (0.18)	0.64 (0.23)	1.23 (0.59)
Planothidium cf. *lemmermannii* Hustedt (Morales)	0.08 (0.13)				0.05 (0.05)
Planothidium delicatulum s.l. (Kützing) Round & Bukhtiyarova m.1		0.08 (0.08)	0.05 (0.05)	0.24 (0.09)	0.29 (0.05)
Planothidium delicatulum s.l. (Kützing) Round & Bukhtiyarova m.2	0.08 (0.13)	0.13 (0.05)	0.10 (0.06)	0.05 (0.05)	0.14 (0.09)
Planothidium delicatulum s.l. (Kützing) Round & Bukhtiyarova m.3	0.08 (0.14)	0.04 (0.04)		0.05 (0.05)	
Planothidium deperditum (Giffen) Witkowski. Lange-Bertalot & Metzeltin				0.10 (0.10)	0.05 (0.05)
Pleurosigma sp.1	0.31 (0.14)	0.32 (0.08)	0.29 (0.05)		0.28 (0.12)
Psammodictyon panduriforme var. *continuum* (Grunow) Snoeijs		0.03 (0.03)		0.16 (0.10)	
Reimeria sinuata (Gregory) Kociolek & Stoermer					0.05 (0.05)
Seminavis sp. 1					0.05 (0.05)
Staurophora salina (W. Smith) Mereschkowsky	0.38 (0.47)	0.50 (0.20)		0.26 (0.13)	0.46 (0.20)
Stephanodiscus rotula (Kützing) Hendey	0.08 (0.13)				
Surirella atomus Hustedt	0.24 (0.24)	0.24 (0.10)	0.17 (0.10)	0.74 (0.21)	0.34 (0.10)
Surirella curvifacies Brun		0.20 (0.11)	0.08 (0.08)	0.14 (0.14)	
Surirella sp.1	0.16 (0.28)	0.06 (0.06)		0.05 (0.05)	0.05 (0.05)
Thalassiocyclus lucens (Hustedt) Håkansson & Mahood	0.16 (0.28)	0.16 (0.09)	0.05 (0.05)	0.33 (0.20)	0.59 (0.25)
Thalassiosira angulata (Gregory) Hasle	0.15 (0.26)		0.08 (0.05)	0.10 (0.06)	0.04 (0.04)
Thalassiosira binata Fryxell	0.08 (0.14)				
Thalassiosira cf. *profunda* (Hendey) Hasle	0.08 (0.13)				0.04 (0.04)
Thalassiosira minima Gaarder	0.24 (0.42)	0.14 (0.09)	0.22 (0.08)	0.56 (0.33)	0.35 (0.26)
Thalassiosira proschkinae Makarova in Makarova. Genkal & Kuzmln	0.62 (0.70)	0.72 (0.47)	0.86 (0.67)	0.83 (0.37)	0.72 (0.27)
Thalassiosira cf. *pseudonana* Hasle & Heimdal	1.24 (0.17)	1.75 (0.20)	1.92 (0.65)	4.93 (1.44)	5.89 (2.47)
Thalassiosira sp.1	0.08 (0.13)				
Thalassiosira sp.2				0.05 (0.05)	
Tryblionella apiculata Gregory		0.17 (0.06)			0.14 (0.09)